2007

Cellmap: An automated multielectrode array cell culture analysis system based on electrochemical impedance spectroscopy

Abdur Rub Abdur Rahman
University of South Florida

CellMap: An Automated Multielectrode Array Cell Culture Analysis System

Based on Electrochemical Impedance Spectroscopy

by

Abdur Rub Abdur Rahman

A dissertation submitted in partial fulfillment
of the requirements for the degree of
Doctor of Philosophy
Department of Electrical Engineering
College of Engineering
University of South Florida

Major Professor: Shekhar Bhansali, Ph.D.
Thomas Weller, Ph.D.
Jing Wang, Ph.D.
Mark Jaroszeski, Ph.D.
Chun Min Lo, Ph.D.

Date of Approval:
June 28, 2007

Keywords: biosensor, bioimpedance, cell-based assays, whole cell assays, cell substrate sensing, cell monitoring, cytology, cellular behavior, biomems

Acknowledgements

This work is supported by National Science Foundation career grant No. 0239262.

I begin by thanking GOD for all things in life.

I thank Professor Shekhar Bhansali for his mentorship and friendship. I am fortunate to have him as my adviser. His support and encouragement have been crucial to my success. He has been very considerate of my professional and personal situations. I look forward to his continued mentorship in future.

I thank my committee members for agreeing to serve on my dissertation committee despite their busy schedule. I thank them for their encouragement and support.

I thank Dr. Chun-min Lo for his research collaboration and teaching. If not for his support, it would have been difficult for me to complete many of my experiments in a timely manner. He is a well wisher and a friend, who has always wished for my betterment.

I would like to thank past and present members of the Microsystems and RF MEMS group at USF. I have benefited greatly from my interactions with them. They have helped maintain a safe and cordial workplace.

I would like to thank my parents for providing me with a good upbringing and education. Their emphasis on service to society by learning and teaching has provided the motivation for my education. I would like to thank my wife for her support, encouragement, patience and love all along. Without her cooperation, this research would not have been possible.

Table of Contents

List of Tables

List of Figures

CellMap: An Automated Multielectrode Array Cell Culture Analysis System Based on Electrochemical Impedance Spectroscopy

Abdur Rub Abdur Rahman

ABSTRACT

The objective of this research is to develop fundamental understanding of cell-substrate (CS) and cell-cell (CC) interactions in the culture space for time evolving cell cultures. Space resolved CC and CS interactions are important indicators of cell-density distribution, localized cellular behavior, and multiple cell-layers which are differentiators of normal and abnormal cell behavior. In this research, CS and CC interactions and the variations therein due to a) Cell growth, 2) cell-drug interaction, and 3) effect of Cytotoxin were studied using multielectrode, multi-frequency Electrochemical Impedance Spectroscopy (EIS). Contemporary impedance based methods sense either CC or CS interaction as a space averaged macroscopic quantity. A major contribution of this research is that, both CC and CS interactions are recorded and analyzed with spatio-temporal resolution. This research led to the development of an automated cell culture monitoring system, namely, CellMap.

A planar eight electrode sensor was fabricated on a glass substrate and interfaced with a switching circuit. The switching circuit sequentially selects consecutive electrodes upon input of a 5V trigger pulse which is generated by the frequency response analyzer at the end of each frequency scan, thereby

facilitating automated switching and recording of multielectrode dataset. Calibration standards and protocols were developed to null the channel parasitics of individual channels. A set of eight impedance measurements for eight electrodes constitutes a "frame". Frames are recorded at regular time intervals over the desired course of time.

Impedance mapping of adhesion, spreading, motility and detachment of OvCa429 ovarian cancer cells was performed over a period of 70 hours. The cell-layer resistance, which indicates cell-cell contact, increased as a function of time until confluence, and decreased thereafter due to cell death and detachment. This was also confirmed by optical microscopy observations. Similarly, the cell layer Constant Phase Element (CPE) parameters, which were found to correlate well with cell density distribution, also increased as a function of time until confluence and decreased thereafter. Additionally, the cell-growth mapping revealed that the CellMap system is able to resolve non-uniform cell distributions in the culture space, which may be useful in differentiating between normal and pathological cells.

Chapter 1: Introduction

1.1 Problem Definition

There are behavioral, macroscopic and microscopic differences between normal and pathological cells in-vivo (tissue) and in-vitro (culture) [1]. Normal cell behavior, which includes adhesion, spreading, motility and apoptosis is influenced by the introduction of foreign organisms [2], effect of chemical compounds [3], and environmental parameters [4] among other causes. These changes have been successfully detected by cell-based biosensors. Among the several classes of cell-based biosensors, Impedemetric sensors provide a non-invasive and label-free method for monitoring cell cultures [5]. The feasibility of Impedemetric sensors has been demonstrated for a variety of applications including wound healing, cell-drug interaction and apoptosis [6, 7]. However, current Impedance-based whole-cell biosensors technology suffers from the following limitations, a) lack of spatial resolution, b) non-specific, non-parameterized quantitative descriptors of adhesion and motility, and c) limited data processing and analysis capabilities.

Many abnormal cell types exhibit adhesion and proliferation characteristics that are different from their normal counterparts [8]. To distinguish these behavioral characteristics, a space and time resolved measurement system is needed. Current real-time impedance-based cell substrate sensors use non-specific space-averaged quantitative descriptors to represent cell substrate interaction and often do not characterize the cell layer [9, 10]. Although these descriptors provide some measure of the cellular activity, the exact

nature of the cell-substrate interactions is unclear. A system is needed which can monitor specific parameters of cell-substrate interactions (e.g. Cell-substrate separation) and cell-cell interactions (e.g. tight junctional resistance) on a real-time basis. Contemporary systems (commercial as well as research) lack the capability for real-time impedance mapping and parameterization of evolving cell cultures.

A primary hurdle in distributed impedance mapping is the additional hardware requirement of switching between electrodes without introducing measurement parasitics. Additionally, data collection, processing, analysis and visualization are difficult to implement and integrate for large multidimensional datasets, especially in a real-time environment.

Impedance Spectroscopy (IS), also referred to as dielectric spectroscopy has been extensively used in the study of cell-substrate interactions among several other investigations of biomaterials' properties [11, 12]. A major challenge in IS is in the interpretation of the impedance spectra. IS data is predominantly interpreted by parameter extraction via equivalent circuit modeling. Traditional spectroscopic measurements involve few datasets which are fit to circuits of choice to extract parameters. A multiple electrode system performing impedance spectroscopy in real-time generates large datasets, where each electrode data has to be individually fit to an equivalent circuit for parameter extraction. This task is cumbersome unless automated. However, no such system has been reported yet that can perform automated parameter extraction from impedance data of time evolving cell cultures. Hence, there is a need for a system that can perform automated data analysis and parameter extraction. A key challenge in the implementation of automated parameterization of evolving cell cultures is that the model representing the system continuously changes.

We address the aforementioned need for an automated cell culture monitoring system which can monitor and report specific changes in cell-

substrate and cell-cell interactions. The problem of automatic parametric extraction of an evolving cell culture is addressed.

1.2 Motivation

Cell culture studies provide valuable information on the cells' physiological condition and by extension the tissue and organism from which the cells originate. Among the many techniques that are currently available for cell culture monitoring, Impedance-based techniques are promising because; they offer label free, low cost, non-invasive, non-destructive, and high throughput screening and detection. However current Impedance-based techniques have a limited functionality as discussed in the previous section and elaborated in section 1.7.

The lack of a spectroscopic, automated, space resolved, time resolved, impedance monitoring system for cell-substrate interactions is the main motivation of this research. We aim to develop a system which will provide the aforementioned functionality. Such a system will provide a detailed account of the cell-substrate and cell-cell interactions which will in turn provide a wealth of information about the adhesion, spreading, motility and state of confluence of the cell layer. By parameterizing the cell-cell and cell-substrate impedance, information such as cell-substrate contact, cell distribution, trans-cell layer resistance, and mono- or multi- cell-layer capacitance can be obtained.

1.3 Research Objectives

The objective of this research is to demonstrate a fully automated, spatially resolved cell culture monitoring system. The specific objectives are,

a) Fabricate a multielectrode cell-substrate impedance sensor

b) Implement a switching methodology with minimal parasitics to facilitate multielectrode data acquisition

c) Perform multichannel Impedance Spectroscopic characterization of cell cultures.

d) Develop software for data acquisition, data processing, parameter extraction, and multi-plane 2D and 3D visualization.

h) Demonstrate the functionality of the aforementioned system in monitoring cell behavior in-vitro.

1.4 Dissertation Outline

The objective f this work was to develop a complete system to study cell cultures called CellMap. The first step in the development cycle of CellMap system is to gain sound understanding in the use of EIS for biological systems. This is done by performing EIS for cell substrate sensing using contemporary tools. Towards this end, Impedance Spectroscopic analysis of OvCa429 ovarian cancer cell cultures was performed using an Electrical Cell Substrate Sensing (ECIS) well plate (8W1E), which is one of the most widely used culture wells for cell substrate measurements. This provided the understanding on identification and interpretation of various components of the impedance Spectra including interfacial, physiological, and high frequency device characteristics (Chapter 4).

In chapter 5, the effect of electrode geometry on the impedance measurements of four different types of analytes is studied. The analytes used are a) simple binary electrolyte (KCl), b) a highly viscous conductive gel (Spectra 360™), c) OVCA429 ovarian cancer cell cultures and d) excised human skin tissue. Impedance measurements of these analytes were performed on an array of electrode sizes ranging from 50 μm to 500 μm. This study provides important understanding of the effect of electrode area and analyte morphology on impedance measurements. Insight is also gained into the effect of aforementioned quantities on current distribution effects.

With this understanding, a planar fabricated 8-electrode radial array with an out-of-plane counter electrode was designed and fabricated. The sensor is illustrated in Figure 1. The eight electrode radial configuration is inspired by the electrical impedance tomography technique which aims to reconstruct the impedance image of an object encircled by the electrode array. In the present case, a 2D impedance map will be constructed during the period of cell adhesion and growth and confluence. The outputs of this device are color-mapped time varying impedance images and quantitative markers which reveal a) rate of cell growth, b) time to confluence, c) cell density and uniformity, d) properties of tight-junctions, and e) Trans-monolayer properties.

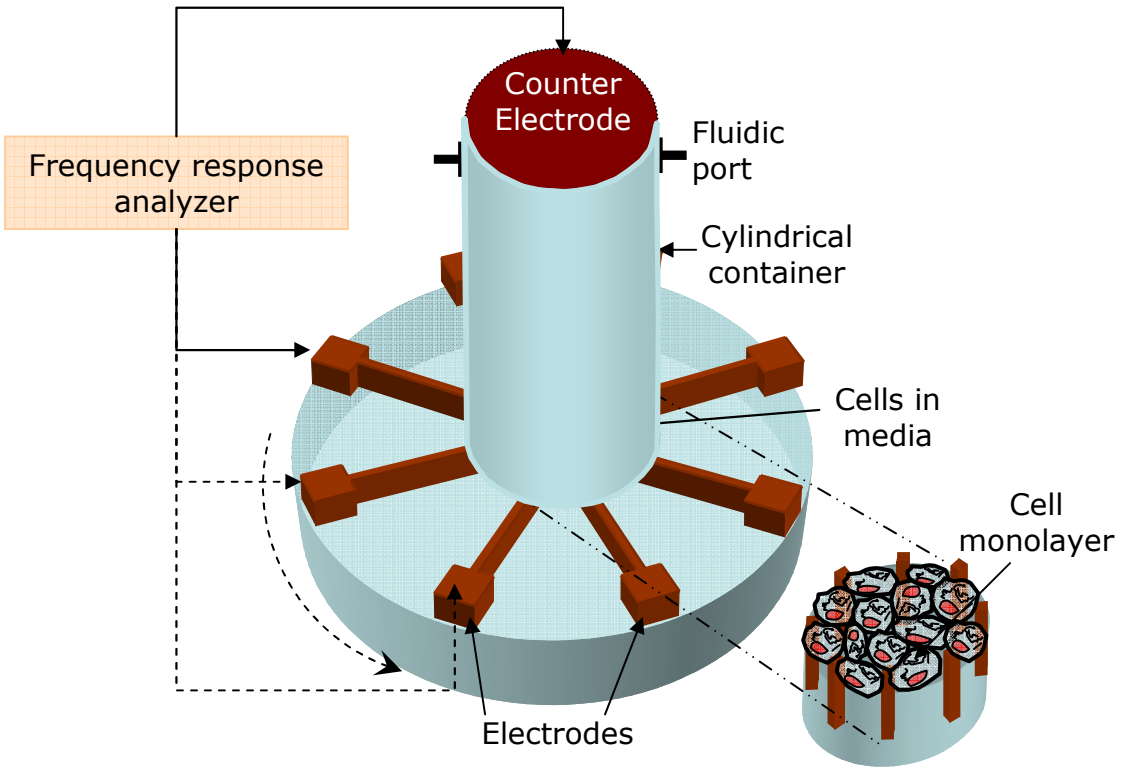

Figure 1: Illustration of the proposed 8-electrode CellMap device.

Cells are cultured in a cloning cylinder attached to the substrate. Impedance is measured across all the electrode pairs at set frequency points. The impedance data is then processed through software routines to create superimposed image of impedance from all electrode pairs in a single scan. A collection of such data from a single sweep is termed as a "frame". Based on data from consecutive frames, information such as cell adhesion, spreading and motility can be extracted.

Chapter 2: Analysis of Cellular Systems

2.1 Introduction

Cells are the building blocks of organisms. In multicellular organisms such as humans, cells are grouped into various types, which posses' unique morphology and function, exemplified by the various organs in the human body. Consequently, diseases manifest at different levels of cellular organization depending upon their progression and may only affect certain cell types (ex. Breast carcinoma). Different techniques have been developed for pathological analysis at these levels. In this chapter, cellular organization and the analysis techniques applicable to different levels of cellular organization are described.

2.2 Pathological Analysis of Single Cells, Cell cultures, and Tissue

A variety of external and internal factors influence disease processes including trauma, infection, poisoning, loss of blood flow, inherited or acquired genetic damage, or developmental errors. The complex scientific field which seeks to understand the mechanisms of alterations in cells and tissues as well as the body's means of responding to these alterations through examination of organs, tissues, cells and bodily fluids is known as pathology. The branch of pathology which examines organs, tissue and cells is referred to as Anatomical pathology and the branch which examines body fluids such as urine, plasma, mucosal secretions etc., is referred to as Clinical pathology. Different forms of pathological analysis provide useful and often complementary information that help develop the understanding of a specific

physiological condition. In this chapter, various techniques in anatomical pathology will be discussed.

2.2.1 Anatomical Pathology

Anatomical pathology is concerned with the diagnosis of disease based on the gross, microscopic, and molecular examination of organs, tissues, and cells. Based on the type of examination (gross, microscopic or molecular) and the level of cellular organization (organ, tissue, cellular or sub-cellular), anatomical pathology is further classified as Autopsy, biopsy, surgical pathology, cytopathology and molecular pathology.

a) Autopsy

Autopsy is the broader examination of the organism as a whole, post-mortem. Autopsies serve two major purposes. They are performed to gain insight into pathological processes and determine what factors contributed to the organism's death. Besides gross macroscopic examination of the organism, autopsies also involve some aspect of tissue and clinical pathology, wherein histological examination and microbiological analysis are performed.

b) Biopsy

A biopsy is a procedure performed to remove tissue or cells from the body for examination under a microscope. Biopsies are usually performed to determine whether a tumor is malignant (cancerous) or to determine the cause of an unexplained infection or inflammation. Biopsy is often the beginning point in many types of pathological analysis including histopathology and cytopathology. The tissue and cells required for biopsy can be acquired in a number of ways depending upon the location of the target tissue. For example, intestinal tissue is acquired with the help of a forceps enabled endoscope, where as cervical cell examination is performed by scraping the area. The types of biopsies and their interpretation are discussed in [13]

c) Surgical Pathology

Surgical pathology involves the gross and microscopic examination of surgical tissue specimens to diagnose a disease or to determine a treatment plan. Surgical pathology includes both the physical examination of the tissue with the naked eye, as well as examining processed tissue under a microscope. A common method of examining surgical specimens is histology which along with other pathological techniques is described in the pathological techniques section.

d) Cytopathology

Diagnosis of diseases based on examination of individual cells and small clusters of cells, is known as cytology or cytopathology. Cytology involves microscopic examination of whole, individual cells obtained from smears or fine needle aspirates. It is used extensively to diagnose cancer. It is also used in screening for fetal abnormalities and in diagnosing infectious organisms. The cells to be examined may be obtained by: scraping the tissue surface, body fluids and fine-needle aspirations.

Cytological analysis includes the study of cellular physiological properties, structure, and intracellular organelles. The study the cells' interactions with their environment, proliferation, division and death are also part of cytological analysis. Cytological examination can be performed at both microscopic and molecular level.

e) Molecular Pathology

Molecular pathology focuses on the use of nucleic acid-based techniques such as DNA sequencing, fluorescent in-situ hybridization, reverse-transcriptase polymerase chain reaction, and nucleic acid microarrays for specialized studies of disease in tissues and cells. Molecular pathology shares some aspects of practice with both anatomic and clinical pathology, and is sometimes considered a "crossover" discipline.

2.2.2 Pathological Techniques

a) Histopathology

Histology or Histopathology refers to the microscopic examination of tissue structure in order to study the manifestations of disease. Histopathology is the most important tool in anatomical pathology in routine clinical diagnosis of cancer and other diseases.

Histological examination of tissues starts with surgery, biopsy or autopsy followed by several steps of sample preparation and staining as briefly listed: Fixation, processing, embedding, sectioning, and staining. First, the sample is mechanically and biochemically stabilized in Phosphate buffer saline (PBS) in a process called fixation, followed by a dehydration, cleaning and waxing procedure, collectively termed as processing. During processing, the sample is immersed in a series of baths containing ethanol, xylene and molten wax in a procedure lasting 12-16 hours. After embedding the tissue in hard paraffin block, the tissue is sectioned into thin slices approximately 2-8 μm thick, which are then placed on glass slides for staining. Staining is performed to give contrast to the tissue being examined.

Staining is an important procedure in histopathology. Staining provides the necessary contrast between cellular morphological features for microscopic examination. Hematoxylin and eosin are the most commonly used stains in histopathology. Hematoxylin colors nuclei blue, eosin colors the cytoplasm pink. Several other types of dyes exist for special examinations of the histological samples [14], [15].

b) Histochemistry and Immunhistochemistry

Immunohistochemistry (IHC) refers to the process of localizing proteins in cells of a tissue section exploiting the principle of antibodies binding specifically to antigens in biological tissues [16]. Each type of antibody recognizes and attaches to specific antigen. Certain types of normal cells and diseased cells contain unique antigens, which can be recognized by specific

antibodies. Cells containing a specific antigen will attract a specific antibody. The sample is then chemically stained to determine the extent of antibody binding. Immunohistochemical staining is widely used in the diagnosis and treatment of cancer. Specific molecular markers are characteristic of particular cancer types. IHC is also widely used in basic research to understand the distribution and localization of biomarkers in different parts of a tissue.

Visualizing an antibody-antigen interaction can be accomplished in a number of ways. In the most common instance, an antibody is conjugated to an enzyme, such as peroxidase, that can catalyze a color-producing reaction. Alternatively, the antibody can also be tagged to a fluorophore. The latter method is of great use in confocal laser scanning microscopy, which is highly sensitive and can also be used to visualize interactions between multiple proteins. Other techniques such as cyclic voltammetry have also been used in the detection and quantification of biochemical reactions.

c) Electron Microscopy

Electron microscopes have much higher magnification and resolving power than a light microscope. Consequently, electron microscopes facilitate a more detailed examination of sub cellular structures. Sample preparation for electron microscopy requires several processing steps such as cryofixation, dehydration, embedding and staining. There are four major types of electron microscopes namely, Scanning Electron Microscope (SEM), Transmission Electron Microscope (TEM), Reflection Electron Microscope (REM) and Scanning Transmission Electron Microscope (STEM).

d) Nucleic acid based techniques

Nucleic acids are found in all cells and viruses. Deoxyribonucleic acid (DNA) is the fundamental hereditary material. It stores and preserves the genetic information that determines the physical characteristics and various functions of living organisms. Ribonucleic acid (RNA) is involved in the transcription

and translation of DNA for the synthesis of proteins. Nucleic acid testing is useful in classifying leukemia's and in finding remnant leukemia cells after treatment.

A widely used nucleic acid based technique is the Polymerase Chain Reaction (PCR). PCR is used to amplify specific regions of a DNA strand, which facilitate detection of small quantities of analyte. The PCR procedure involves disruption of cell wall to release cytoplasmic material, from which the DNA is extracted. The DNA is then processed through a series of temperature cycles to achieve the required amplification.

Several other nucleic acid based techniques have been developed in recent years for applications ranging from genetic finger printing to diagnosis of infectious and hereditary diseases. A classification of nucleic acid based techniques and recent developments in the field can be found in

e) Flow Cytometry

Flow cytometry is a technique for counting, examining, and sorting microscopic particles suspended in a stream of fluid. It allows simultaneous multiparametric analysis of the physical and/or chemical characteristics of single cells flowing through an optical and/or electronic detection apparatus.

The tissue sample is broken up into single cells and held in a test tube, which is placed into the flow cytometer. The liquid containing the cells is drawn up from the test tube and pumped into the flow chamber. A small laser beam of very bright light illuminates the cells as they pass through the flow chamber. Small angle scattering is known as forward scatter and large angle scattering is known as side scatter. Each type of cell has a unique combination of forward and side scatter. The scattered light is detected by a light detector and color detectors and processed through a computer.

f) Electrical techniques for anatomical characterization

The use of electrical signals for probing biological objects has long been in use in a variety of applications ranging from neural probes to patch clamps. Electrical techniques provide a quantitative, direct, label free alternative to microscopy and biochemical methods, many of which are qualitative and indirect. Commonly used electrical techniques for cellular probing are listed as follows

The Patch-Clamp Technique

The cell membrane is a semipermeable bilipid membrane common to all living cells. The cell membrane physically separates the intracellular components from the extracellular environment. The membrane is selectively permeable and regulates the transport of material between intra and extra cellular environments. This is accomplished by integral proteins known as ion channels. The ion channel activity can be monitored by the patch clamp technique.

A glass pipette with an opening of the order of a few microns is used to form a tight seal around the ion channel by using suction. Once a good seal is established, an extracellular voltage is applied to the cell and its response to stimulus measured by recording the change in ion channel activity.

Voltammetry

In voltrammetry, the potential applied to the electrochemical cell is varied from a lower limit to upper limit. Specific electrochemical reactions occurring in the cell are characterized by a voltage peak at a particular voltage. The cycle is repeated for various voltage scan rates to determine reaction rate limiting phenomenon. Besides cyclic voltammetry which is the most commonly used, several other types such as pulsed, linear and sine wave voltammetry are also in use.

Voltammetry is an invasive technique in which the electrochemical system is sufficiently deviated from its equilibrium potential. This method frequently requires the use of another detection modality to validate the presence of reaction byproducts. The use of voltammetry in monitoring living systems is complicated by the difficulty in establishing the non-interference of applied signal with the system under investigation.

Electrical Impedance based physiological monitoring

Electrical impedance is a non-invasive, quantitative, label free and real-time physiological monitoring modality. Unlike voltammetry, the applied signal is smaller than the thermal noise at room temperature (< 25 mV), which makes this modality non-invasive and non-destructive. In contrast to fluorescence microscopy and biochemical methods, no labels or reporters are required for impedance monitoring. Since the measured output is the opposition to the flow of electrical current, it is quantitative. Owing to its advantages over other techniques and the emergence of convenient impedance measurement equipment, the impedance technique has gained importance in physiological investigations.

Classical works in the field of bioimpedance were contributed by Kenneth Cole, Peter Debye, Robert Cole and Herman Schwann. The works of Kenneth Cole included investigation of electrical impedance of squid axon [17], and dielectric dispersion of spheres [18] , among others. Herman Schwan contributed to the understanding of electrical characterization of tissues [19] and electrode polarization [20], among several other major contributions to the field of bioimpedance. Much of the early bioimpedance work is summarized in the review by McAdams and Jossinet [21].

In summarizing the review of various pathological techniques, it can be stated that various techniques provide diverse and often complementary information about the state of the sample. Histological and biochemical analysis provide information at the cellular and multicellular level whereas

nucleic acid based techniques provide information at the sub-cellular level. Many of the aforementioned techniques terminate the cell cycle at a predetermined time period and record the physiological end state. A non-destructive technique that can provide real-time information on cellular activity is highly desirable as it can provide a wealth of information about the biophysics and biochemistry of cells.

The study of cell cycle processes such as adhesion, spreading, division and death is accomplished by the use of "cell-based" or "whole cell" assays. "Cell-based" assays. Cell based assays often use anchorage dependent cells which are cultured invitro. Majority of live cell imaging techniques are optical microscopy based which use fluorescent markers to identify various cellular processes. As labeling involves chemical treatment sample, the effect of label itself on the analyte is unknown. Moreover, optical methods provide a qualitative analysis of cellular processes. Impedance based real-time cellular monitoring on the other hand facilitates quantitative, label free real-time cellular monitoring. Impedance based cellular monitoring is

Prior to introducing impedance based cellular monitoring it is useful to review the activities of living cells invitro. These activities are the subject of investigation by live cell sensors. The following section reviews some important aspects of invitro cell behavior.

2.3 Theory of Cell-Cell and Cell-Substrate Interactions

Biological cell cultures are colonies of living cells that have long been utilized to gain fundamental understanding of various physiological mechanisms of complex organisms [22-24]. These colonies are dynamic environments where processes responsible for proper function or dysfunction of the organism occur. Thus, it is of interest to understand the fundamental aspects of cell's interaction with its environment and with other cells.

Most mammalian cell types are anchorage dependent [25] cells that require a favorable substrate to grow and multiply. Cell culture based impedance

measurement systems often study anchorage dependent cells. A typical two electrode impedance measurement system consists of a small working electrode and a large counter electrode. The counter electrode is designed to be approximately 100 times the area of the working electrode to discount its contribution to the overall impedance [26]. In the absence of cells, the impedance of this system comprises of the electrochemical interfacial capacitance and the solution resistance, explained in chapter 2. This interfacial impedance is considerably modified due to the presence of anchorage dependent cells.

The study of cell's interaction with its environment has improved with the advent of Microtechnology. Microtechnology provides an interface of comparable dimension to that of an individual cell, which improves spatial resolution in the study of cellular processes. Microelectrode based devices have been applied in impedance-based [27-29] and electrochemical [30, 31] characterization of cell cultures. Several other electrophysiological manipulations of cells such as electro-fusion [32] and electroporation [33] have also been reported.

Microelectrode based devices offer many advantages such as spatial resolution, small signal, batch fabrication, and portability. In microbiological and cell culture studies, the spatial resolution of microelectrodes offers the ability to investigate a single cell [34], [35] or a group of cells [36], [37]. Literature in this subject is vast despite the relatively recent nature of Micro-Electro-Mechanical Systems (MEMS), reflecting the rapid strides in this field of research [38].

Although cell-substrate studies are capable of detecting micromotion of cells [39], the observed impedance changes are an averaged effect of cellular motion over a large electrode area (compared to the cellular dimensions of approximately 30 μm). Moreover, the parameter describing the cell micromotion is non-specific. For example, due to the cell's close approach to

the interface, the electrical double layer capacitance is modified (section 3.7.2), this is a specific quantifier because it refers to a particular aspect of cell-substrate interface. The existing methods quantify the cell-substrate interaction in terms of normalized resistance [40] or a cell index [9] (non-specific quantifiers), not in terms of changes in interfacial capacitance or cell-junctional resistance (specific quantifiers). With currently available impedance-based cell-substrate sensing methods, it is not possible to predict the directionality of cell growth and the cell density distribution, which are important indicators of "orderliness" of growth which in turn is an important distinction between normal and cancer cells [41, 42].

In the following sections the relevant biological concepts in cell adhesion, spreading and motility are introduced. The intent is to familiarize the reader with the terminology and basic concepts. References are provided for in-depth coverage of these topics.

2.3.1 In-vitro Cell Kinetics

The cell is the structural and functional unit of all living organisms, and is sometimes called the "building block of life." A whole cell is the smallest biological entity which is self-sustaining. Millions of cells come together to form organs and tissues, which collectively form the organism. Diseases often manifest at the cellular level, even if they are asymptomatic to the organism as a whole. The science of understanding abnormalities at the cellular level is referred to as cellular pathology.

Cells are highly dynamic: they crawl, change shape and divide. In many critical biological processes, cells both exert and respond to forces in their surroundings; the mechanical properties of the cell are intimately related to this behavior. They also continually remodel their internal structure and thereby change their mechanical properties. An integrated understanding of cell structure and mechanics is thus essential for elucidating many fundamental aspects of cell behavior, from motility to differentiation and

development. A variety of experimental techniques show that cells have both elastic and viscous characteristics, and thus are viscoelastic materials [43] .

Despite constituting a simplistic simulation of the organism's inner workings, cell culture has become an essential tool in cell and molecular biology as well as in applied biotechnology. Cell culture systems inherently lack the three-dimensional, multicellular architecture found in an organism's tissue but offer precious advantages over whole-animal (in vivo) experimentation. The parameters necessary for cell function can be isolated without interference from more complex, whole-organism or whole-organ responses. Animal care expenses, human labor costs and animal suffering are reduced because many experimental conditions can be tested with the cells from only one sacrificed animal, or a small portion of one. The cells are distributed in a thin layer; therefore, optical observation under a microscope is unobstructed by other cell layers. With cell lines, the researcher effectively circumvents the time necessary to raise the animal and its very sacrifice [44].

The phenomenon of cell adhesion is involved in most physiological cell functions, including survival, proliferation, differentiation, migration or activation, as well as pathological situations such as metastasis formation, tissue invasion by pathogens, atherosclerosis, inflammation, or host-biomaterial interaction. Cell behavior is frequently dependent on deformability. Thus, a cell cannot form durable attachments with a surface without undergoing micrometer-scale deformation to form an extensive interaction zone allowing molecular contact. This deformation can be obtained with either passive or active mechanisms.

The processes of cell adhesion, spreading and motility are dependent on an intricate network of macromolecules known as the extracellular matrix. The make-up of extracellular matrix and its function in cell physiology is described in the following section.

a) The Extracellular Matrix

Most of the cells in multicellular organisms are surrounded by a complex mixture of nonliving material that makes up the extracellular matrix (ECM). In some cases, the ECM accounts for more of the organism's bulk than its cells. The ECM is often referred to as the connective tissue, which is composed of 3 major classes of biomolecules: a) Structural proteins (collagen and elastin), b) Specialized proteins (e.g. fibrillin, fibronectin, and laminin), c) Proteoglycans. Proteoglycans are composed of a protein core to which are attached long chains of glycosaminoglycans (GAGs) forming extremely complex high molecular weight components of the ECM [45].

Control of cell shape by ECM is critical for regulation of cell growth, differentiation, cell polarity, and tissue pattern. ECM regulates cell and tissue morphogenesis by altering the structure of the intracellular cytoskeleton (CSK) which, in turn, serves to orient much of the cell's metabolic machinery [46]. Most normal vertebrate cells cannot survive unless they are anchored to the extracellular matrix. This anchorage dependence is often lost when a cell become cancerous. HeLa cells, for example, are among the few types of vertebrate cell that can be grown in liquid culture.

Cells attach to the ECM by means of transmembrane glycoproteins called integrins. The extracellular portion of integrins binds to various types of ECM proteins: collagens, laminins and fibronectin. The intracellular portion binds to the actin filaments of the cytoskeleton [47].

b) Focal Adhesion

Many cells grown in tissue culture adhere tightly to the underlying substrate through discrete regions of the plasma membrane, referred to as focal adhesions. In these regions where the surface of the cell comes closest to the substrate, the plasma membrane is specialized at its cytoplasmic face for anchoring stress fibers, the large bundles of microfilaments that are prominent in many cultured cells. A large group of cells, including fibroblasts,

epithelial cells, endothelial cells, and platelets, form focal adhesions when plated onto appropriate substrates.

Several factors affect focal adhesions including tumor promoters, hormones and growth factors, and viral transformations. Commonly used techniques to monitor focal adhesions include, electron microscopy and Interference reflection microscopy [48].

c) The cell Junctions

In many animal tissues (e.g., connective tissue), each cell is separated from the next by an extracellular coating or matrix. However, in some tissues (e.g., epithelia), the plasma membranes of adjacent cells are pressed together. Four kinds of junctions occur in vertebrates: Tight junctions, Adherens junctions, Gap junctions and Desmosomes.

Tight Junctions

Epithelia are sheets of cells that provide the interface between cell masses and a cavity or space. The portion of the cell exposed to the lumen is called its apical surface. The rest of the cell make up the basolateral surface. Tight junctions seal adjacent epithelial cells in a narrow band just beneath their apical surface. Tight junctions perform two vital functions: a) they prevent the passage of molecules and ions through the space between cells. So materials must actually enter the cells (by diffusion or active transport) in order to pass through the tissue. This pathway provides control over what substances are allowed through. b) they block the movement of integral membrane proteins between the apical and basolateral surfaces of the cell.

Adherens Junctions

Adherens junctions provide strong mechanical attachments between adjacent cells. They hold cardiac muscle cells tightly together as the heart expands and contracts. They also hold epithelial cells together. They seem to be

responsible for contact inhibition. Some adherens junctions are present in narrow bands connecting adjacent cells. Others are present in discrete patches holding the cells together. Adherens junctions are built from cadherins — transmembrane proteins and catenins.

Gap Junctions

Gap junctions are intercellular channels about 1.5–2 nm in diameter. These permit the free passage of ions and small molecules (up to a molecular weight of about 1000 daltons) between the cells. They are cylinders constructed from 6 copies of transmembrane proteins called connexins. Because ions can flow through them, gap junctions permit changes in membrane potential to pass from cell to cell.

Desmosomes

Desmosomes are localized patches that hold two cells tightly together. They are common in epithelia (e.g., the skin). Desmosomes are attached to intermediate filaments of keratin in the cytoplasm. Carcinomas are cancers of epithelia. However, the cells of carcinomas no longer have desmosomes. This may account for their ability to metastasize. Hemidesmosomes are similar to desmosomes but attach epithelial cells to the basal lamina ("basement membrane") instead of to each other [49].

Several methods exist for characterization of cell-substrate interaction in vitro. These methods are listed and discussed in the following section.

2.4 Cell Substrate Sensing Technologies

The significance of cell-substrate interactions was discussed in the previous section. In this section, contemporary methods in cell-substrate investigations are examined. Generally, the methods employed to study cell-substrate interaction can be classified into three major categories and several subcategories as listed below

The aforementioned techniques can be broadly classified as either label and reporter based or label free. Label and reporter based technologies require elaborate sample preparation, pre- and post-treatment. Label free technologies are preferred due to their non-invasiveness and non-interference with biological functions.

The most widely used method for assessing and quantifying cell adhesion and spreading is to seed the cells onto the surface and allow the cells to adhere and spread for a length of time. The unbound cells are then washed away in a buffer solution. The attached cells are labeled with a fluorescent reagent and viewed in an inverted or confocal microscope. Alternatively the cells can be stained and counted using light microscopy. The cells can also be prelabeled with a fluorescent dye. After washing the unbound cells, the bound cells are quantified using a plate reader. An additional method for assessing the role of adhesion proteins is to coat the surface with antibodies or peptides that are specific for various receptors and then seed the cells that are expressing the appropriate receptors. The interaction of the receptor on the cell surface with the antibody or peptide can then be detected using one of the aforementioned methods.

The assays described above are known as endpoint assays. They provide one time information about the cell system at the end of an observation point [50]. They require pre-labeling, post-labeling, fixation and permeabilization. Additionally, the peptides, dyes or proteins introduced for signal transduction may interfere with the biological function and add background noise to the data. Alternatively, Electrical Impedance-based techniques offer several advantages such as a) non-invasive, b) non-destructive, c) label free, d) real-time and e) dynamic monitoring of cell culture systems.

Electrical Impedance-based cell substrate sensing is fast emerging as a viable and reliable technique for investigating cell substrate interactions. In

the following section we review the current state of the art in commercial and non-commercial (research) impedance-based cell-substrate sensors.

2.5 Impedance-Based "Whole Cell" Biosensors

The terms "whole cell biosensors" and "cell-based biosensors" have been used to refer to devices that characterize the attachment and spreading of anchorage dependent cells on a substrate and the changes therein due to environmental variables as well as variables such as the effects of virus, bacteria and pharmaceutical agents [51], [52]. The tracking of cell attachment and motility plays an important role in cell biology to elucidate biological phenomena such as cell division, tumor invasion/metastasis, and embryonic cell migration/sorting [53].

Impedance-based whole cell biosensors can detect morphological and physico-chemical changes. A simple Impedemetric sensor consists of a two planar electrode arrangement on which cells are grown. Impedance is either continually monitored or a single impedance recording is made when cell confluence is reached. In continuous monitoring of cell culture events, the following information is available: 1) cell motion, 2) attachment and spreading, 3) mitosis, 4) confluence and 5) apoptosis. In addition, if impedance recordings are made over a broad frequency range (few Hz to several hundred MHz), specific dielectric characteristics of cells and their interfaces due to polarization, interfacial effects, and dipole rotations can be detected [54]. At even higher frequencies the dispersion characteristics of biological microstructures can be observed [55].

A variety of impedance-based measurements have been recorded in-vitro on cell cultures using microelectrodes [56]. An impedance recording of cell cultures and tissues falls into two categories, namely, 1) Differential Impedance and 2) Absolute Impedance. In differential recording, a blank or control sample is measured and compared with the impedance (or part of it) of the analyte [57]. For example, a control could be a medium in which

bacteria are grown and analyte could be medium containing bacteria. In this approach, the absolute electrical properties are unknown and only their deviations act as markers for variability. In the second category, absolute electrical properties of cells are recorded, with the view of characterizing a particular type of cell in terms of its electrical characteristics such as complex conductivity and permittivity [58].

Most microelectrode devices reported in literature are of the first category. The reasons for that are two fold. Firstly, most microelectrode devices are planar, and in such geometries it is difficult to define the low frequency current paths and hence the cell constant of the measurement cell, in the presence of biological cell layer. Secondly, interfacial polarization is dominant in microelectrode devices. Interfacial polarization is the result of electrostatic interaction of a metal and its immediate surrounding electrolytic environment. In two electrode measurements of electrode electrolyte interface, the electrode polarization in the form of double layer capacitance dominates the low frequency impedance spectrum due to the inverse relationship between electrode area and impedance. When cells are present in the vicinity of the electrodes, they alter the interfacial capacitance, which is detected by the change in impedance.

In multielectrode system, several small area counter electrodes are spread across the culture space with a common counter electrode. This system may provide information such as cell density distribution, directional motility and cell clustering. However, the advantages of multielectrode mapping are offset by the data handling and analysis complexity, where tasks such as data fitting have to be repeated as many times as the number of electrodes. Another hurdle in multielectrode recordings is the arrangement of electrodes and their connecting leads, which could contribute parasitics, especially at higher frequencies, if not compensated individually.

2.6 State of the Art in Multi-Electrode Impedance Sensors

Impedance techniques have been used to study organs in the body [Dijkstra, et al., 1993], explanted neural tissues [Cole and Curtis, 1939; Hodgkin and Huxley, 1952], whole blood and erythrocytes [Fricke and Morse, 1926; Fricke and Curtis, 1935], cultured cell suspensions [Schwan, 1957], bacterial growth monitoring [Hause, et al., 1981], and anchorage dependent cell cultures [Giaever and Keese, 1984]. While all but the latter are not directly related to this research, there is a great deal of relevant information regarding the characteristics of biological material to be obtained from those studies.

a) Electrical Cell Substrate Impedance Sensing (ECIS), Applied Biophysics Inc, NY

The pioneering work of Ivar Giaever and Charles keese has led to many applications of Electrical Cell Substrate Impedance Sensing (ECIS) as a viable tool for physiological analysis [59-61]. ECIS is a two electrode impedance measurement system, consisting of a 250 μm diameter working electrode (WE) and a large counter electrode (CE). A 1 μA current perturbation is applied between the electrodes and the resulting complex voltage is measured across the same electrode pair [40]. The resulting impedance is a space averaged quantity over the area of the WE. The design of ECIS makes discrimination between evenly and unevenly distributed cell layer difficult. The in-plane arrangement of working WE and CE creates uncertainty in the current paths in the presence of a cell layer, thereby making it difficult to define cell layer properties. The output of the ECIS system is a time versus normalized resistance plot, where normalized resistance is the ratio of electrode resistance between the presence and absence of cells.

Figure 2 illustrates the ECIS electrodes with the measurement setup. Impedance of cell culture is recorded at a single frequency of 4 KHz. Real-time monitoring of cell layer characteristics such as cell layer capacitance and tight junctional resistance are not available in the ECIS system. The resulting

data has been fit with a few different models [62-64]. Of these, the model presented by Gode et al [62] is electrochemically relevant and fundamental. Although ECIS has been successful in detecting micromotions of mammalian cells and monitor phenomenon such a wound healing. This system does not provide real-time electrochemical parameterization of impedance data to monitor cell-substrate and cell-cell interactions. For example, in Figure 3, the interfacial capacitance is absent.

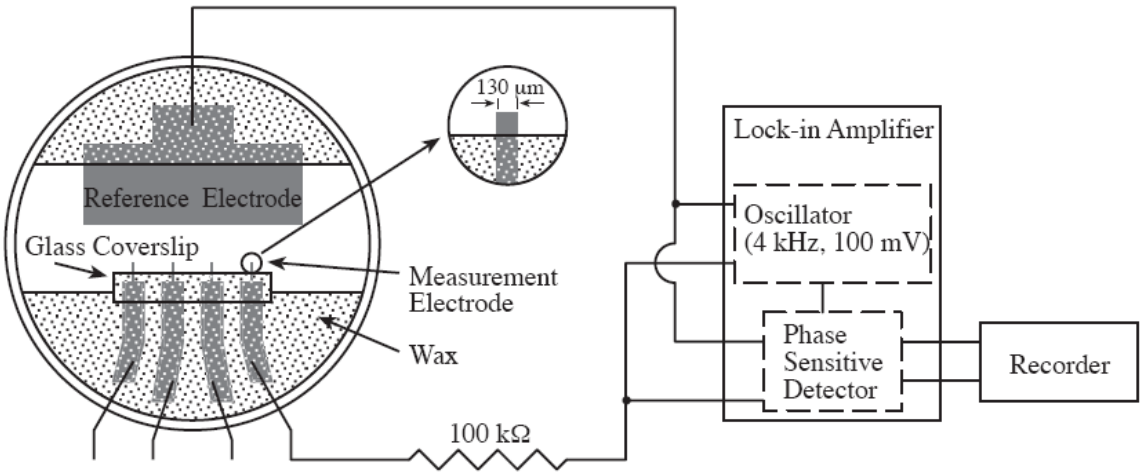

Figure 2: Illustration of the ECIS system. Source [51].

At 4 KHz, the AC signal in the linearity regime cannot fully penetrate through the interfacial capacitance. It is not clear as to whether a resistance can be used to completely represent the interfacial regime. Development of fundamental models is already underway, particularly in the works of Wegener [65], Lo [66] and Goda [62].

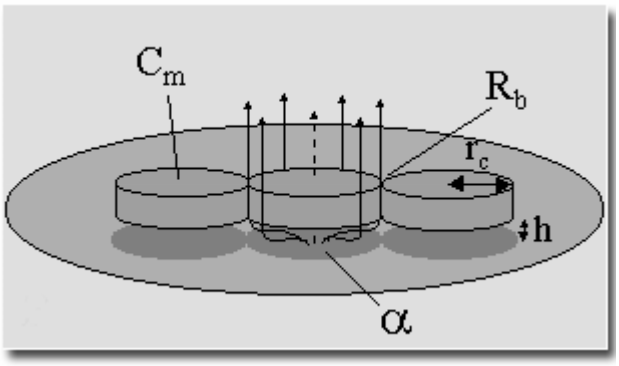

Figure 3: Model used to parameterize impedance data obtained using ECIS. Source: Biophysics.com.

In many reports of parameterization of ECIS data, the statistical estimates of the fit have not been reported. These estimates provide insight into the goodness of the fit, appropriateness of the parameters to the fit, and determination of an optimum model among several candidates, which is the recommended method for model based analysis of impedance data [67]

b) Cell-Based Biosensor, Stanford University, 2003

Borkholder [51], demonstrated a 40 electrode array sensor for characterization of the effects of pharmaceutical compounds on cell membrane. He recorded the action potentials as well as impedance of cultured cells to determine the effect of pharmaceutical compounds. The device used for this application is shown in Figure 4. Borkholder performed impedance spectroscopy to characterize the electrode and cell impedance. The applied voltage was 100 mV, well over the limit of linearity in IS, which is approximately 25 mV at room temperature [67]. Non-linear behavior was observed in the recorded data. Parameter extraction was not carried out, neither was cell spreading and motility monitored. Although impedance measurements were recorded over a range of frequencies, the results were not interpreted by electrical equivalent modeling.

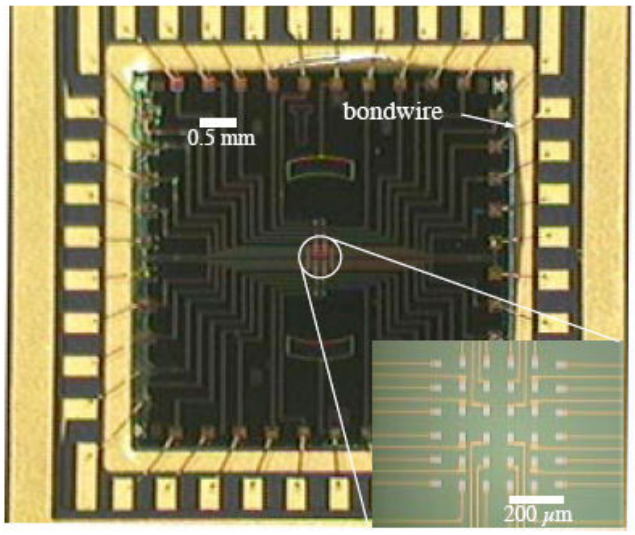

Figure 4: Multielectrode array for recording action potential and impedance of cultured cells. source: [51].

c) Impedance-based sensing of Mammalian cell colonization, Carnegie Mellon University, 2004.

Huang et al [68] developed a multielectrode impedance system for cell behavior study. They investigated two different device geometries, a) an array of devices with variable area WE with a dedicated CE and b) an array of fixed area WE with a common CE. However, no spatial mapping of cell distribution is reported in their work and the system is not automated. Moreover, the cell layer was not parameterized to determine the junctional resistance and cell layer capacitance.

Nguyen [69] reviewed several microelectrode devices to justify their work on a multielectrode device for space resolved cell growth monitoring. He noted that many of the cell-substrate interaction sensors in his review suffered from area averaging effect of the cell micro-motion and hence were not able to detect individual cell motion. To circumvent this difficulty, he fabricated the sensor set reproduced in Figure 5. However, nguyen's design has a few drawbacks. In device A, the sensing electrodes are of different sizes positioned at 4 edges of the culture area, considering the size of an average cell to be 30 μM; the spatial resolution would be poor. A 2D impedance map

of the culture area was not attempted which would provide the impedance distribution of the culture space.

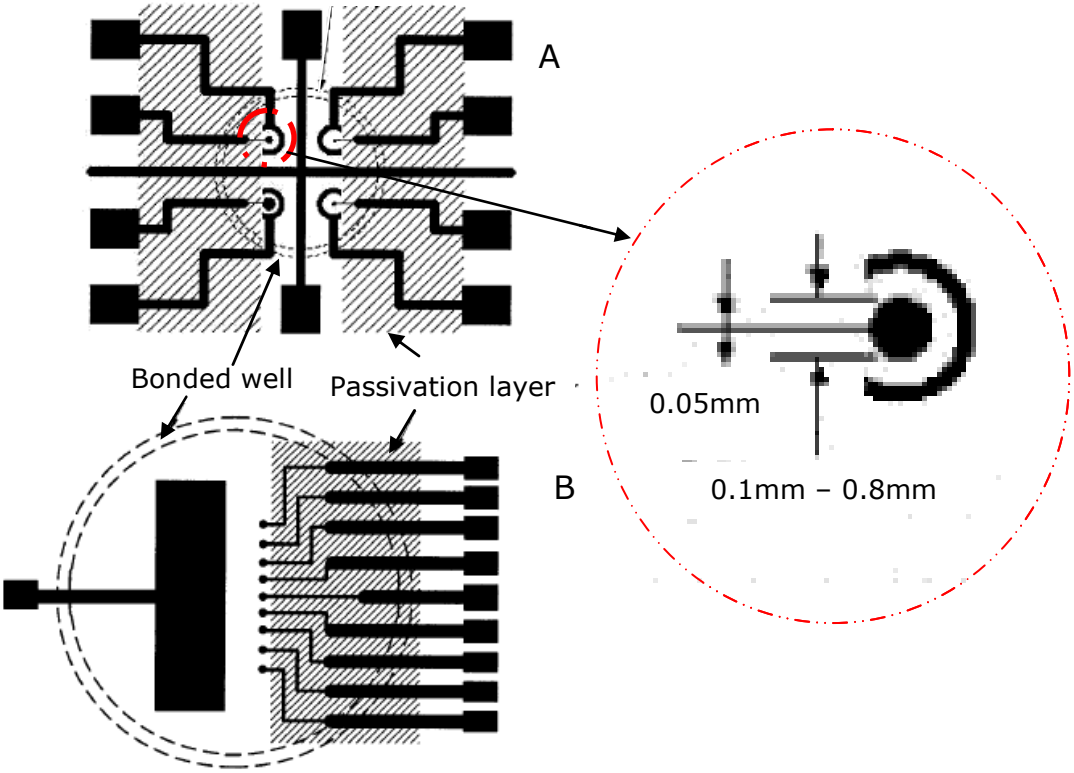

Figure 5: Multielectrode array biosensor for cell culture monitoring. Source [66].

d) Real-time Cell Electronic Sensing (RT-CES™), ACEA Biosciences Inc, San Diego

Real-Time Cellular Electronic Sensing (RT-CES™), manufactured by ACEA Biosciences, is a cell culture monitoring device based on a microelectronic cell sensor array integrated into the bottom of standard format micro-titre plates. RT-CES™ works by measuring electrical impedance across the sensors to detect the presence, absence, or change in condition of cells. For cell-based assays, cells are grown in the individual, sensor-containing wells of the micro-titre plate and placed in a standard incubator. The system can be programmed to collect data as frequently as every minute by sending nominal current through the sensors at the user defined intervals. The electronic sensors provide information on impedance values, which is then

converted to a measure known as Cell Index, CI (the impedance of the cells normalized for the impedance of the media alone) [70].

The cellular status is continuously monitored using the real-time cell electronic sensing (RT-CES™) system. Effector-mediated cytotoxicity results in target cell death which is accompanied by morphological changes such as a loss of the integrity of the actin cytoskeleton and cell rounding that is ultimately accompanied by deadhesion of the cells. All these morphological events leads to a loss of cell-substrate impedance signal over time. The integrated software is able to display entire history of the experiment from seeding the cells to termination of cytotoxicity. The time and effector-to target ratio (E/T)-dependent curves can be displayed in real-time allowing dynamic monitoring of NK cell cytotoxic activity. The RT-CES™ electrode geometry is shown in Figure 6. The output of the RT-CES™ system is shown in Figure 7.

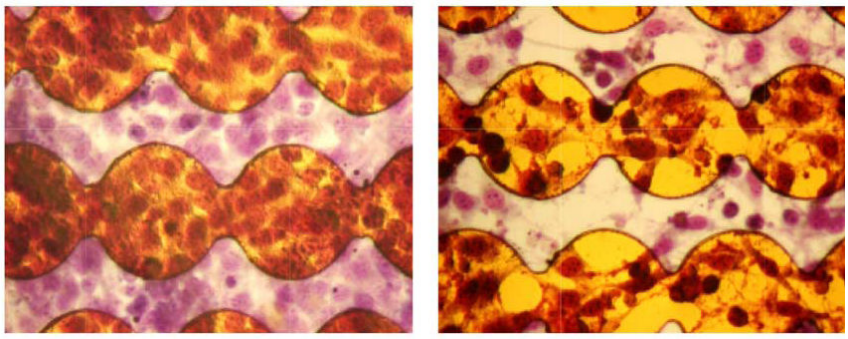

Figure 6: Electrode geometry of RT-CES™ cell-substrate sensing system. Source [71].

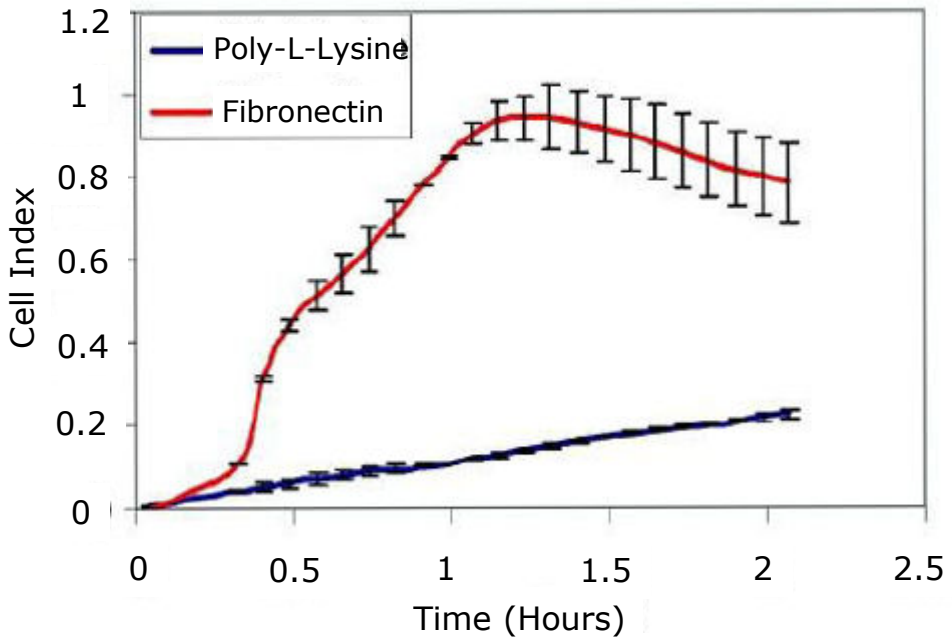

Figure 7: Output from a RT-CES™ system. Source [67].

The adhesion, spreading and confluence of cells is reflected in a quantity referred to as Cell Index (CI), given by the following expression

$$CI = \max_{i=1,..,N}\left[\frac{Rcells(f_i)}{Rb(f_i)} - 1\right] \qquad 1.1$$

where Rcells is the frequency dependent electrode resistance with the cells and Rb is the resistance without cells, and N is the number of frequency points. Thus CI is a quantitative measure of status of cells in the electrode containing well. More number of cells leads to higher CI. To quantify the lysis at specific time points, the data was exported to excel and percentage cytotoxic activity at specific E/T ratio at a given time was determined by using the following equation:

Percent cytotoxicity = (1- (CI at given E/T ratio)/(CI without NK))/100.

Similar to the output parameter of ECIS, the output of RT-CES™ is a non specific descriptor based on the aggregate of frequency response. This does

not provide insight into specific aspect of cell-substrate or cell-cell interaction; neither does it provide information about cell density distribution.

e) EVOHM and REMS, World Precision Instruments (WPI), Sarasota, FL

WPI is the world leader in Trans Endothelial Electrical Resistance (TEER) measurements. The TEER device consists of a resistance meter and a four electrode culture chamber. The current electrodes are made of silver-silver chloride. The Epithelial cells are cultured in the culture cup. The current flows from bottom electrode to top electrode, which ensures the passage of current through the cell layer. Illustration of TEER electrode measurement system is shown in Figure 8.

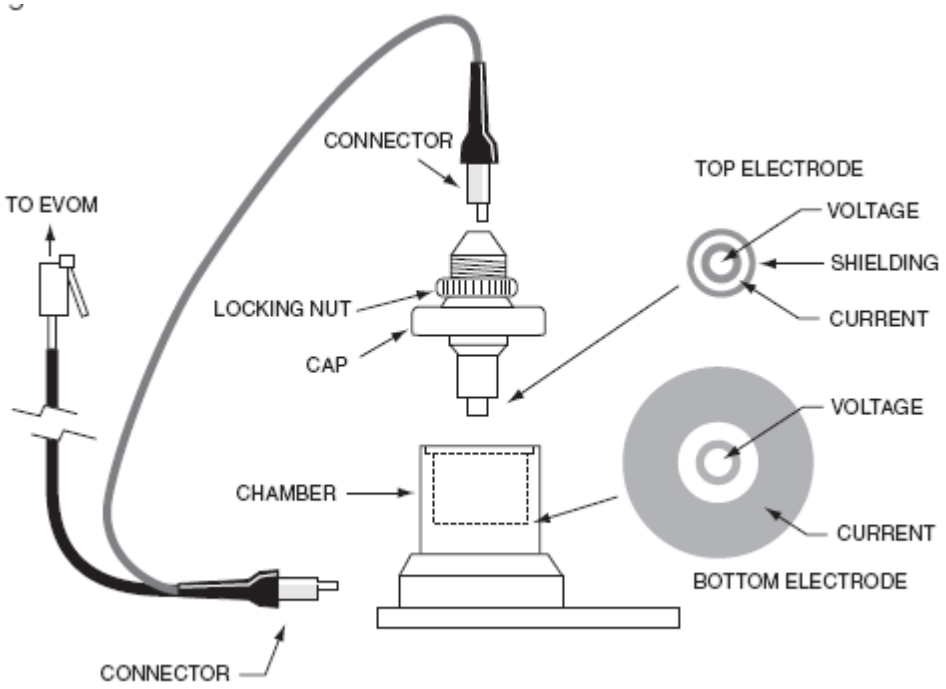

Figure 8: The EndOhm chamber for use with EVOM resistance meters.

WPI markets an automated REMS system, which measures TEER on multiple wells. The REMS AutoSampler automates measurements of electrical resistance of transepithelial, transendothelial or Caco-2 cell membranes being grown to confluence on microporous filters of high throughput

screening (HTS) 24 and 96 well microplates. It is a PC-controlled, tissue resistance measurement system that offers multiwell monitoring capability.

f) CellKey™, MDS Sciex, San Francisco, CA

MDS Sciex has recently released the CellKey™ System, which uses cellular dielectric spectroscopy (CDS) to quantitatively and kinetically measure endogenous cell surface receptor responses to ligands in live cells. Using the CellKey™ system, a series of receptor-specific, frequency-dependent impedance patterns (called CDS response profiles) resulting from changes in cellular bio impedance are collected every two seconds as spectrum of frequencies (1KHz to 10MHz). The characteristics of the CDS response profiles are used to determine the identity of the signalling pathway being activated by the receptor-ligand interaction and provide easy to access information on compound selectivity. In addition, these profiles allow quantitative pharmacological analyses such as potency and Schild analysis. Recently published work demonstrates the effectiveness of the system in profiling many endogenous ligand- induced cellular responses mediated by the three major classes of G-protein-coupled receptors, Gs, Gi, and Gq, as well as a number of protein tyrosine kinase receptors in many different cell types including primary cells7 [72].

The CellKey system uses polynomial fitting using Legendre polynomials to fit the difference between control and ligand initiated impedance data. This is an empirical, non-descriptive method of detecting biochemical changes by dielectric spectroscopy. This device suffers from the drawback that it does not provide specific details of cell-cell and cell-substrate interactions. The commercially available CellKey™ system is shown in Figure 9

Figure 9: CellKey™ system for cellular dielectric spectroscopy.

g) The CellMap system

The need for a space and time resolved cellular behavior and cell layer characterization system in a fully automated environment is addressed in the CellMap system. The CellMap system uses a commercial impedance measurement instrument, PGSTAT 30, a PCB based multielectrode device with an out-of-plane counter electrode, a switching circuit and MATLAB programming to achieve fully automated, spatially distributed impedance mapping of cell behavior and properties. The key features of this system are 1) automated impedance data acquisition 2) data analysis and visualization, and 3) automated parameter extraction. This system was employed to study the adhesion, spreading, motility, confluence and detachment of OvCa429 cells. The CellMap system is contrasted with the currently available tools for impedance -based cell-substrate interaction monitoring in the following discussion.

Table 1: Comparison of contemporary techniques available for studying cell-substrate interactions.

Device/system	Automated Impedance Parameterization	Immittance analysis	frequency Spectroscopy	3D visualization
CellMap	yes	yes	yes	yes
ECIS™	no	no	Yes	no
Nguyen	no	no	yes	no
CellKey™	no	no	no	no
EVOhm™	no	no	no	no
RT-CES™	no	no	no	no
Borkholder	no	no	yes	no

Table 1 summarizes the contemporary impedance-based cell-substrate analysis systems. In all of the aforementioned systems except CellMap, non-homogenous cell density distribution, impedance image mapping and automated cell-cell and cell-substrate parameterization have not been successfully demonstrated. The aforementioned systems provide an aggregate quantity measured over either a single frequency or a group of frequencies to represent cell-substrate interactions.

Chapter 3: Theory of Electrochemical Impedance Spectroscopy and Bioimpedance

3.1 Introduction

In this chapter, the theory of Electrochemical Impedance Spectroscopy (EIS) is presented. Impedance data and its interpretation using Bode and complex plane plots are explained with examples. The concept of bio-impedance spectroscopy is introduced and explained with emphasis on impedance of biological cell cultures. Various methods of impedance data presentation and their advantages are discussed with the help of examples. Finally, the method of electrical equivalent circuit analysis used for modeling impedance spectroscopy data is explained.

3.2 Impedance Spectroscopy

Impedance is the opposition to the flow of Alternating Current (AC) signal in the material of interest. Electrical responses of solids and electrochemical systems are complex functions of frequency. The real and imaginary components of the complex function are known as resistance and reactance respectively. The study of frequency dependence of these complex functions is known as Impedance Spectroscopy (IS).

In IS an AC sinusoidal signal is applied at a certain frequency across the sample and the resulting current (magnitude and phase) is measured. For a linear system, the applied voltage and measured current will be of the same frequency. The complex ratio of applied voltage to measured current is the impedance. When these measurements are performed over a range of

frequencies, it constitutes an Impedance Spectrum. The magnitude and phase angle of impedance spectrum contain information about the properties of the material.

IS has been applied in applications such as material characterization, corrosion, and fuel cells among others [67]. The advantages of this technique are its economy, simplicity, non-invasiveness as well as its ability to cover a wide span of time-constants which is unrivalled by other techniques [73]. In IS, frequency is the independent variable and impedance, admittance, permittivity or electric modulus, collectively known as immittance is the dependent variable.

In IS, the material or system to be characterized is connected between 2, 3 or 4 terminals of an impedance measurement instrument and impedance is recorded at different frequencies. For analysis, the magnitude and phase of impedance are plotted against the logarithm of frequency (Bode plots) and the real part of impedance is plotted against the imaginary part (complex plane impedance plot). Depending upon the type of response and prior knowledge of the material or system under test, one can arrive at plausible conclusions about the state of the material or system.

A commonly observed response is a semicircular arc in the complex impedance, admittance or permittivity plane. In corrosion of materials this could be interpreted as the electrochemical response of a corroding metal in a conductive solution, with the solution resistance given by the high frequency intercept of the semi-circle (closest to imaginary axis) and the charge transfer resistance estimated by the diameter of the semi-circle. Based on the values of these parameters, many physical quantities such as solution conductivity, exchange current density etc., can be determined. In dielectric material characterization, a semicircular arc in the complex permittivity plane ("Cole-Cole plot") can be interpreted as the dielectric relaxation of the material.

In the case of a known electrical circuit made of active or passive electrical elements, the impedance as a function of frequency can be measured or simulated. This is the forward problem. In EIS, the material or system whose properties are to be determined can be considered as a black box with two terminals. Based on the impedance spectrum of the black box, the properties of the system are to be inferred. This is the inverse problem. Electrochemical Impedance spectroscopy of solid materials, electrochemical interfaces and biological systems is an inverse problem.

For non-linear systems such as most electrode material systems, IS measurements are useful and meaningful only for small applied signals of magnitude such that the overall electrode-material system response is electrically linear. For an applied potential magnitude less than the thermal voltage, VT Ξ RT/F Ξ kT/e about 25 mV at 25 °C, it can be shown that the basic differential equations describing the response of the system become linear to an excellent approximation. Here k is the Boltzmann's constant, T the absolute temperature, e the proton charge, R the gas constant and F the faraday. For a system, where power is only dissipated, not stored, a sinusoidal input will result in sinusoidal output of same frequency and phase but lesser amplitude. For a system, where power is stored and dissipated, a sinusoidal input will result in a sinusoidal output with both amplitude and phase shift.

To understand and interpret the impedance spectrum of an unknown system (black box), familiarity with spectra of known systems is necessary. In fact, the most common method of interpreting impedance spectra of unknown systems is by approximating its behavior with that of a known system. This is known as electrical equivalent circuit modeling. In the following sections the impedance response of some simulated circuits are analyzed and compared with real-world systems.

3.3 Electrode Kinetics

3.3.1 Faradaic and Non-Faradaic Electrode Processes

Two types of processes occur at electrodes namely, faradaic and non-faradaic. In faradaic processes charges are transferred across the metal electrolyte interface. Since electron transfer reactions are governed by faraday's law, these processes are termed as Faradaic processes. If the charges transfer reaction is thermodynamically or kinetically unfavorable it will not occur. However adsorption and desorption can occur with changing potential. Such processes are termed as non-faradaic processes. Although charge does not cross the interface in non-faradaic processes, transients current are present due to the charging and discharging of the interface. Both faradaic and non-faradaic processes occur when electrode reactions take place. Hence both have to be considered while evaluating the current potential response of the system.

3.3.2 The Electrical Double Layer

Electrodes where no charge transfer occurs are termed as Ideally Polarizable Electrodes (IPE). Since charge cannot cross the IPE interface when the potential across it is changed, its behavior is analogous to that of a capacitor, with one plate of the capacitor being the metal electrode and the other plate located on the electrolyte side. The space charge layer in the vicinity of the electrode is illustrated in Figure 10.

The solution side of the double layer is made up of several layers. The closest to the electrode, the inner layer contains solvent molecules and sometimes other species that are specifically adsorbed. This layer is also called the compact, Helmholtz or stern layer. The centers of the specifically adsorbed ions constitute the Inner Helmholtz Plane (IHP). The locus of the centers of the nearest solvated ions to the metal electrode constitutes the Outer Helmholtz Plane (OHP). The solvated ions are said to be nonspecifically

adsorbed. Due to thermal agitation in the solution, the solvated ions are distributed in a three dimensional region called the diffuse layer.

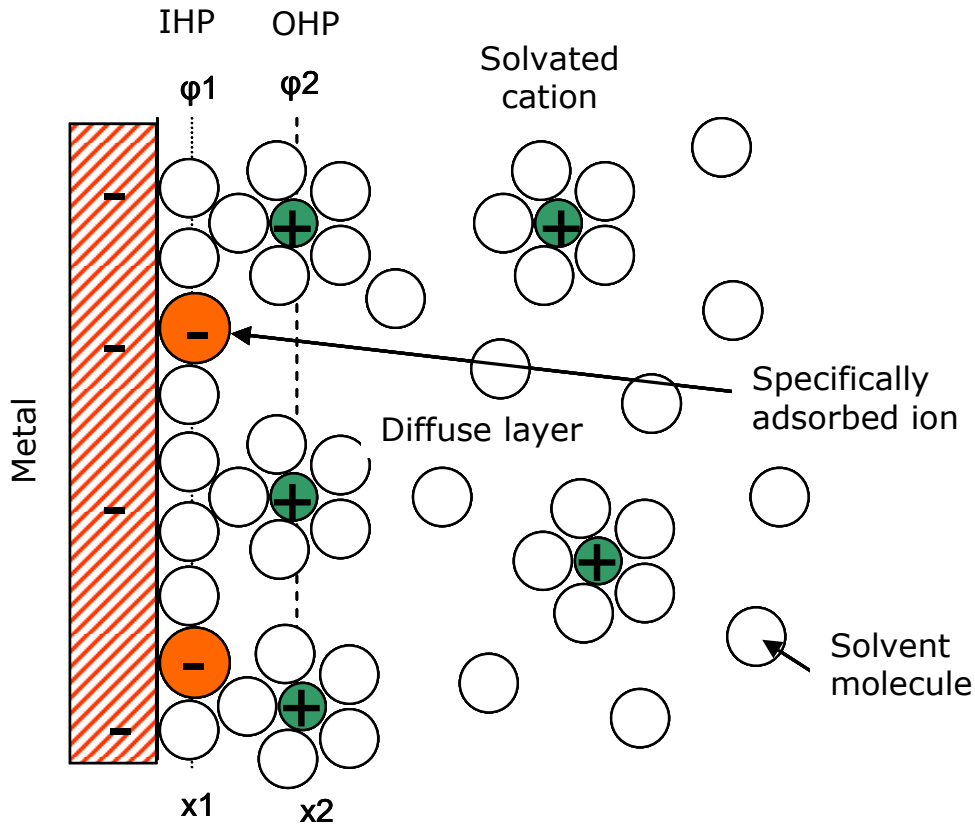

Figure 10: Ionic charge distribution in the vicinity of the electrode. IHP is the Inner Helmholtz Plane, OHP is the Outer Helmholtz Plane.

The total thickness of the diffuse layer depends on the total ionic strength of the solution. Majority of the voltage drop across the electrode-electrolyte interface occurs in the double layer. The distance from the metal electrode where the potential is 1/e times the value at metal surface is known as the Debye length, where is the proton charge. The Debye length is dependent on the ionic strength of the electrolyte. Figure 11 is the plot of variation in Debye length as a function of electrolyte concentration.

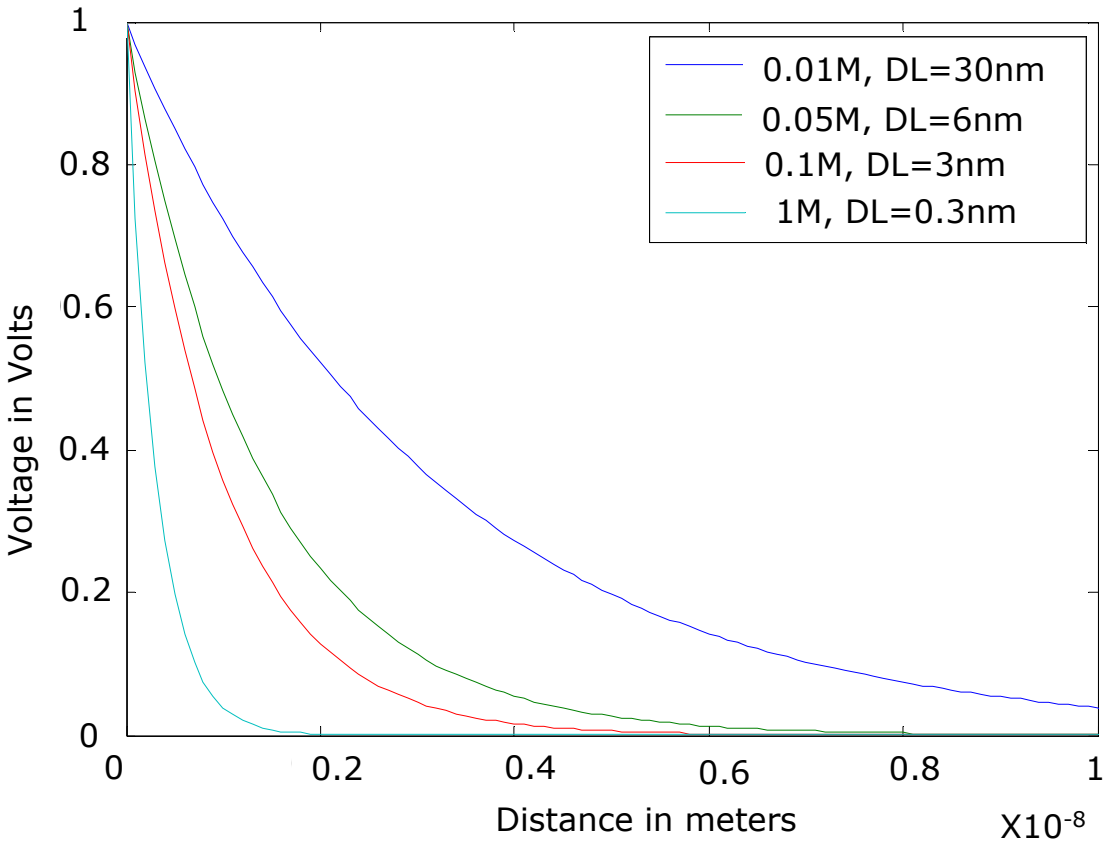

Figure 11: Debye length as a function of electrolyte concentration.

3.3.3 The Constant Phase Element (CPE)

An ideal capacitor's impedance is represented as $Z=1/j*\omega*C$; where Z is the impedance, $\omega=2*pi*f$; is the angular frequency, where f is the frequency in hertz, and C is the capacitance. In electrochemical interfaces and liquid metal inter-phase boundaries, the capacitance does not display the ideal capacitors $1/(f)^1$ dependence, but displays a $1/(f)^n$ dependence, known as power law dependence. The power factor n, accounting for deviation from ideality of capacitive behavior, could be for example due to the fractal nature of the electrode surface. Such behavior is represented by what is known as a Constant Phase Element (CPE).

The CPE is used in IS to describe several scenarios such as surface roughness, non-uniform current distribution and distribution of reaction rates,

among other processes. It is also used to model the cell-layer capacitance, which is due to a space charge distribution on either side of the membrane.

When represented in the form of a Bode diagram, the magnitude of this element exhibits a slope and the phase exhibits a constant value less than 90°, throughout the measured frequency range, hence the name Constant Phase Element (CPE).

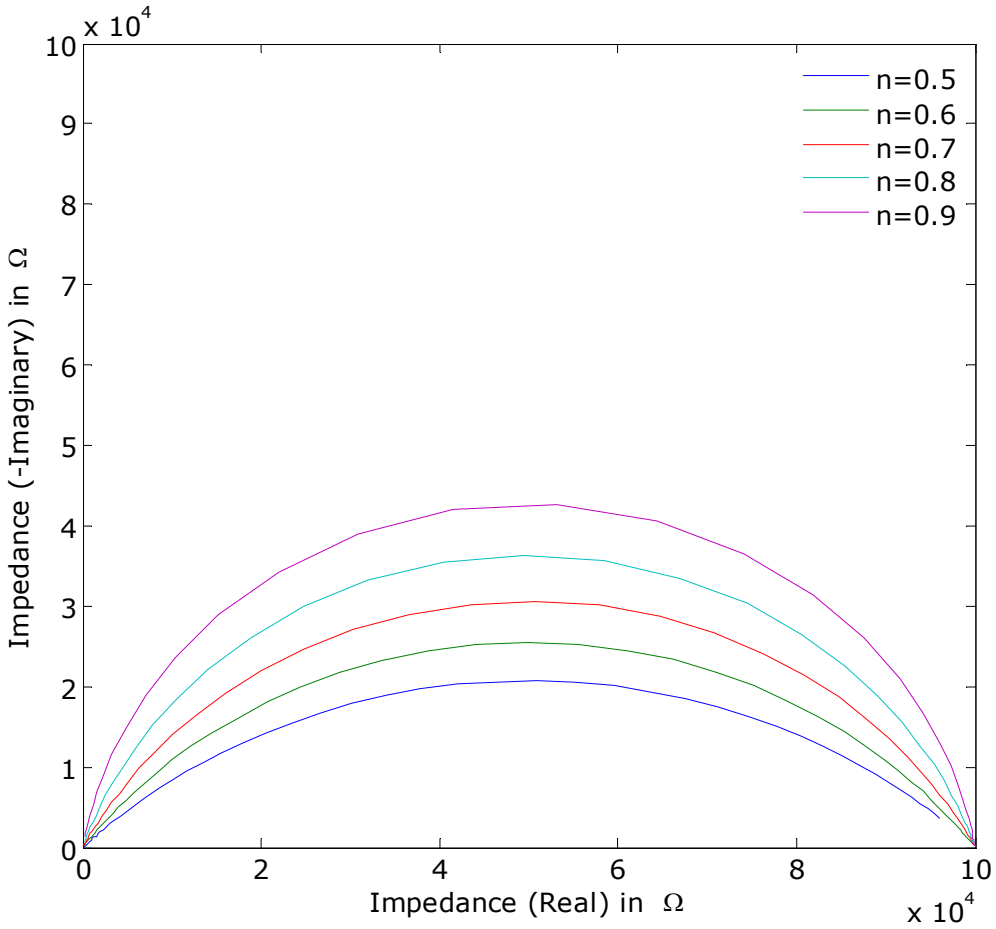

Figure 12: The complex impedance plot of a parallel combination of resistor and CPE for various values of CPE-n. R= 1e5, CPE-magnitude=.5e-10.

When the CPE is in parallel with a resistor, the impedance of this combination gives rise to a semicircle in the complex plane impedance plot. The center of this semi-circle does not lie on the real axis but below it. It is sometimes

referred to in EIS as a depressed semi-circular arc. Figure 12 is the complex plane impedance plot of a parallel combination of resistor and CPE, plotted for a range of n-values.

The slope of the CPE is described by the impedance equation for a constant phase element (CPE), which has the form:

$$CPE = Y * \frac{1}{(i * \omega)^n} \quad \text{..... (2.1)}$$

where $0 \leq n < 1$ and $n = 1$ represents an ideal capacitor, Y is a scalar with units of Siemens.(second)^n, and is equal to an ideal capacitance when n = 1, and ω is the angular frequency. The value of n is determined by the slope of the Bode magnitude plot. Some factors that affect electrode polarization include temperature, electrode roughness, electrode potential and ionic concentration.

3.4 Stability of Gold Electrode – Pourbaix Diagram

Pourbaix diagrams are used in corrosion to study the stability of materials in a given environment. Figure 13 is the pourbaix diagram of gold in NaCl solution at room temperature. Under room conditions gold exhibits excellent stability characteristics, as seen from the upper bound of the black line. The voltage band within which water is stable in the presence of a gold electrode is indicated as the area between the blue lines. Above the upper bound of the blue line, water dissociates resulting in oxygen evolution and below the lower bound hydrogen evolution occurs. A stable electrode is necessary for material characterization; otherwise a corroding electrode might interfere with the impedance characteristics of the analyte. Gold is routinely employed in bio-impedance investigations owing to its stability in biological environments.

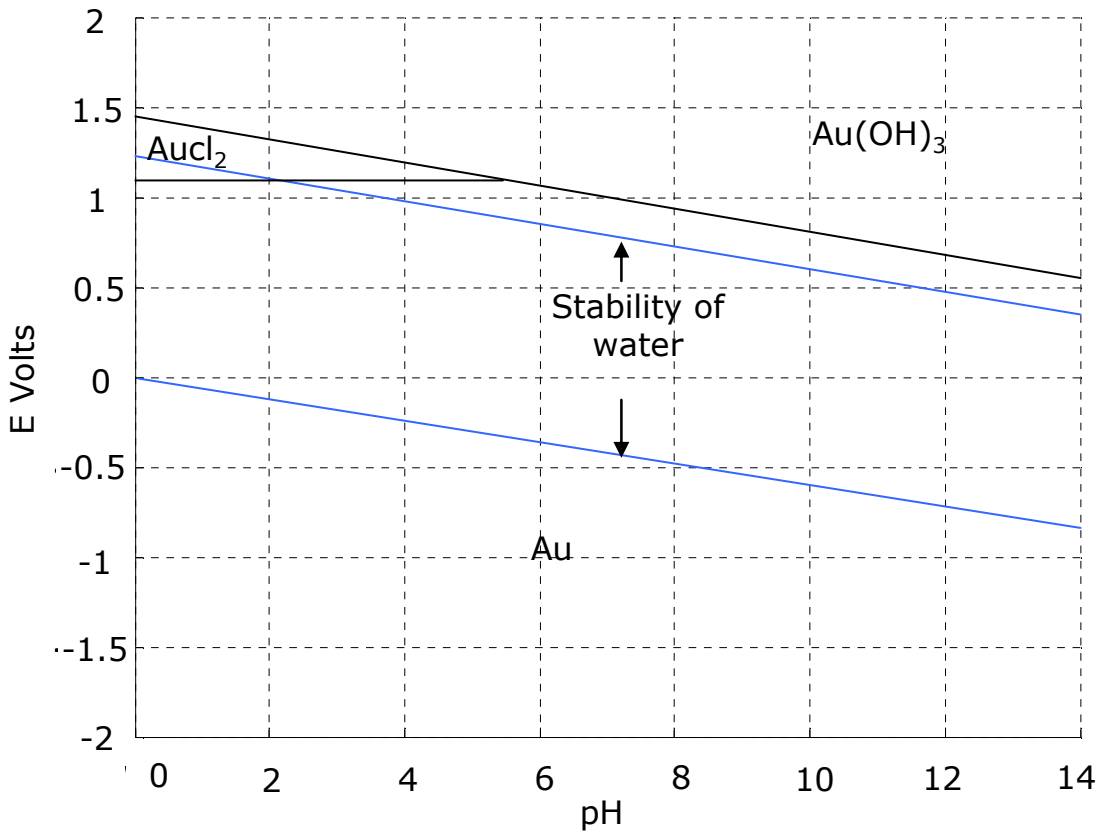

Figure 13: Theoretical Pourbaix diagram of gold in a solution with NaCl: 250mg/l, at 25ºC. The stability region of water is within the two blue lines.

3.5 Impedance Data Representation

3.5.1 Bode Diagrams

Bode diagrams are widely used in Impedance data representation. A Bode diagram comprise of two plots, a Bode magnitude plot and a Bode phase plot. The Bode magnitude plot is a logarithmic plot of frequency versus impedance. The Bode phase plot is a semi logarithmic plot of frequency (log) versus phase angle in degrees. Since impedance data have a wide range and are usually spread out over a wide range of frequencies, logarithmic representation enhances data points that would otherwise be obscure.

3.5.2 Complex Plane Immittance Diagrams

In EIS the complex data can be visualized in several forms such as real part of impedance versus imaginary part of impedance or imaginary part of permittivity as a function of square root of frequency. Various representations have their advantages. Four of the most commonly used forms of complex plane representation of impedance data are a) Impedance, b) Admittance, c) permittivity and 4) Electric Modulus. The transformations between the various forms are given by,

Impedance, Z

Admittance, Y=1/Z

Permittivity, E = Y/(i*ω*CC*ε0)

Modulus, M= 1/permittivity

Where, CC is the cell constant, ε_0 is the permittivity of free space and ω=2*pi*f, where f is the frequency in Hertz.

Data can be visualized in each one of these planes by plotting real part in the horizontal axis versus imaginary part in the vertical axis.

3.5.3 The Importance of Immittance Representation in EIS

Figure 14 and Figure 15 are examples of usefulness of immittance plotting in IS. Figure 14 A and B are the complex plane representation of conductivity and permittivity data of Trypticase Soy Broth, a bacterial culture medium, monitored for 100 hours in a closed environment. The drift in the sensor is clearly visible in the permittivity plane, where as the admittance plane does not reveal the drift. Similarly, Figure 15 A and B are the complex plane impedance and admittance representations of impedance data of a partially coated system. The conductivity plane clearly reveals two dispersions, where as the impedance plane does not.

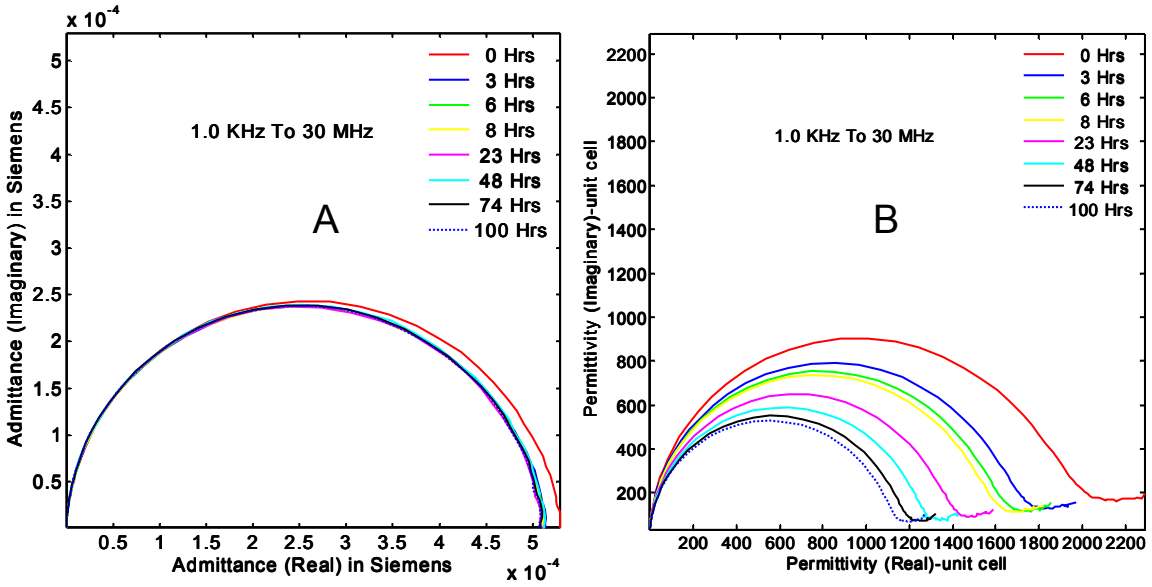

Figure 14: A) Complex plane admittance and B) complex plane permittivity plot of Trypticase Soy broth in a closed system.

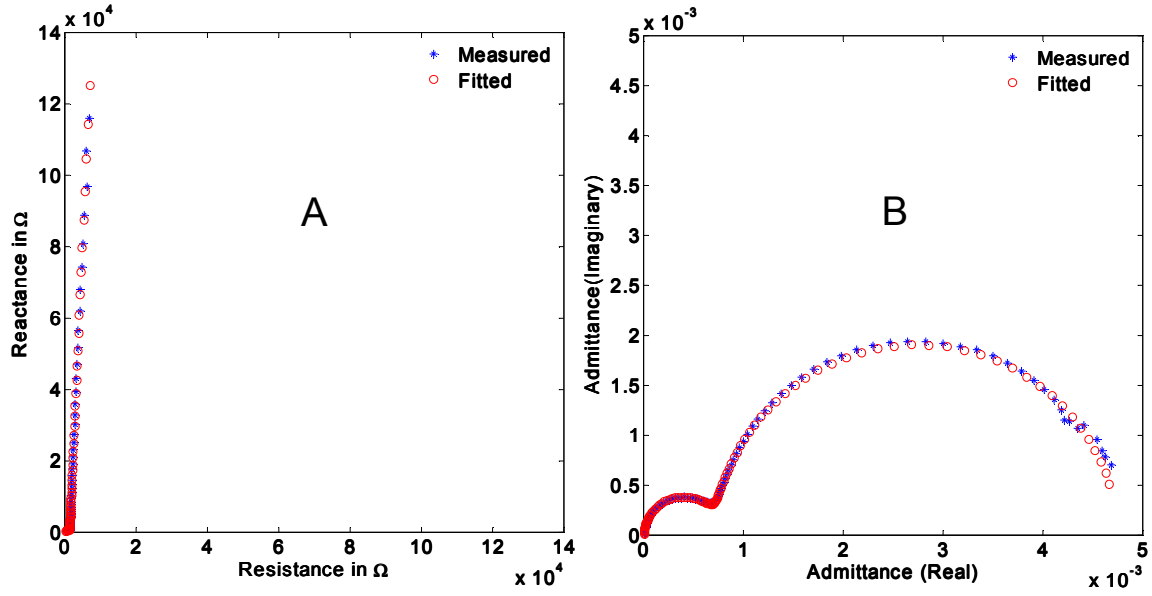

Figure 15: A) Complex plane impedance and B) Complex plane admittance plot of partially coated metal electrodes.

These examples underline the importance of immittance plotting of complex data. The same data set can reveal hidden trends when viewed in different

planes. The CellMap GUI developed in this research facilitates viewing of the entire dataset (in time and space) in all four immittance planes.

3.6 Simulation of Electrochemical Impedance Spectra

3.6.1 Interfacial Impedance

Figure 17 is the simulated impedance magnitude and phase diagram (Bode diagram) of a Resistor-capacitor parallel combination in series with a resistor shown in Figure 16. For the choice of an array of values for the parallel capacitor (R_{ct}), the resulting changes in bode diagram are plotted in Figure 17.

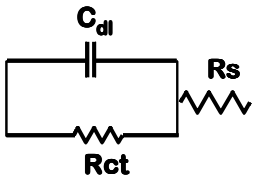

Figure 16: An example circuit to illustrate the effect of variations in Rct on the impedance spectrum. This circuit is often employed in corrosion monitoring and analysis using EIS.

The circuit shown in Figure 16 is a classical example of an electrochemical system undergoing charge transfer at the interface. The capacitance is due to the double layer capacitance, explained in Section 3.3.2 and the resistance is due to the resistivity of the solution. Two observations are worthy from the Bode diagrams of Figure 17, the changes in R_{ct} shift the low frequency plateau along the horizontal axis and shifts the characteristic frequency of the dispersion. This is due to the change in RC time constant of the circuit, which leads to a change in decay time.

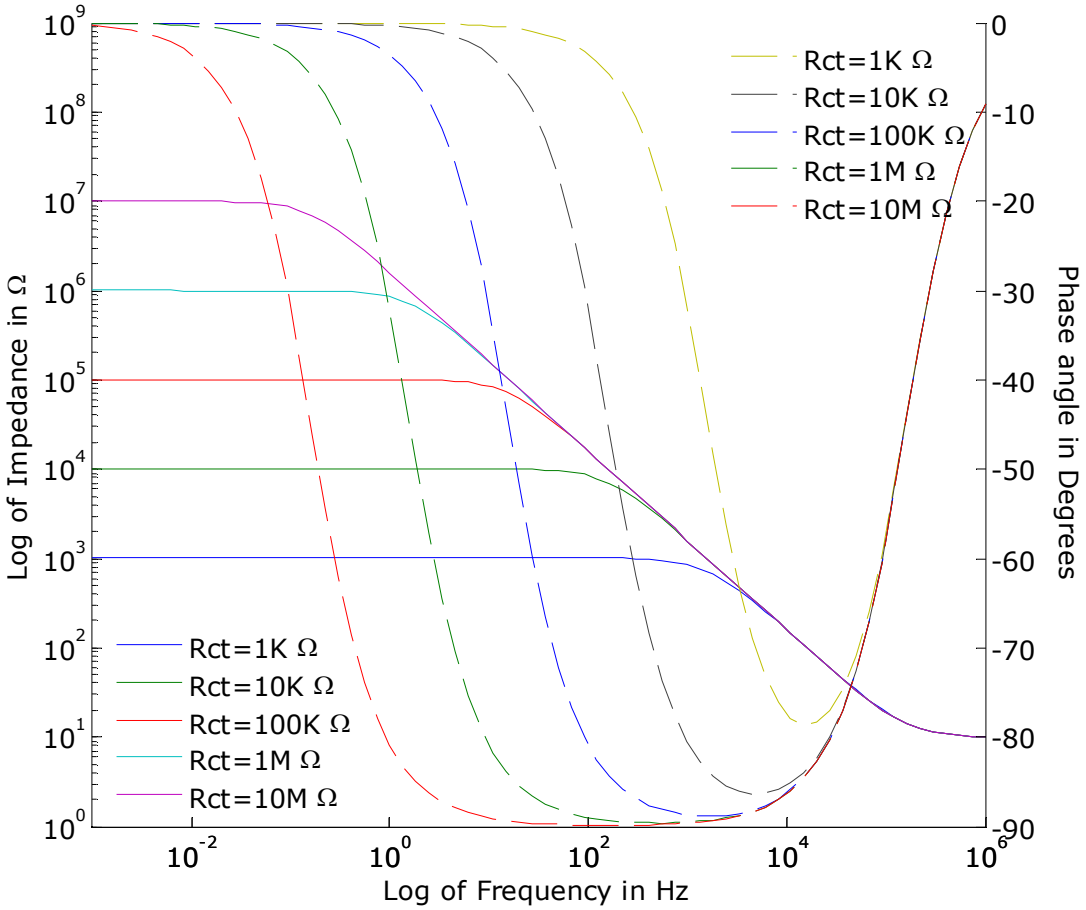

Figure 17: Bode diagrams of a resistor-capacitor parallel combination in series with a resistor. The capacitance, C_{dl} is 0.1 μF, and R_s=10 Ω.

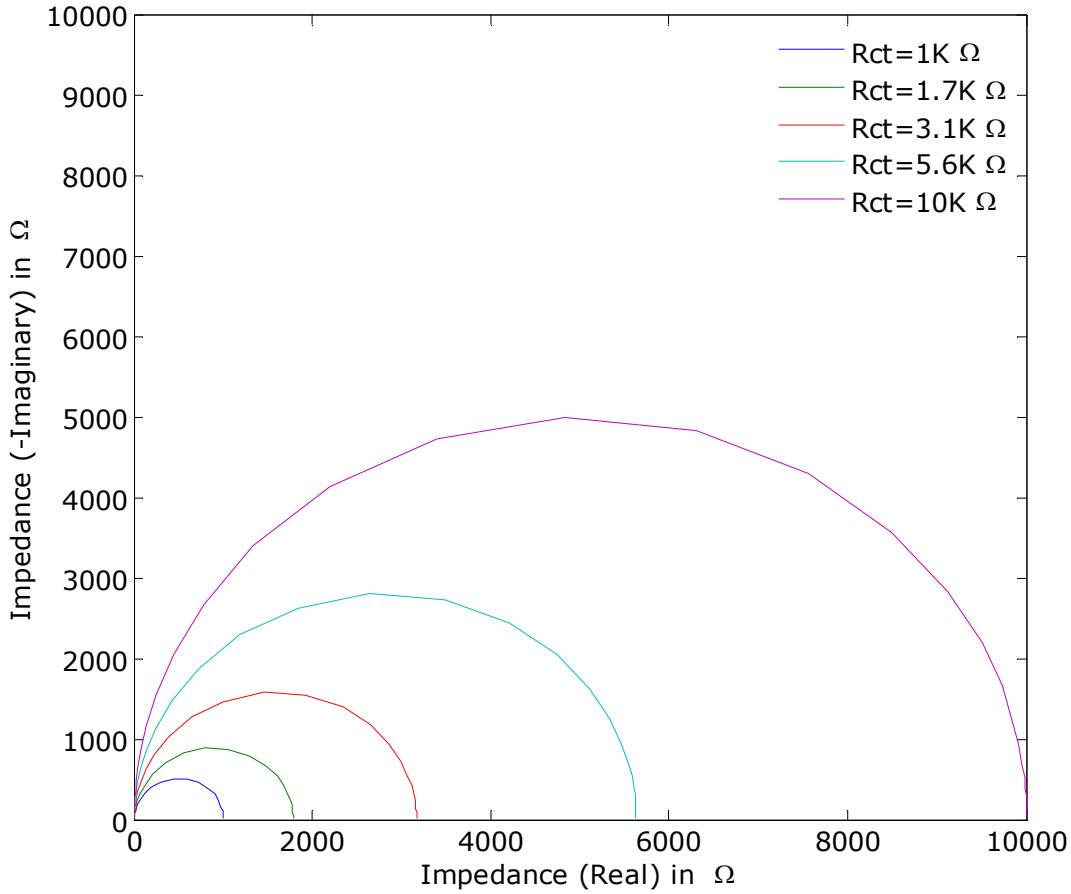

Figure 18: Complex impedance plot of circuit of Figure 16 for a range of R_{ct} values. R_{ct}= [1, 1.7, 3.1, 5.6, 10]*1E3, c_{dl}=1e-7 F, R_s=10 Ω.

The effect of R_{ct} in the complex impedance plane is shown in Figure 18. Changes in Rct shift the low frequency intercept of the semi-circle along the real axis.

For real electrochemical systems this is a simple way of determining the charge transport across the interface and hence electrochemical erosion or deposition can be monitored directly from the Bode or complex plane plot. However many electrochemical systems are not as simple as the one represented by the circuit of Figure 16. In more complicated situations knowledge of the physico-chemical makeup of the system is needed to

interpret the impedance spectrum. In the following section a slightly more complicated scenario is presented, one which involves both interfacial and bulk phenomenon.

3.6.2 Bulk and Interfacial Impedance

In spectroscopic characterization of materials, the sample is sandwiched between two electrodes and impedance spectrum is recorded. In these experiments, the interfacial phenomenon is a parasitic; unfortunately it cannot be avoided in bipolar measurements. However, recognition of interfacial and bulk phenomenon will help in proper parameterization of the impedance spectra. Moreover, methods have been developed to facilitate subtraction of a specific parameter or combination of parameters from the complex impedance dataset. Using these methods, the interfacial impedance component can be excluded from the overall impedance data.

In situations where a bulk (material) effect follows the interfacial effect, the Bode diagram appears as the one shown in Figure 19. The circuit used to simulate this impedance response is the one shown in Figure 20.

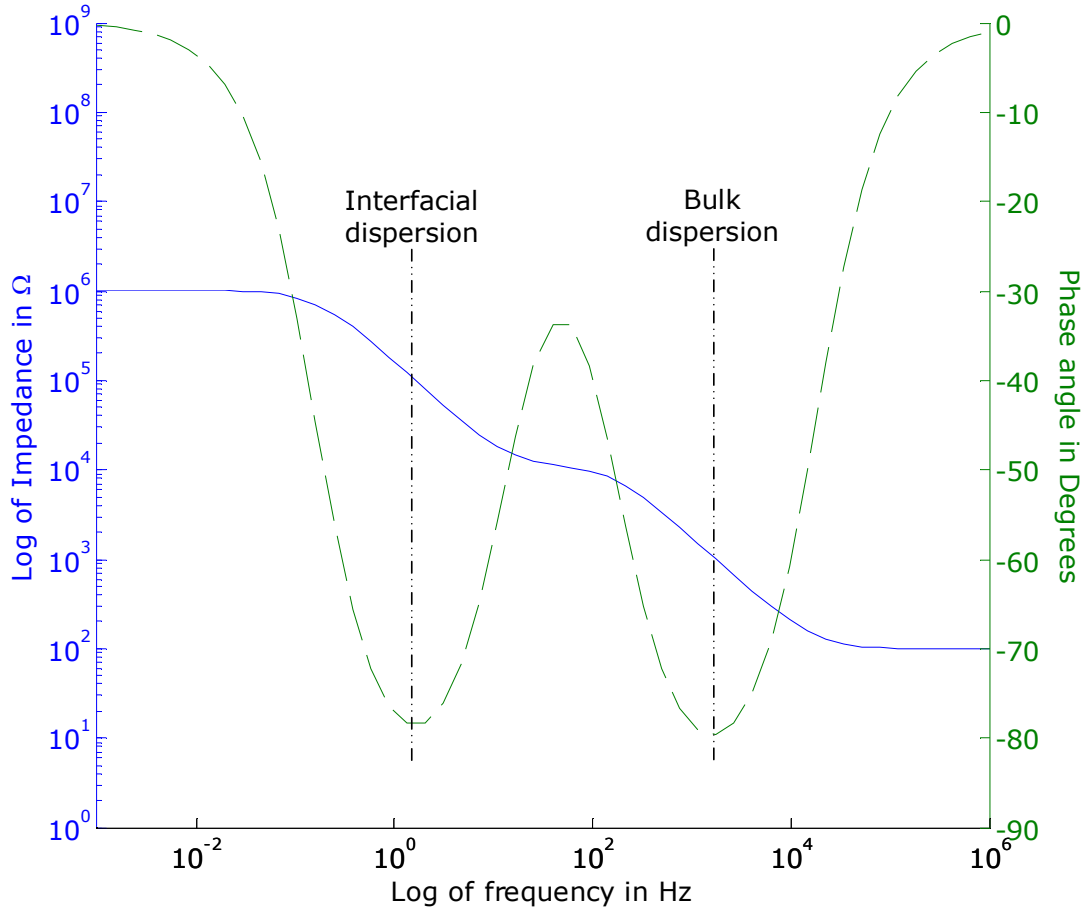

Figure 19: Bode diagram of a circuit approximating interfacial and bulk effects. R_b=1e4, C_b=1e-7, R_{ct}=1e6, C_{dl}=1e-6, R_s=1e2.

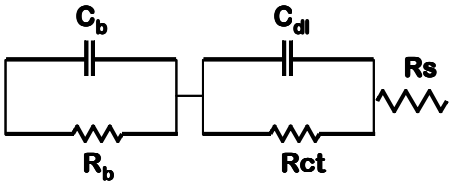

Figure 20: An example circuit to illustrate the interfacial and bulk effects. R_b and C_b are bulk parameters, C_{dl} and R_{ct} are interfacial parameters, R_s is the solution resistance.

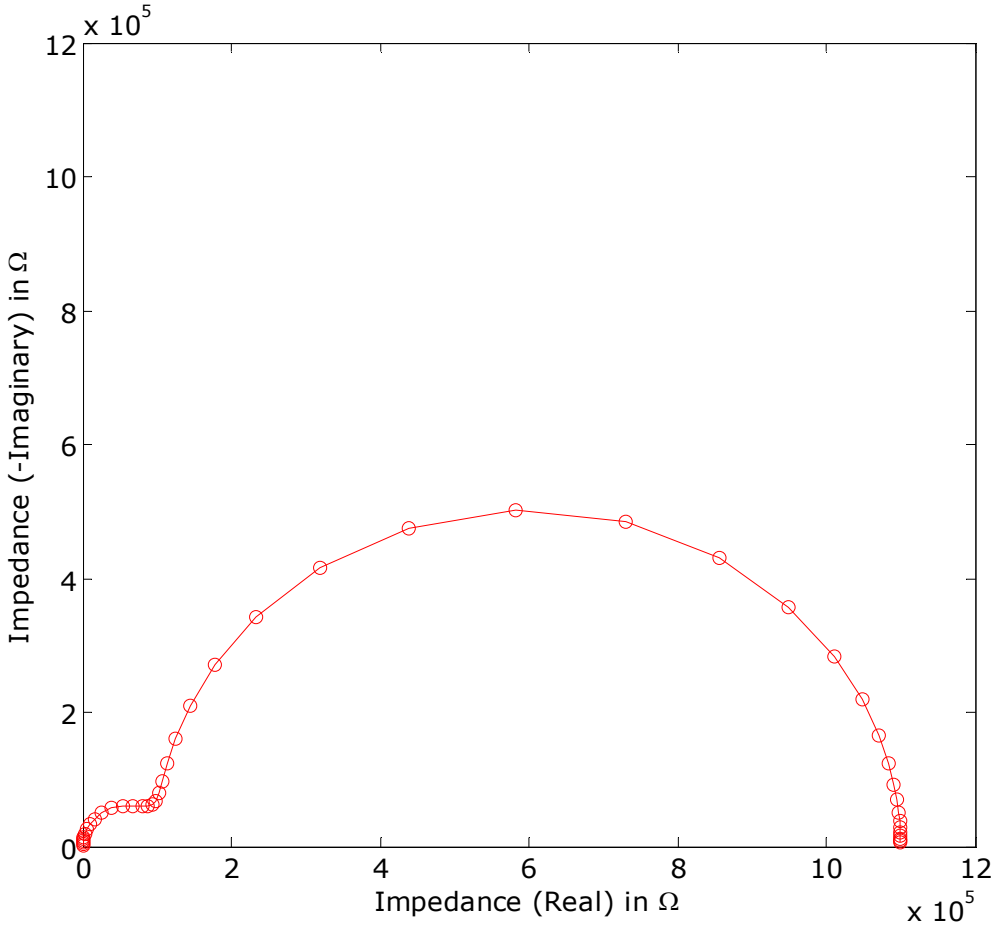

Figure 21: The complex plane representation of the impedance response of circuit in Figure 20.

Figure 21 is the complex plane representation of a two time constant system, displaying two distinct dispersions. In systems involving multiple dispersions, additional experimentation is typically carried out to ascertain the correctness of interpretation. For example, in the data presented in chapter 5, two dispersions are present in impedance spectra (Figure 47) of Gold (electrode) – potassium Chloride (electrolyte) system, whereas one was expected. The second dispersion was determined to be due to the polymer covered regions of the electrode metal. To confirm the interpretation, the area of the electrode is varied. The interfacial polarization which is directly proportional to the area of gold electrode displays a proportional increase

with electrode area. By examining the impedance spectra of different electrode sizes, the section of the impedance curve due to the interfacial component can be easily recognized. In the Bode diagram of Figure 47, the low frequency slope of the Impedance magnitude plot is ascribed to the interfacial polarization.

3.7 Bio-Impedance Spectroscopy

Biological and electrochemical systems obey general laws of physics in the limits of linearity. Their response to electrical stimulus can be approximated by a set of linear differential equations, such as the ones used to describe the time decay of current in an RC circuit excited by a step voltage. In other words, a measured frequency response of a biological system can be approximated by an equivalent electrical or mechanical (mass-spring-damper) or a fluidic (pressure-pipe-reservoir) circuit. Due to the nature of input stimulus (electrical) and direct correlation of quantities, an electrical equivalent circuit is chosen for biological system in IS measurements. This forms the basis of equivalent circuit analysis. This is an excellent feature of IS as well as a drawback. The drawback results from the fact that, by Voigt-Maxwell equivalence, a lumped parameter electrical circuit does not uniquely define a frequency response [74]. In order to interpret the impedance response by equivalent circuit analysis, a physical insight of the system under study is needed; otherwise the analysis can be ambiguous. Most impedance spectra in dispersion and relaxation studies are evaluated by equivalent circuit modeling.

3.7.1 Biological Dispersions

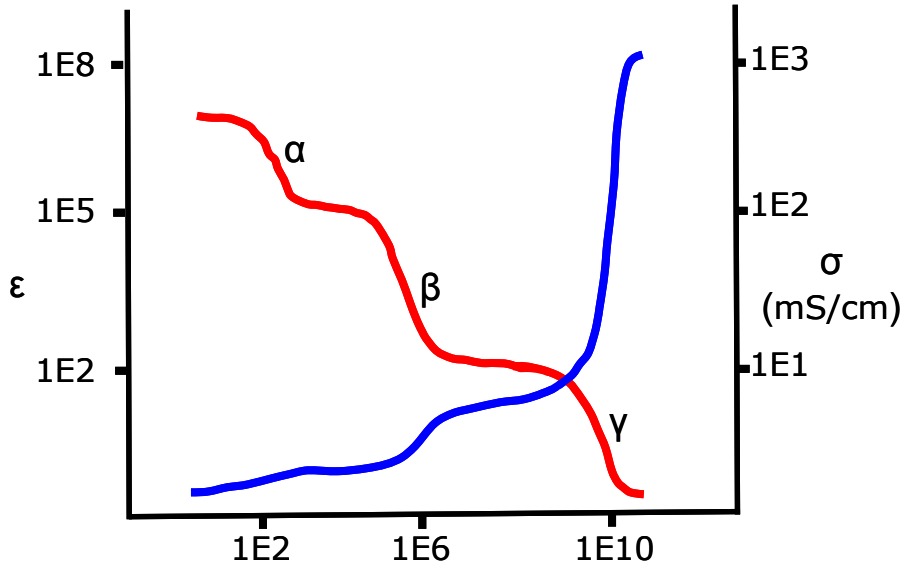

Figure 22: Frequency dispersions in biological materials.

The electrical properties of tissue and cells change with frequency in three distinct steps. These steps are referred as biological dispersions first introduced by Schwan [75]. These dispersions known as α, β, and γ disperions are due to various phenomenon that occur in biological tissue at different frequencies. The γ dispersion has been ascribed to abundant tissue water, where as the β dispersion is ascribed to Maxwell-Wagner induced dipole effect.

The α dispersion is thought to be due to a few different mechanisms including counter ion relaxation and frequency dependence of the cell membrane at low frequencies due to ion channel kinetics. Cell suspensions also display the as α, β, and γ dispersions but at different characteristic frequencies and magnitudes due to different cell sizes. The α and γ dispersions of tissue and cell suspensions are comparable. Several researchers have tabulated data on a variety of biological materials and their dispersive properties. These properties reflect the microscopic morphological makeup of the tissue and cells.

Cells and their environments are highly ionic conductors. Cell membranes and interfaces block the free passage of ions and therefore are capacitive. Hence, a network of biological cells and its extracellular matrix can be considered equivalent to an electrical network. In addition to the passive electrical properties that are exhibited by the cells and their surrounding environment, there are active electrochemical processes that are associated with living cells exemplified by the electrochemical potential gradient across a living cell membrane [76].

3.7.2 Electrical Elements of Biological Impedance

In bipolar investigation of bio-impedance, biological materials are placed between two electrodes and impedance measurements are recorded as a function of frequency. The biological cell consists of a bi-lipid membrane that is devoid of conductive ions but has ion channels to facilitate transcellular communication. The bi-lipid membrane can be represented as a parallel combination of resistor and capacitor. The intracellular environment comprises of cytoplasm containing ion rich fluids and membrane bound organelles. The intracellular environment is usually approximated by a resistance, neglecting the effect of membranes of organelles, Figure 23. The electrode electrolyte interface itself gives rise to complex impedance as discussed in the interfacial capacitance earlier.

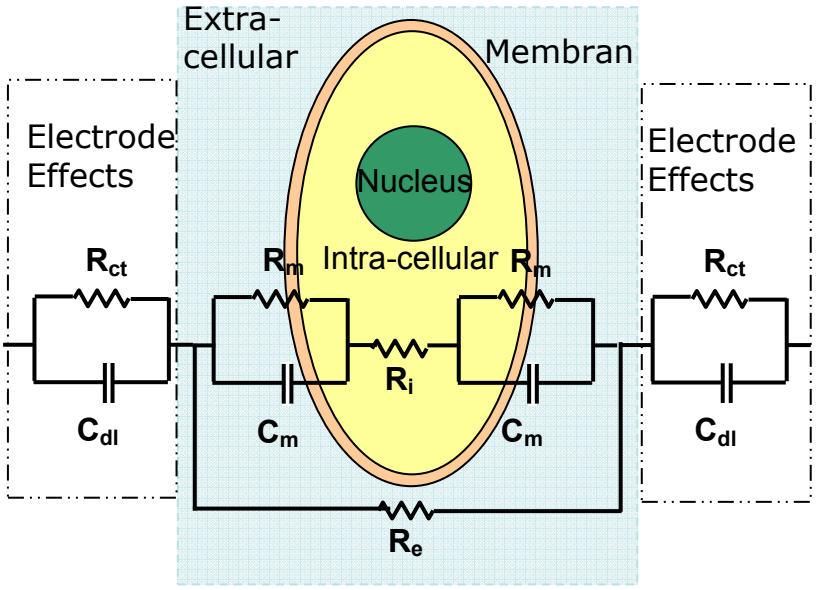

Figure 23: Illustration of equivalent circuit components of biological cell and the electrode-electrolyte interface.

In-vitro, anchorage dependent cells attach to the substrate and spread by multiplication. When full coverage of the substrate is achieved, the cells are considered to be confluent and the cell layer is termed as a monolayer. Generally, normal cells cease to multiply upon confluence, where as neoplastic cells continue to multiply and form multiple layers. This difference is illustrated in Figure 24.

Depending upon the number of layers and binding between cells (tight-junctional resistance) the impedance characteristics will vary. The process of attachment and spreading of biological cells and its electrical investigation have been well researched [64]. By performing IS on a biological cell systems, it is possible to differentiate between normal and tumor tissue [77], [78] , characterize ischemia [79], and other cell conditions [80], [56].

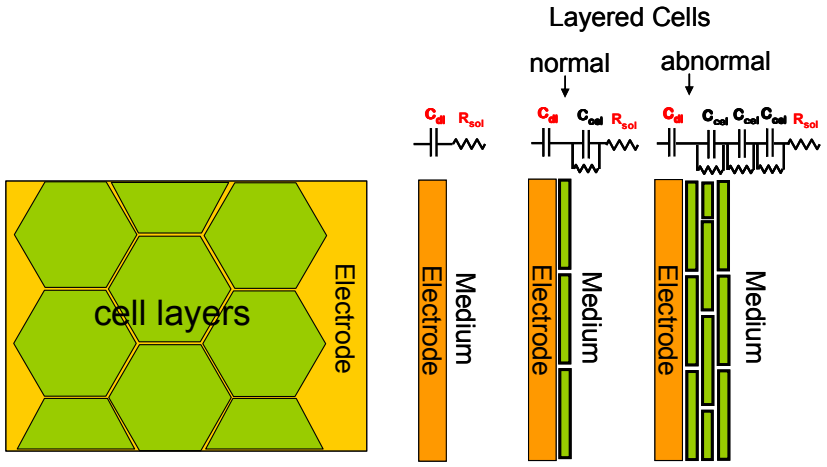

Figure 24: Illustration of cell monolayers and multi layers of electrode surface.

3.8 Summary

Concepts in electrochemical impedance spectroscopy and bio-impedance spectroscopy are reviewed. The importance of immittance representation of impedance data is emphasized with examples. The applicability of gold as an electrode material for bio-impedance measurements is examined. The impedance spectrum of simulated electrochemical interfaces is explained and the analysis is extended to real-world systems. Interfacial polarization and the modification therein due to cell growth is examined.

Chapter 4: Fabrication, Assembly and Programming of CellMap System

4.1 Introduction

In this chapter, fabrication, assembly and programming of the CellMap system are discussed. The CellMap device is discussed followed by the description of the switching circuit used for multielectrode recordings. The development of MATLAB based GUI developed for data acquisition, processing, analysis, parameterization and visualization is described in detail.

4.2 CellMap Electrode Array Fabrication

The CellMap electrode array fabrication is a single mask liftoff process. PY 3000 negative resist is spun onto the glass wafer. The electrode mask is used to expose the photoresist to make the molds for electrodes. A 1000^0 thickness of gold is deposited into the molds to form the electrodes. Liftoff is performed to isolate the electrodes. This is the process flow for the 8-electrode device on glass substrate.

4.2.1 Electrode Device Assembly

The Microfabricated and assembled 8-electrode device is solder-mounted on an 8-lead PCB board. The PCB board was fabricated with contact holes at the end of the leads. Pins are soldered into the contact holes. The PCB switchboard was also fabricated with matching holes to those of the lead board. Receptacles are soldered into the holes in the switching board. The device can be plugged and unplugged from the switching board.

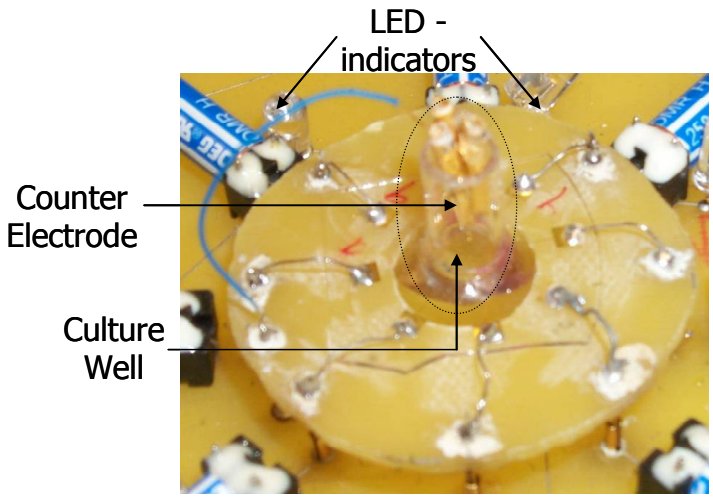

Figure 25: Assembled 8-electrode device. The Microfabricated device is mounted on a 8-lead PCB board.

In the case of PCB based device, standard commercial fabrication process is employed to form the electrode array. The PCB tracks are then electroplated with an approximately 2 µm layer of gold. Upon completion of device fabrication a glass cylinder is attached at the center of the electrode array using commercial two-part epoxy. The assembled device is shown in Figure 25.

4.3 PCB Switch Matrix

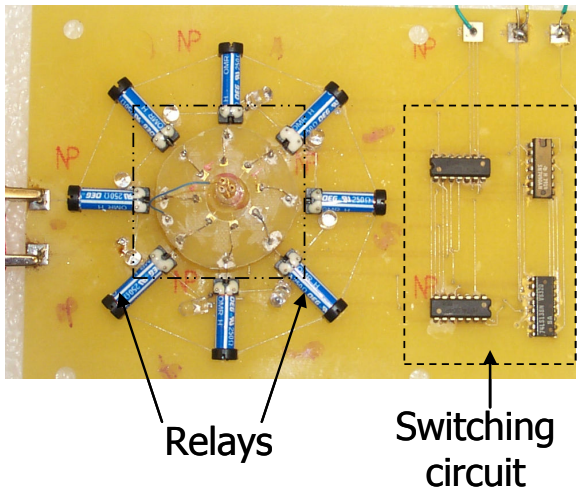

Figure 26: Switching circuit used for multichannel data recording.

The switching circuit consists of a) decade ripple counter-SN7490AN b) 3 to 8 decoder; -SA74LS138N c) inverters-HD74LS04P d) reed relays e) LEDs. At the end of each IS scan, a digital high (5V) is output to a selected pin of the digital I/O port of the PGSTSAT equipment. This output is fed to the trigger input of decade counter. Initially, the value of the counter is set to '000' in 3 digit binary representation. The output of the counter is decoded using 3 to 8 decoder to represent 11111110. This value is inverted using inverters to 00000001. These binary digits are fed to the control terminal of the eight reed relays, which are connected to eight working electrodes. The logic '1' in the first position of this value will switch (ON) the first relay. At this stage the input signal from the PGSTAT is routed to that particular working electrode and the impedance is recorded. At the end of the measurement scan, a digital high (5V) is fed to the trigger input of the decade counter. The count increases from 000 to 001. After decoding and inverting, the corresponding output will be 00000010. This will switch on second relay and hence the second working electrode. Impedance is recorded using FRA2 impedance analyzer for each electrode and the process repeats till measurements are recorded at all 8 electrodes. Reed relays were used as switching elements because of their high isolation. LEDS indicate the active channel.

4.3.1 Programming the Frequency Response Analyzer (FRA) for Multichannel Impedance Measurements

Impedance spectroscopy was performed over a frequency range of 25 Hz to 1 MHz using the frequency response analyzer (FRA2) module of the PGSTAT 30 potentiostat/Galvanostat. To achieve 8-electrode IS scan; the FRA programming interface is utilized. In the FRA programming utility, a procedure is a particular type of measurement, e.g. a frequency scan from 1 Hz to 10 Hz. A project could be a collection of such procedures as well as other I/O utilities.

For an 8-electrode scan, a new project is created which performs the IS procedure 8 times. At the end of each IS scan, a digital high (5V) is output to

a selected pin of the digitial I/O port of the PGSTSAT equipment. This output is fed to the trigger input of the 8-electrode switch circuit. This facilitates automatic switching to electrode n+1 upon completion of measurements on electrode n. The code for programming AUTOLAB FRA is provided in the appendix.

4.4 Measurement Protocol

Cell growth is sensitive to substrate conditions. A good clean substrate is important for cell growth. Upon fitting the cell culture cylinder to the 8-electrode device, and after a 10 minute drying period, DI water is dispensed in the culture well. The device is placed in a 50 °C incubator for 12 hours. This is done to allow chemicals to diffuse out of the epoxy into the liquid. The device is washed in acetone, methanol and DI water for 2, 2 and 5 minutes respectively. Prior to cell culture, the device is inoculated with cell culture medium overnight. The purpose of inoculating with cell culture medium was to normalize the surface with proteins and to facilitate the evolution of open circuit potential.

Cells were inoculated on the 8-electrode device in the form of suspension. After dispensing the cells, the devices were placed inside the incubator for a period of 2 hours. This period is crucial to cell attachment and spreading. Experiments performed without this inoculation period did not yield cell growth. After 2 hours, the device was transported to the measurement facility. After measurements were performed for all 8 electrodes, the device was transported back to the incubator. This procedure was repeated until completion of the experiment. The lack of an incubator in the measurement lab necessitated the transport of devices back and forth between the incubator and measurement facility.

4.5 Data Collection, Processing, Modeling and Visualization

Several computational steps are involved in the data processing and visualization of complex impedance data. An automated GUI-based MATLAB

routine was developed to facilitate data collection, analysis, parameterization and visualization. Figure 27 is the outline of the task flow for the MATLAB based GUI.

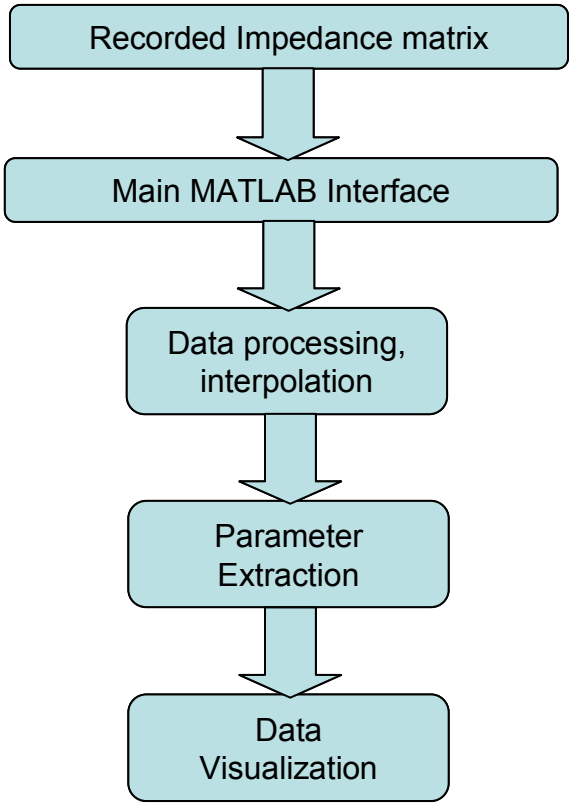

Figure 27: Outline of proposed data processing and analysis algorithm.

The goals of the software routine can be listed as follows,

1) Data processing, 2) Interpolation (if required), 3) Equivalent circuit parameter extraction, 4) Data conversion to different immittance forms, 5) 2D and 3D data visualization.

Data is imported from the primary AUTOLAB directory (source) on the PC into the MATLAB directory (destination). The program requires user input in pointing out the source and destination directories. This is necessary to avoid cross-mining of data and overlapping variable assignments in MATLAB. The data is then converted into time frames. Each time frame consists of a NX8 matrix, where N is the number of frequency points and 8 is the number of

electrodes. Each column of this matrix corresponding to a particular electrode consists of a complex vector. Each element of this vector is a complex number representing the impedance of a particular electrode at a particular frequency at a particular time. The entire dataset is 5-dimensional. Data is then processed through a "for" loop which extracts the parameters of the complex impedance data for each electrode at any given time instance.

4.5.1 Equivalent Circuit Analysis and Least Square Complex Data Fitting

Most electrochemical impedance measurements are interpreted with the help of equivalent electrical models. In this approach, impeding elements to the flow of ions and the exchange of charge (Faradaic processes) are represented by resistances. Charge storage elements in the system, such as the double layer capacitances are represented by capacitors. Initially, a circuit is assumed to represent the physical system under test, based on prior knowledge of the system. Using computational tools, such as least square data fitting and regression analysis, the model parameters are varied to fit experimental observations. The quality of the fit is then evaluated. This process is repeated by refining the model until a good fit is obtained.

The parametric description of an electrochemical system depends on its dimension, composition, and the measurement frequency range. For example, in the case of gold-medium system, impedance over a frequency range 10 Hz to 100 KHz may be represented by a series combination of a CPE and a resistor. However, for an extended lower frequency range, other parameters to account for diffusion or adsorption may have to be included.

4.5.2 Parameter Extraction

One of the most important aspects of the CellMap GUI is the parameter extraction. It is this step that facilitates monitoring several cell-substrate and cell-cell interaction parameters in tandem. A four parameter circuit is identified, which represents the impedance of the electrode in the presence

of cells. The same circuit can be used to model the data in the absence of cells, however, the cell layer parameters will not be well determined. The confidence interval of a parameter can be used to identify the importance of a parameter to the fit. The equivalent circuit used to model the data for presence and absence of cells is shown in Figure 28. Even though two separate circuits are shown for the purpose of illustration, the circuit b of Figure 28 is sufficient to represent the presence and absence of cells.

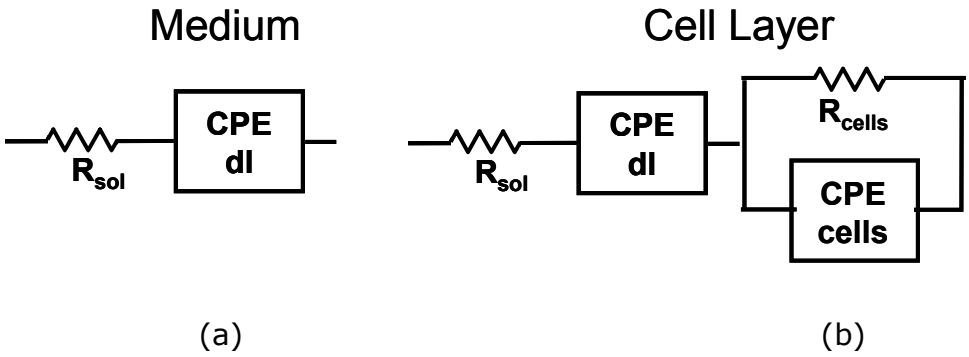

Figure 28: Equivalent circuits used to parameterize medium only (a) and cell layer (b) impedance data.

Three MATLAB functions are utilized to perform parameter extraction namely, FMINSEARCH, LSQNONLIN and LSQCURVEFIT. These and other curve fitting and parameter extraction tools can be found under the optimization toolbox of the MATLAB root directory.

a) FMINSEARCH

Fminsearch finds the minimum of a scalar function of several variables, starting at an initial estimate. This is generally referred to as unconstrained nonlinear optimization. The function to be minimized is given in Eq.3.

$$\frac{1}{Z_{cell}} = \frac{1}{R_{cell}} + (i * \omega * C_{cell})^{n-cell} \quad (3.1)$$

$$Z_{\text{interface}} = R_s + \frac{1}{(i * \omega * C_{dl})^{ndl}} \quad (3.2)$$

$$Z_{total} = Z_{\text{interface}} + Z_{cell} \quad (3.3)$$

The fminsearch algorithm minimizes this function and returns the estimates of parameters. It does not, however, provide the confidence intervals of the estimated parameters. To estimate the confidence intervals we make use of the Lsqnonlin and Lsqcurvefit functions.

b) Lsqnonlin

Lsqnonlin solves nonlinear least-squares (nonlinear data-fitting) problems. Specifically, it solves nonlinear least-squares curve fitting problems of the form given in eq. (4).

$$\min_x(f(x)) = f_1(x)^2 + f_2(x)^2 + ... + f_m(x)^2 \qquad (3.4)$$

lsqnonlin requires the user-defined function to compute the vector-valued function

$$F(x) = \begin{bmatrix} f_1(x) \\ f_2(x) \\ . \\ . \\ f_m(x) \end{bmatrix} \qquad (3.5)$$

Then, in vector terms, this optimization problem can be restated as

$$\min_x \frac{1}{2}\left\|F(x)\right\|_2^2 = \frac{1}{2}\sum_1 f_i(x)^2 \qquad (3.6)$$

The function Lsqnonlin returns the parameters estimates, residuals, normalized residuals, Eigen vectors and jacobian.

c) Lsqcurvefit

Lsqcurvefit solves nonlinear curve-fitting (data-fitting) problems in the least-squares sense. The problem is defined as finding the coefficients x, that best fits the equation

$$\min_x \frac{1}{2}\left\|F(x, xdata) - ydata\right\|_2^2 = \frac{1}{2}\sum_{i=1}^{m}(F(x, xdata_i) - ydata_i)^2 \qquad (3.7)$$

given input data xdata, and the observed output ydata, where xdata and ydata are vectors of length m and F (x, xdata) is a vector-valued function.

The latter methods need an initial parameter estimate very close to the final parameter value, whereas the fminsearch method can minimize with a higher degree of initial parameter latitude. In the parameter extraction algorithm, fminsearch is used to first extract the parameter estimates. These parameters are then supplied to Lsqnonlin and Lsqcurvefit for final estimates.

Figure 29 is the measured and simulated (using estimated parameters) plot of OvCa429 cell culture impedance. The plot 'Fitted' is simulated with estimated parameters obtained using Fminsearch. The plot 'Estimated' is simulated with parameter estimates obtained using Lsqnonlin. It is observed that the parameter estimates from LSQNONLIN and LSQCURVEFIT are very close to each other. The usage of two algorithms serves the purpose of cross validation and back-up if one function fails to minimize.

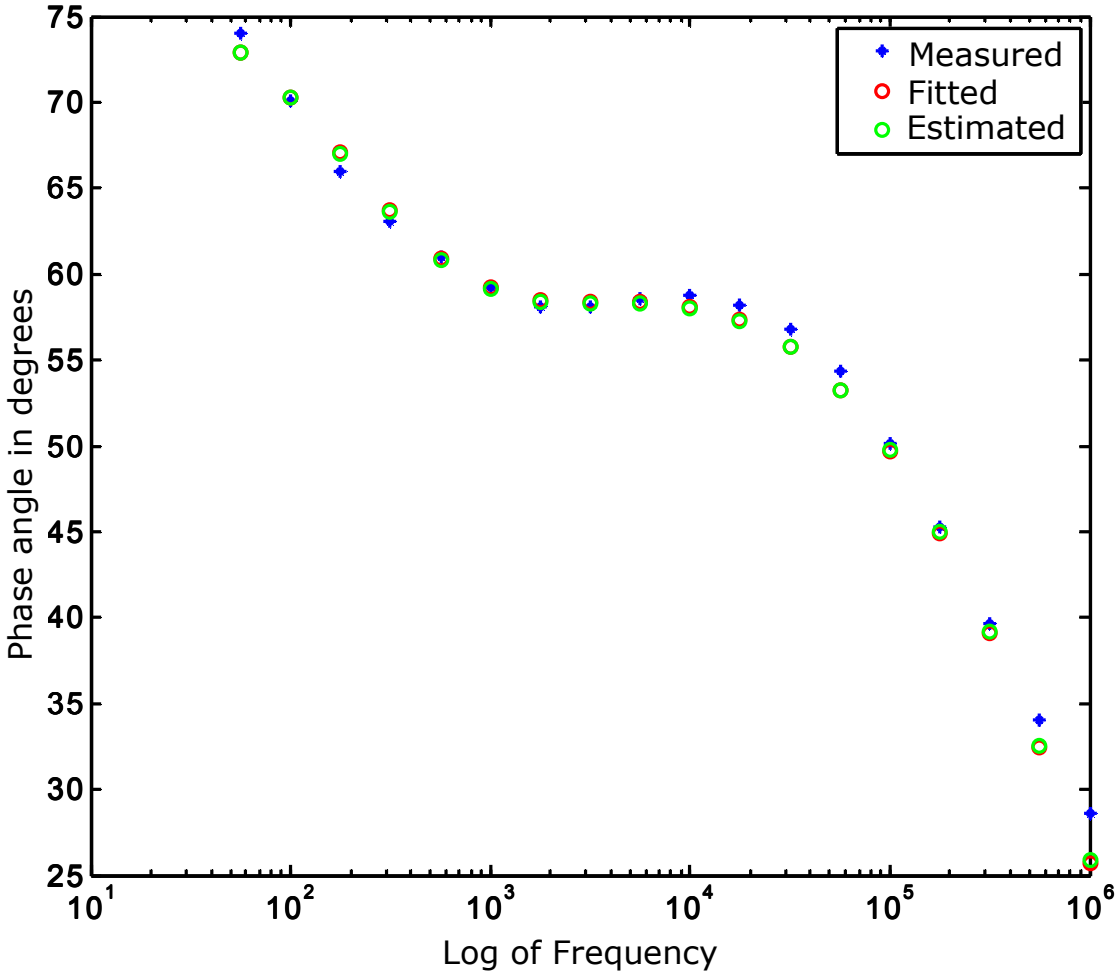

Figure 29: Measured, estimated and fitted data of OvCa429 cell culture.

d) Data visualization

Data visualization routines output fully formatted plots at any one of the four immittance levels for visual analysis. Visualization is available at all four immittance levels. The Graphical User Interface (GUI) developed for automated data analysis and visualization is shown in Figure 27. Additionally, movie and report capabilities are also available.

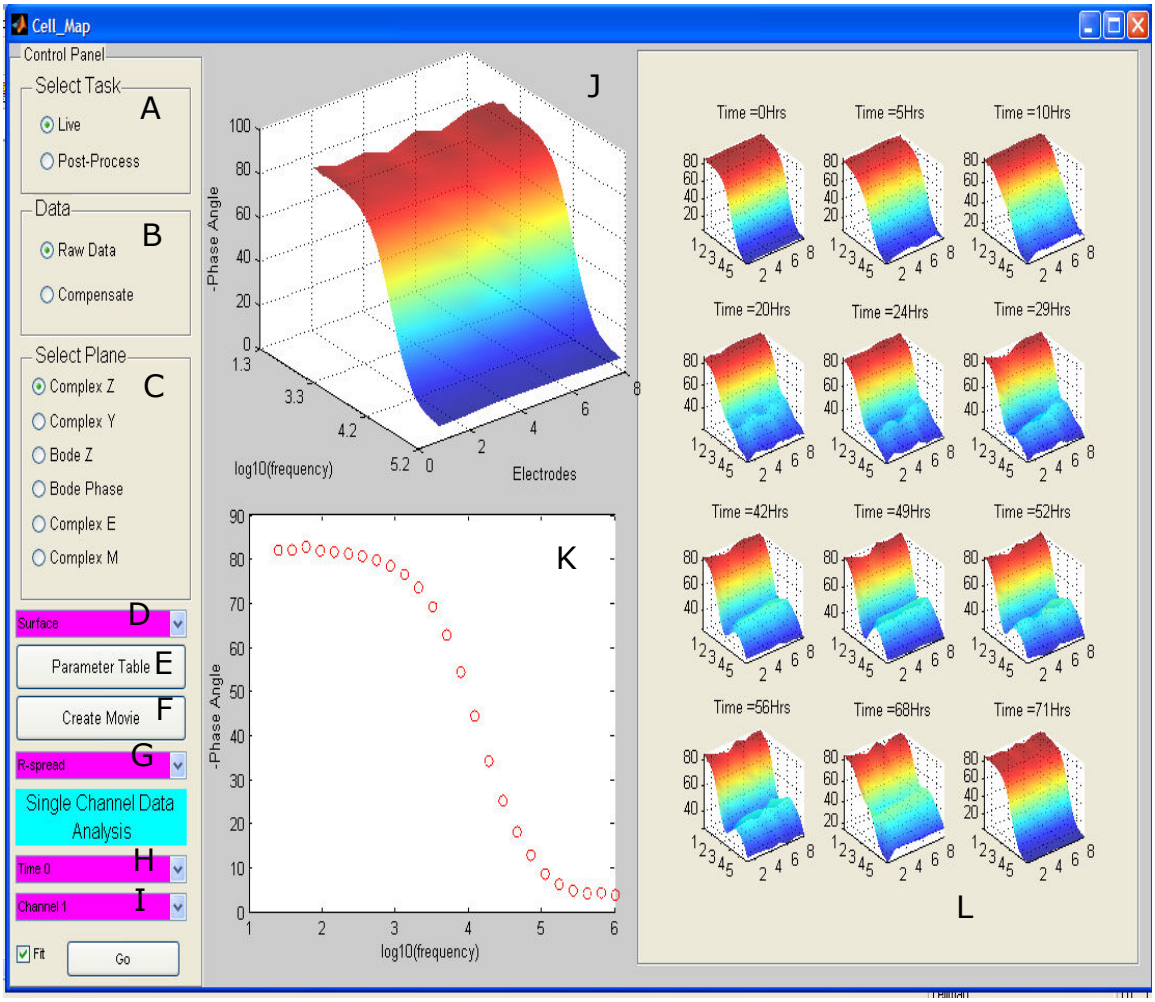

Figure 30: MATLAB based graphical user interface for data analysis and visualization.

The various modules and their functions are described as follows:

A: This module selects the appropriate functionality based on two scenarios a) an ongoing (Live) experiment and b) Post processing; Data processing and visualization upon completion of the experiment.

B: Selects if the user wishes to work with raw data or compensate the data (open-short-load compensation).

C: Selects the immittance plane for data visualization. The various planes available and their advantages are explained in section (3.5.2. The available

options are a) Bode magnitude, b) Bode phase, c) Complex Impedance, d) Complex admittance, e) Complex permittivity and f) Electric modulus.

D: Selects the type of plot. Available options are a) 3D line plot, b) Mesh plot and c) surface plot.

E: This push button control generates a word document containing a list of estimated parameters for all time instance and channels including the confidence intervals of the parameters.

F: Creates a time sequenced movie of the measurement "frames".

G: Select individual parameters to monitor their evolution over time course of the cell culture. The equivalent circuit parameters can be individually monitored.

H and I: Select time and channel for individual plot examination and fitting.

J: Axis showing the most current "frame" of cell culture state.

K: axis showing the most current channel data

L: Montage display of all the time "frames" of measurements across the electrode array.

4.6 Summary

Fabrication and experimental methods used in the implementation of CellMap system are discussed in this chapter. The switching mechanism used for multielectrode data acquisition is presented. Details of automated parameter extraction and development of MATLAB based GUI for data visualization and processing are presented.

Chapter 5: Impedance Analysis of OvCa429 Ovarian Cancer Cell Culture

5.1 Introduction

In this chapter, impedance analysis of OvCa429 cell cultures performed using a commercial cell substrate sensing electrode well plate (8W1E) is presented. 8W1E is widely used in contemporary cell-substrate sensing research. The aim of this study is to understand the impedance response of confluent cell cultures in-vitro using impedance spectroscopy. By using a commercially available and widely used device, data and analysis could be cross referenced and validated. The understanding developed in this experiment will not only aid in the implementation of CellMap system and interpretation of its results, but also provide the necessary data for benchmarking the CellMap system with reference to a contemporary system. The high frequency impedance response of 8W1E filled with HBSS is recorded and analyzed in order to identify the interfacial and measurement fixture impedance components. Similar analysis is performed with OvCa429 culture in 8W1E in order to identify and isolate the response of cell layers from interfacial and device components.

5.2 Materials Used

5.2.1 8W1E Cell Culture Well Plate

In this research, the 8W1E cultureware is used with an Agilent 4294 A impedance analyzer to record impedance measurements. The 8W1E substrate is an 8-well device. Each well is equipped with a 250 μm working electrode at the base of the well, fabricated using metal deposition and

lithography techniques. The working electrode is formed by lithographically defining a 250 μm area (expose) in a large area electrode. All wells share a common counter electrode which is several times the area of the counter electrode. The well plate in discussion is shown in Figure 31.

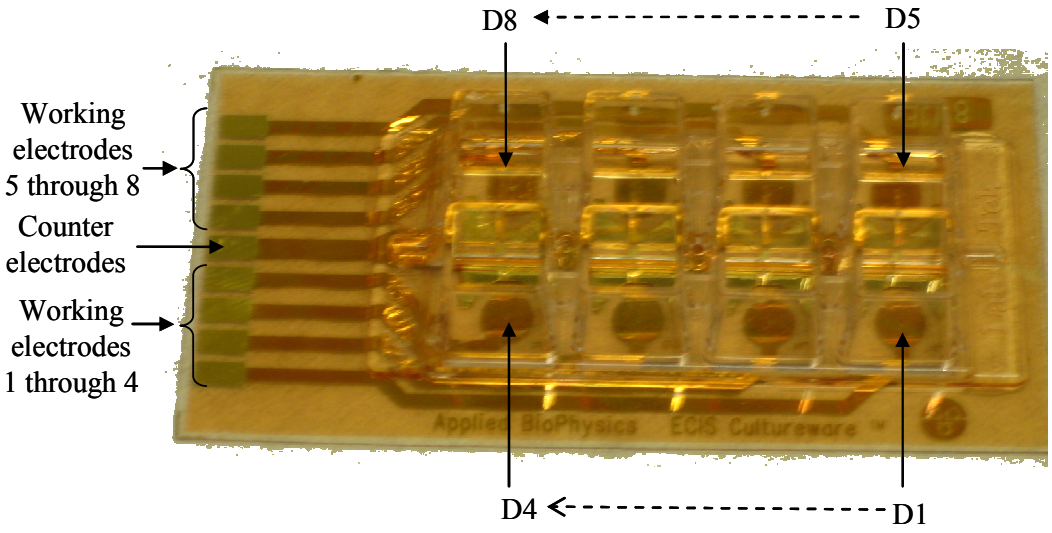

Figure 31: An 8-well ECIS cell substrate culture plate. The 8W1E model culture plate consists of 8 independent devices.

5.2.2 OvCa429 Cell Culture

Ovarian cancer line OvCa429 was provided by Samuel Mok at Harvard Medical School. These cells were grown in M199 and MCDB 105 (1:1) (Sigma, St. Louis, MO) supplemented with 10% fetal calf serum (Sigma), 2mM L-glutamine, 100 units/ml penicillin, and 100 μg/ml streptomycin under 5% CO2, and 37°C high-humidity atmosphere. Cell culture medium was changed every 2-3 days, depending on the rate of cell growth, and cells were sub-cultured at 80% confluence using 1X trypsin solution. Forty-eight hours after inoculating cells into electrode wells at $8\times10^4/cm^2$, confluent cell layers were formed and the normal medium was replaced by Hanks' Balanced Salt Solution (HBSS; Mediatech, Inc., Herndon, VA) without phenol red. Impedance data was taken under room temperature at about 22°C.

5.2.3 Agilent 4294A Based Measurements

The measurement set-up consists of an Agilent 4294A impedance analyzer in tandem with a Cascade™ microprobe station as shown in Figure 32. The Agilent 4294A Impedance Analyzer is a pseudo 4 point probe which facilitates bipolar measurements. Cabling and open-short-load calibrations were performed to null the connection and fixture parasitics. Measurements were performed from 40 Hz to 100 MHz, with a signal level of 25 mV. The signal level was selected to ensure linearity criterion of impedance spectroscopy.

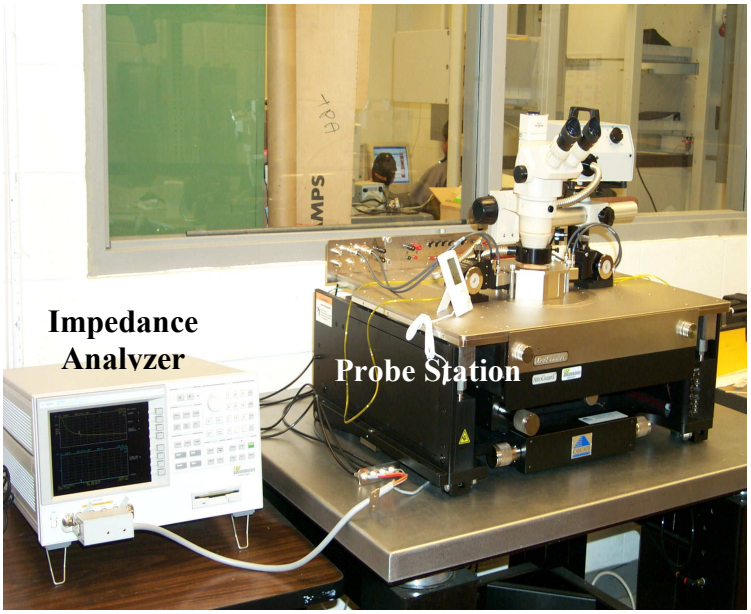

Figure 32: Agilent impedance analyzer based measurement setup.

5.3 Theory

The capacitance of a coated metal-electrolyte interface is 2 nF for a 2 μm thick coating with a relative permittivity of 5, when the coating is dry. When immersed in an aqueous medium, this capacitance is modified by water uptake and time duration of immersion. The modified value of capacitance is a few orders of magnitude less than the double layer capacitance. This implies that at low frequencies, current will tend to travel through the exposed regions of the electrode surface. However, at higher frequencies due to water uptake in polymers as well as disproportional area distribution of the

coated and uncoated regions, the capacitive reactance of the polymer coated region will decrease, making it comparable to the impedance of the exposed regions. This is particularly true in the case of microelectrodes where long lead lines often coated with thin polymer layer or other passivation layers are used to connect the microelectrode area to measurement ports. The lead line area could be several times longer than the area of the microelectrode. In the present case, the 8W1E culture device has a total area of approximately 14.179 mm2 (0.142 cm^2) which is then lithographically patterned to achieve an area of 0.049 mm2 ($4.9*10^{-4}$ cm^2), leading to an approximately 1: 300::exposed: coated metal area ratio. The effect of coated to exposed metal area ratio on high frequency measurements of OvCa429 cells is examined in the following sections.

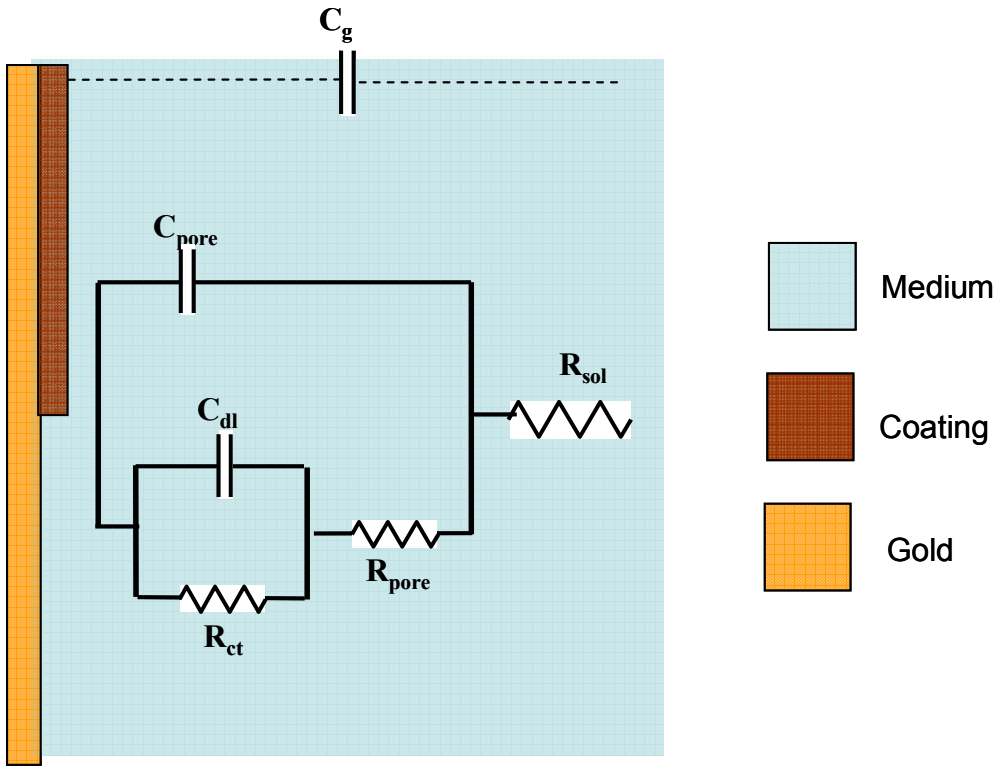

Figure 33: Illustration of a polymer coated metal surface. If the polymer layer is sufficiently thin, its impedance will contribute to the overall impedance substantially.

In Figure 33, Cg is the geometric capacitance of the electrolytic cell, whose impedance contribution can generally be neglected until very high frequencies (GHz). R_{sol} is the solution resistance, C_{dl} is the double layer capacitance, R_{ct} is the charge transfer resistance, C_{pore} is the pore capacitance, R_{pore} is the pore resistance.

5.4 Results

5.4.1 Measurements with Hanks Balanced Salt Solution (HBSS)

For a gold-electrolyte system, under normal room conditions of temperature and pressure, the expected response is due to a combination of interfacial capacitance and solution resistance. In electrical equivalent terms, the representative circuit will comprise of a series combination of resistance and CPE. The Bode magnitude plot should indicate a slope followed by a plateau. The Bode phase plot should exhibit a transition from capacitive to resistive behavior from low to high frequency, respectively.

Figure 34 is the Bode plot of OvCa429 cell culture medium, HBSS. As expected, the low frequency section of the Bode magnitude plot is a slope due to the interfacial capacitance. However, a frequency dispersion follows the double layer CPE slope, instead of the expected solution resistance plateau. This dispersion is due to the coating that was used to define the 250 μm working electrode area. An illustration of the covered electrode and its representative circuit is shown in Figure 33.

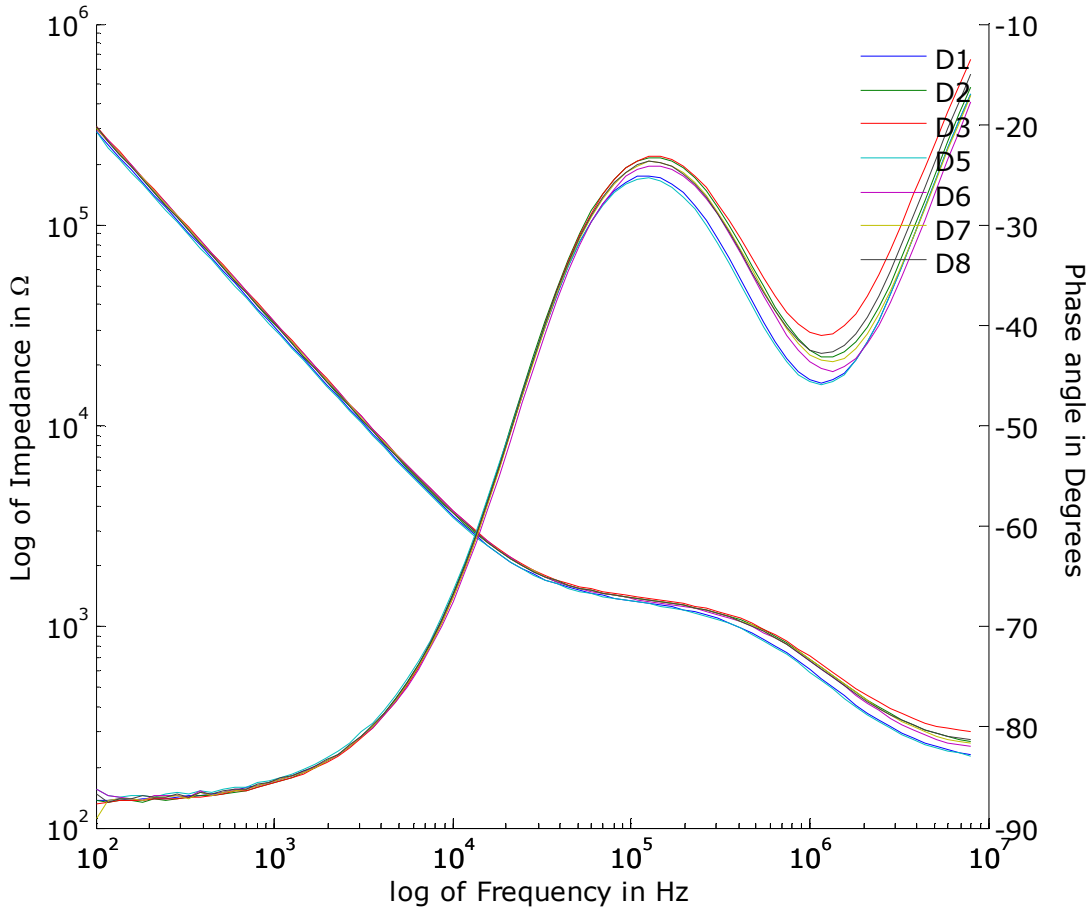

Figure 34: Bode magnitude and phase plots for 7 devices of the 8W1E well plate. Data from device 4 was an outlier and hence omitted from analysis. Secondary frequency dispersion due to the electrode coating is observed beyond approximately $3x10^5$ Hz. The spread in the solution resistance is due to the varying length of electrode leads for various devices (Figure 31).

Figure 35 is the complex plane admittance plot of the 7 devices of the 8W1E culture plate filled with HBSS. Two well separated time constants contribute to the admittance spectrum. In general, a parallel combination of conductance and capacitance gives rise to a semi-circle in the admittance plane. The circuit shown in Figure 36 is used to parameterize the admittance data of 8W1E devices containing HBSS. This circuit models the observed behavior very well as seen from the plot of data and fit Figure 37. The fit

quality factor, sigma F, is a quantitative indicator of the correlation between data and fit. A summary of fit parameters, their standard deviations and the overall quality of the fit for HBSS containing 8W1E devices is tabulated in Table 2.

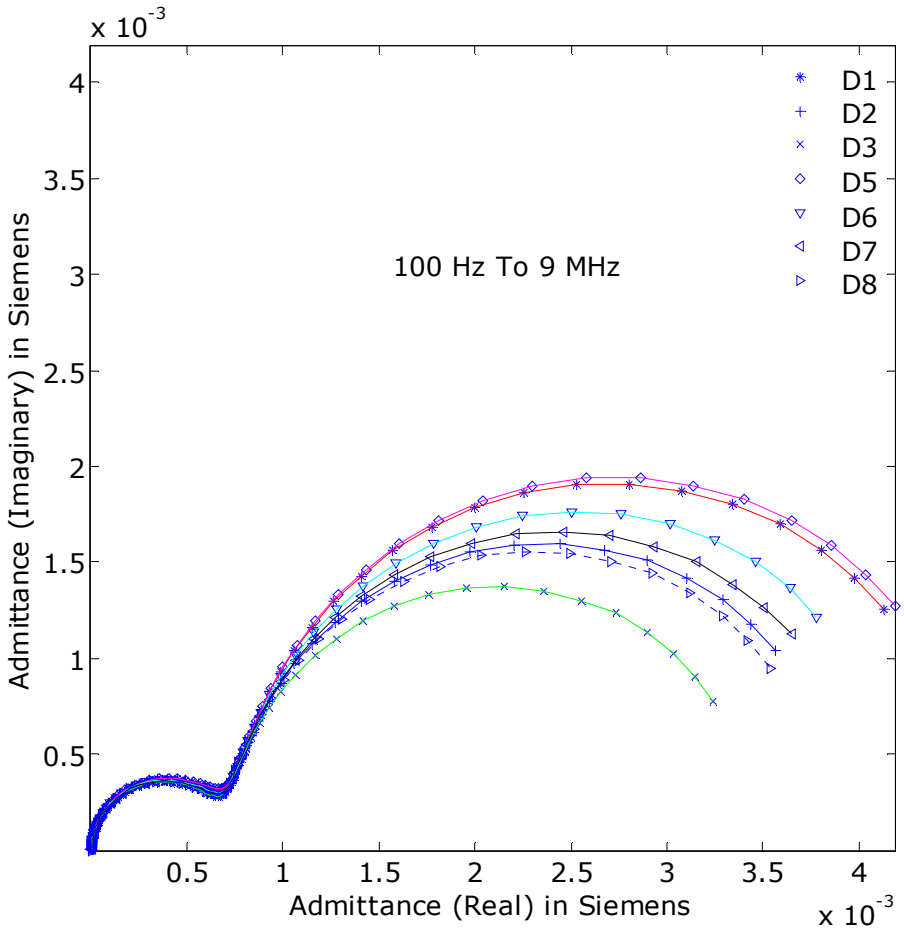

Figure 35: Complex plane admittance plot of 8W1E devices containing HBSS.

The circuit of Figure 36 is commonly used in corrosion measurements in the evaluation of coating effectiveness. Pores in the coating allow restricted access to the metal, which is analogous to the present situation with the 250 μm diameter exposed metal area representing a macroscopic pore. In addition to the macroscopic pore, microscopic pores are also present; but their effect is masked by the dominant effect of the macroscopic 250 μm

diameter pore forming the electrode. The resistor connected by dotted lines was not required in the fitting model. This indicates a very high charge transfer resistance which is consistent with noble metal behavior of gold electrodes.

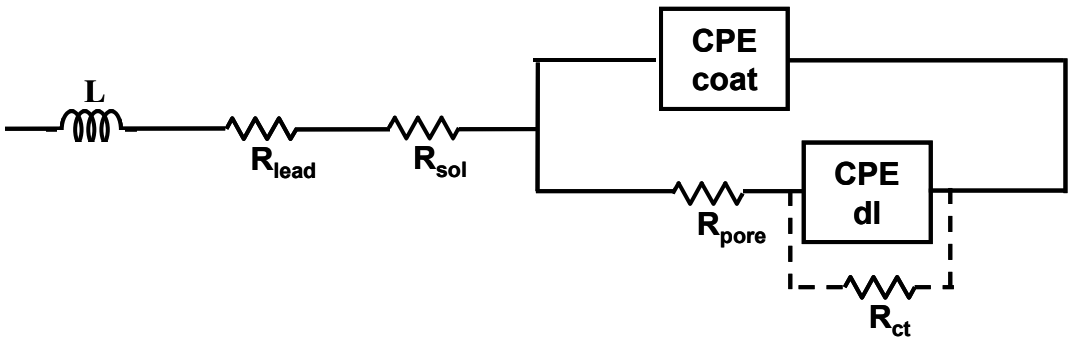

Figure 36: Equivalent circuit used in modeling the HBSS data of 8W1E devices.

The expression for the overall impedance of the electrode system with HBSS is given by following expression.

$$Z_{HBSS} = R_{sol} + R_{lead} + j\omega L + \frac{1}{\dfrac{1}{R_{pore} + \dfrac{1}{\dfrac{1}{R_{ct}} + (j\omega)^{n_{dl}} A_{dl}}} + (j\omega)^{n_{coat}} A_{coat}} \quad \text{.....}$$

where, R_{sol} is the solution resistance, R_{lead} is the lead resistance, L is the lead inductance, R_{pore} is the pore resistance, R_{ct} is the charge transfer resistance, A_{dl} and n_{dl} are the double layer CPE parameters, A_{coat} and n_{coat} are coating CPE parameters.

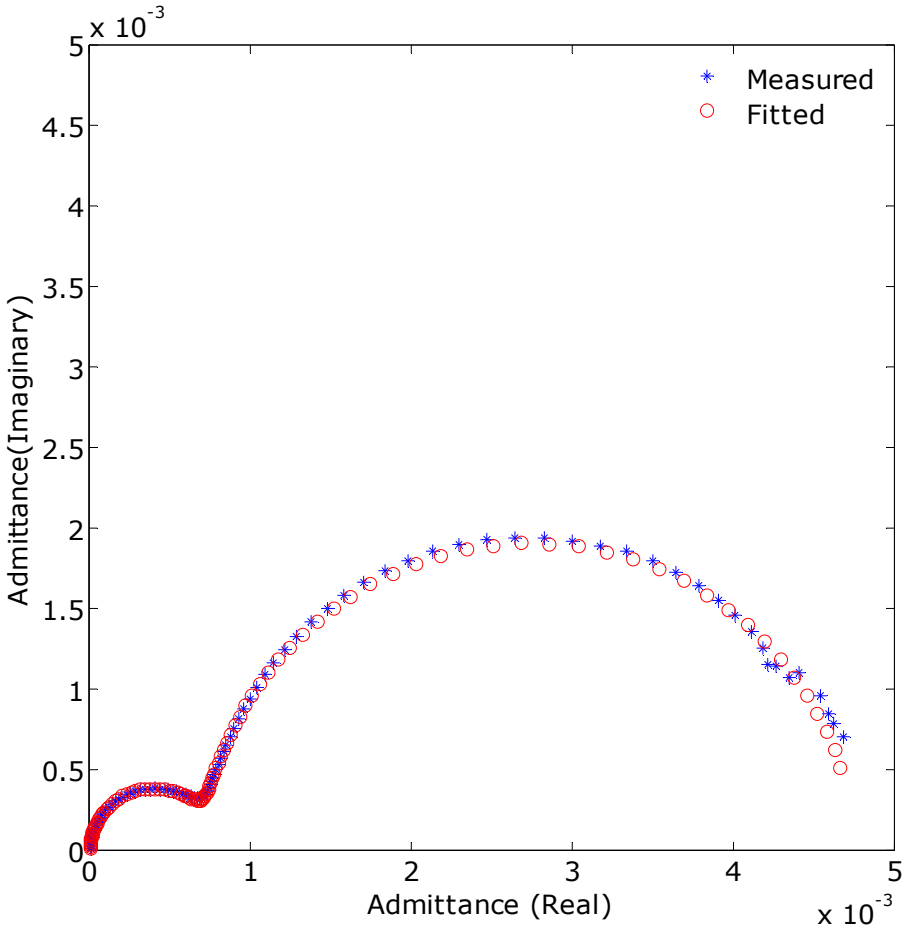

Figure 37: Measured and fit values of HBSS impedance in 8W1E device 5.

In the complex plane diagrams shown in Figure 35, which are the admittance spectra of 7 devices in the 8W1E culture array, the high frequency "tail" of the spectrum shows a systematic deviation while progressing from device 1 to 3 and from device 5 to 8. This is due to the contact lead length increase for these device sequences as observed from Figure 31.

Table 2: Parameters of HBSS impedance in 7 devices of 8W1E culture plate.

PARAMETERS	DEVICE-1	SD	DEVICE-2	SD	DEVICE-3	SD	DEVICE-5	SD	DEVICE-6	SD	DEVICE-7	SD	DEVICE-8	SD
Rsol*1E2	2.07	0.28	2.42	0.27	2.74	0.23	2.23	0.31	2.33	0.29	2.47	0.27	1.84	1.56
Rpore*1E3	1.24	0.21	1.23	0.23	1.23	0.23	1.23	0.25	1.25	0.24	1.24	0.24	0.17	1.95
CPE(dl)*1E-9	5.86	0.43	5.66	0.49	5.46	0.48	5.71	0.53	5.63	0.51	5.70	0.51	5.36	1.30
α(dl)*1E-1	9.75	0.04	9.77	0.05	9.77	0.05	9.73	0.05	9.75	0.05	9.75	0.05	9.87	0.10
CPE(coat)*1E-1	6.10	2.24	5.40	2.56	5.58	2.49	5.32	2.79	5.70	2.66	5.67	2.65	13.04	10.41
α(coat)*1E-1	9.52	0.16	9.51	0.18	9.50	0.17	9.52	0.19	9.47	0.18	9.50	0.18	8.99	0.88
L*1E-7	1.87	7.25	2.39	4.65	3.17	3.18	1.73	7.04	2.16	5.39	2.62	4.15	2.84	9.64
Sigma F	0.0048		0.0058		0.0056		0.0063		0.0060		0.0061		0.0063	

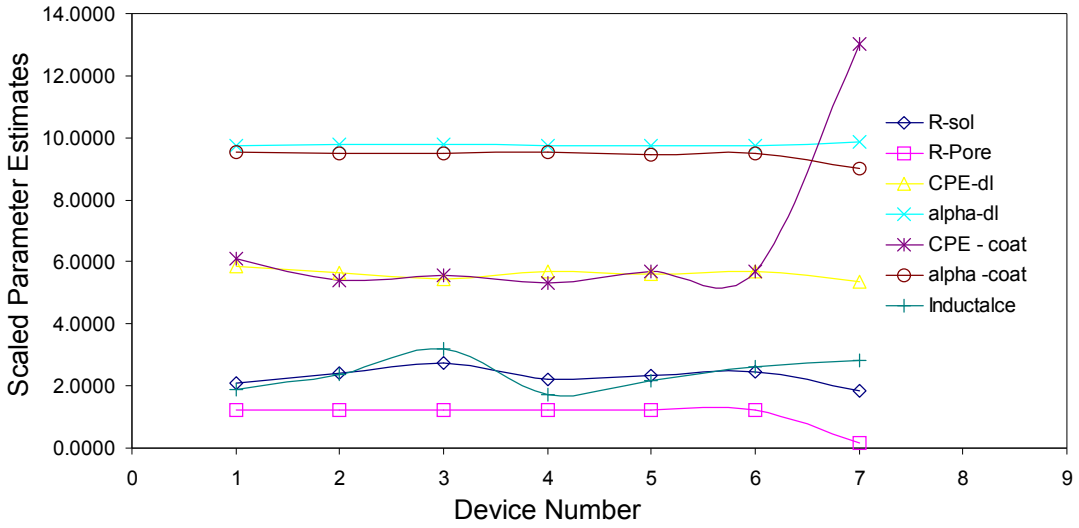

Figure 38: Parameter variation of HBSS impedance as a function of device.

Table 2 summarizes the model parameters of the equivalent circuit of Figure 36. Figure 38 is a graphical representation of the variation of parameter estimates. With the exception of coating capacitance of device 8, all parameters show very little deviation across the 7 devices. This is expected because of batch fabrication of the devices and the constant nature of the electrolyte used (HBSS). The effect of lead resistance has been approximated into the solution resistance as indicated by the increase in the solution resistance with the device index (Table 2). Assigning two separate resistors, one for solution resistance and another for lead resistance led to poor fitting results, indicating the inability of the solver to resolve these components. The pore resistance is approximately 1.23 KΩ, for all devices as expected.

The power factor of coating CPE is very close to ideal capacitance (approximately 0.975), indicating a good quality coating. The double layer CPE is also close to ideal capacitance (approximately 0.95), which is a characteristic of thin film deposited noble metal coatings, which have a smooth and uniform surface. The magnitudes of the two CPE's are separated by roughly one order of magnitude, which is due to water uptake by the polymer as well as a large area of the coated metal, which make the coating capacitance comparable to the double layer capacitance. Finally, the lead inductance also displays a significant variation with device index. This quantity is well determined in all the datasets, which indicates its importance and inclusion in the fitting circuit.

5.4.2 Measurements with OVCA429 Ovarian Cancer Cells

OVCA429 cells upon culturing form a cell layer or layers which cover a broad region of the substrate including the working electrode (coated and exposed) and the counter electrode. The cell layer can be conceptualized as a blanket coating throughout the surface area of the electrodes. Consequently, it is expected that the response of the cell layer should be in series with that of the blank (HBSS) device. Since the cells form close contact with the electrode, the interfacial impedance parameters will also be altered. The cell layers are usually approximated by a parallel resistor – CPE combination. The CPE of the cell layer represents the averaged effect of the membrane capacitance over the area of the electrodes, where as the resistance is due to extra and intracellular ions.

Figure 39 is the Bode plot of cultured OVCA429 cancer cell layer(s) in 8W1E devices. Unlike the HBSS-gold electrode system, there is a substantial low frequency slope variation in the case of OVCA429. This is due to the formation of intimate contact between the substrate and the cell. Moreover, cell layers are dynamic and motile, which explains the variability of device-to-device impedance. However, despite the unevenness that may be present in the cell layer, there are two characteristic properties of the layer, which

vary from device to device. These are, the cell layer resistance, due to the cell-cell contact and the cell layer capacitance, due to the cell membrane.

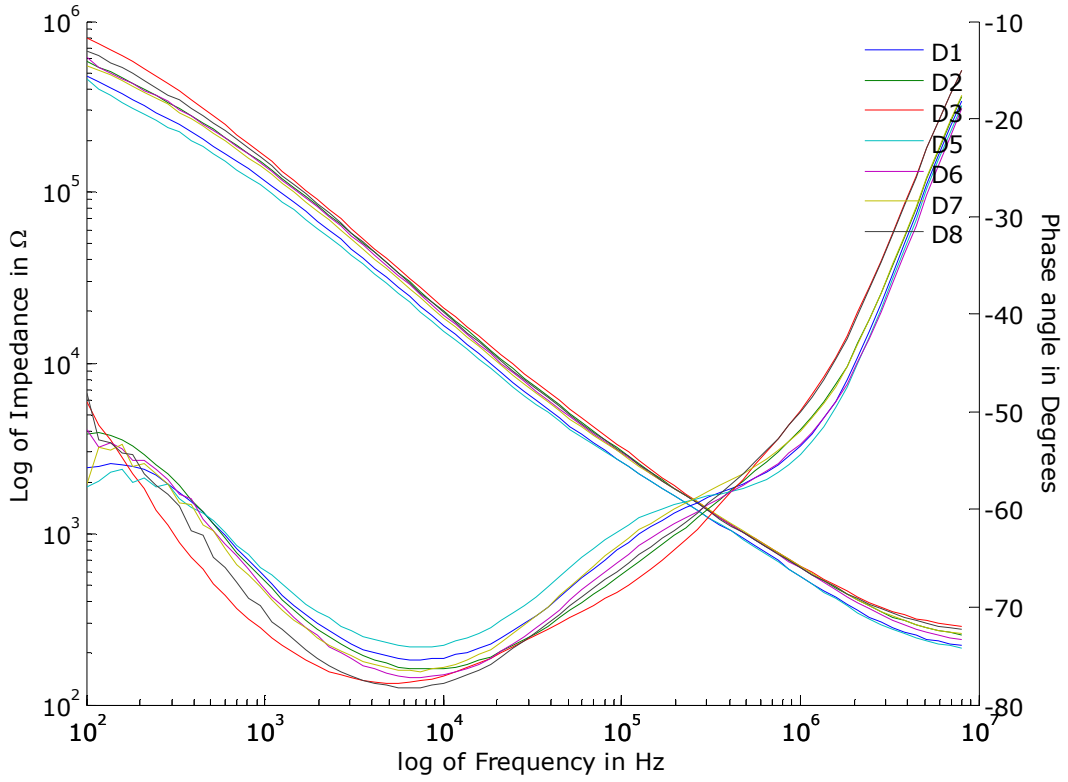

Figure 39: Bode magnitude and phase plots for 7 devices of the 8W1E well plate. Data from device 4 was unreliable and hence omitted.

From Figure 39 it is observed that the high frequency section, that is the frequency range where the impedance of polymer coating on the electrode dominates, is fairly unchanged between HBSS data and OVCA data. The double layer slope is substantially shifted upwards in relation to the HBSS data. Further insight can be gained by examining the immittance diagrams of the OVCA dataset.

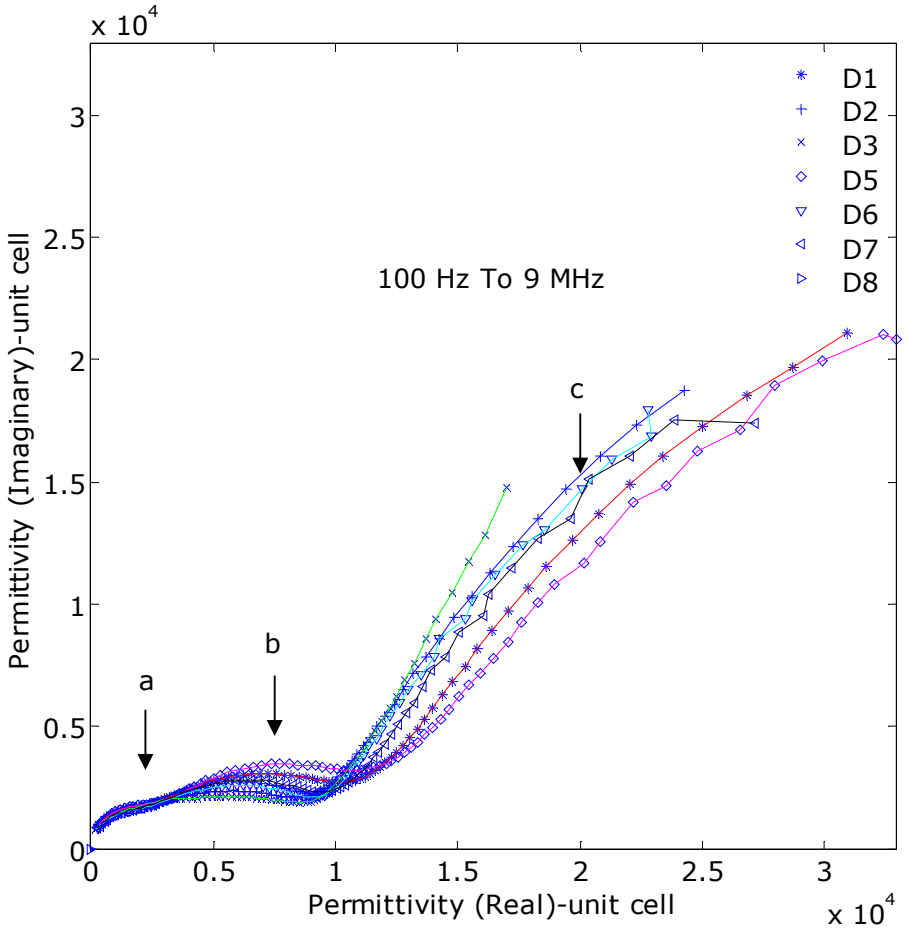

Figure 40: Complex permittivity plot of OVCA429 cell cultures in 7 devices of 8W1E.

Figure 40 is the complex permittivity plot of OVCA429 cell cultures. Data points in the descending order of real axis represent increasing frequency. Three distinct regions can be identified in the permittivity plane. The lowest frequency dispersion (c) is due to the double layer, the mid-frequency dispersion (b) is due to the cell layer capacitance and the highest frequency dispersion (a) is due to the polymer coated regions of the electrode.

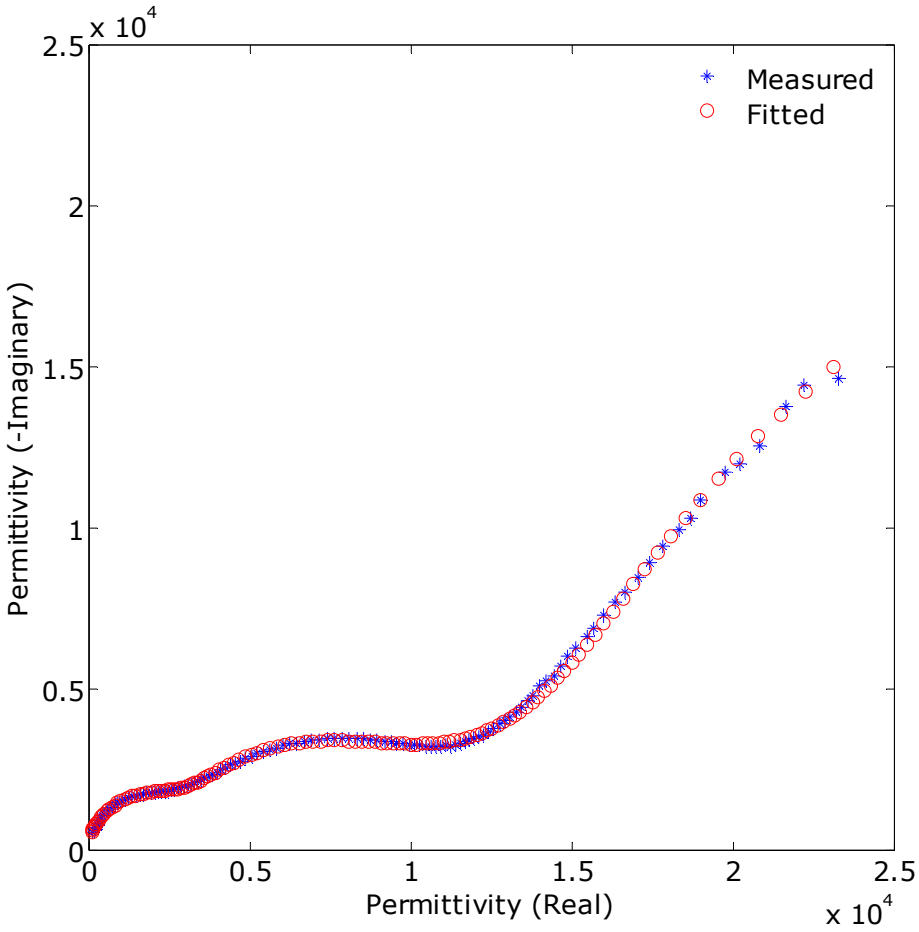

Figure 41: Complex permittivity plot of measured data and fit data using the equivalent circuit of Figure 42.

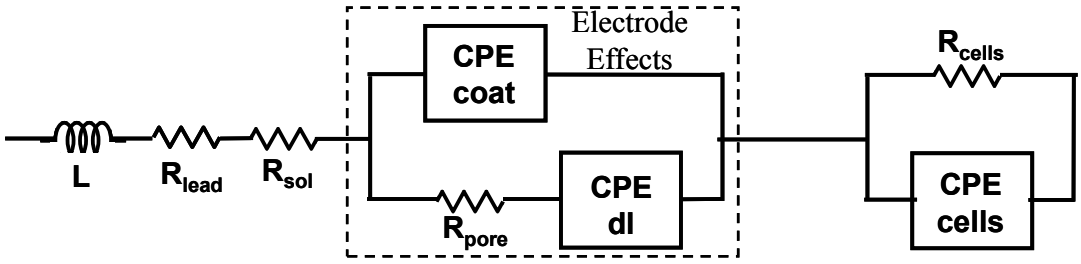

Figure 42: Fitting circuit used to parameterize the OVCA429 impedance data.

The expression for the overall impedance of the electrode system with OVCA429 cell layers is given by the following expression

$$Z_{cells} = R_{sol} + R_{lead} + j\omega L + \cfrac{1}{\cfrac{1}{R_{pore} + \cfrac{1}{\cfrac{1}{R_{ct}} + (j\omega)^{n_{dl}} A_{dl}}} + (j\omega)^{n_{coat}} A_{coat}} + \cfrac{1}{\cfrac{1}{R_{cells}} + (j\omega)^{n_{cells}} A_{cells}} + \ldots.$$

where R_{cells} is the resistance due to the cell layers, A_{cells} and n_{cells} are the CPE parameters due to the cell layers.

Three time constants are observed in the complex plane permittivity plot in Figure 41. The low frequency semi-circle of the "blank" device has been considerably altered by the presence of cells. Figure 42 is the fitting circuit used to model the OvCa429 coated electrode data. As expected, the cell layers contribute an additional R-CPE element to the overall impedance of the blank device which is in series. For comparison, Figure 40 shows the complex permittivity plot of OvCa429 cells on 8W1E device. The admittance plot (not shown) in this case does not lend itself to easy interpretation, where as the 3 time constants are readily discernible in the permittivity plane.

The generally accepted value of cell membrane capacitance is 1 μF/cm^2. Cell membranes are composed of Phospholipid bilayers which act as insulators, except for ion channel openings which conduct transcellular currents. Unlike the membrane capacitance, cell layer capacitance indicates the capacitance of a cell monolayer or multi layers. Cell layers consist of transcellular junctions, folded cell walls, and multiple cell layers which lead to a capacitance value different from that of a flat sheet cell wall capacitance of 1 μF/cm^2. Since the cell capacitance is in series with the double layer

capacitance, the effect of the cell layer capacitance will be visible in the frequencies higher than those at which the double layer capacitance appears.

Table 3: Parameters of OVCA429 cell culture impedance in 7 devices of 8W1E culture plate.

PARAMETERS	DEVICE-1		DEVICE-2		DEVICE-3		DEVICE-5		DEVICE-6		DEVICE-7		DEVICE-8	
		SD		SD		SD		SD		SD		SD		SD
Rsol*1E2	1.93	0.56	2.19	0.90	2.55	1.04	1.88	0.63	1.95	1.05	2.16	0.72	2.36	1.04
Rcells*1E5	2.04	4.45	3.04	4.18	5.24	4.69	1.63	6.42	3.20	6.72	2.81	3.92	3.99	5.51
Rpore*1E3	1.54	3.78	1.48	7.00	1.59	10.12	1.70	4.46	2.03	19.20	2.18	6.52	2.82	18.05
CPE(cells)*1E-9	5.11	3.31	3.94	3.46	2.66	3.60	6.51	4.50	4.36	4.76	4.13	3.76	3.33	4.28
α(cells)*1E-1	8.98	0.75	8.98	0.74	9.43	0.77	8.89	1.05	8.83	1.07	9.01	0.75	9.14	0.89
CPE(dl)*1E-9	9.54	8.78	7.08	17.25	12.28	11.99	11.00	9.40	1.13	28.21	3.87	17.19	1.58	38.82
α(dl)*1E-1	8.36	1.51	8.42	2.16	7.62	1.28	8.26	1.78	10.18	3.18	9.05	2.10	9.50	2.55
CPE(coat)*1E-9	2.43	11.48	4.06	21.42	3.00	29.81	2.07	11.46	10.71	10.73	6.30	12.50	11.03	14.38
α(coat)*1E-1	8.90	0.69	8.56	1.44	8.66	1.98	9.01	0.68	8.02	1.23	8.25	0.91	7.95	1.37
L*1E-7	1.87	8.29	2.65	9.58	2.81	11.10	1.53	11.44	3.36	8.20	3.34	6.36	4.00	7.54
Sigma F	0.0068		0.0085		0.0093		0.0082		0.0112		0.0086		0.0121	

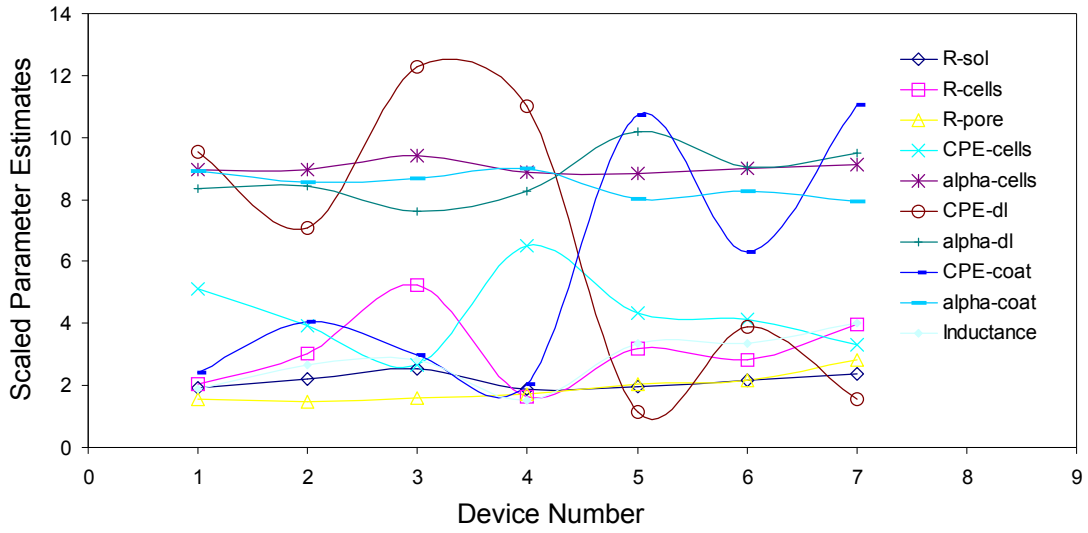

Figure 43: Parameter variation of OVCA429 impedance as a function of device.

Table 3 summarizes the extracted parameters from the circuit model of Figure 42. Figure 43 is the plot of parameter estimates of the equivalent circuit. The addition of cell layers has not only contributed 2 additional impedance elements to the circuit, but also modified the other parameters such as double layer capacitance and pore resistance. The conjugate behavior of the double layer and the coating capacitance is clearly observed

in the plot of Figure 43. This is due to the fact that, given a fixed overall area of the electrode, the double layer capacitance has to decrease to accommodate an increase in the coating capacitance and vice versa. The presence of cells has considerably altered the double layer capacitance. This is because the cells form an intimate and adherent layer to the substrate thereby altering the equilibrium charge density distribution which is spread over a few μm into the bulk of the electrolyte. This alteration of the electrode-electrolyte environment also leads to changes in pore resistance. An important factor to consider is that, unlike their normal counter parts, cancer cells do not cease to multiply upon reaching confluence, hence multiple layers can be formed, which explains the greater device to device variability in the case of OvCa429 measurements (Figure 43) when compared with HBSS measurements (Figure 38). To calculate the area specific parameters, a parameter average for the 7 devices is calculated. This average is then divided by the area of exposed gold electrode (0.049 mm^2) to calculate the cell layer capacitance and multiplied by the area to calculate the cell layer resistance.

Figure 44 is the Bode diagram of device 3 of 8W1E culture well plate with OvCa429 cells and with medium. As indicated earlier, the high frequency region is common to HBSS and OvCa systems. This implies that this section of the impedance spectra is independent of the cells. Hence it is attributed to the polymer covering the gold electrode. Other indicators to this effect are the CPE parameters, namely, magnitude (A) and power factor (n). Due to the thickness of the polymer and its relative permittivity, the A is small compared to the double layer CPE. The n of the coating CPE is closer to unity in the case of good (void free) polymer coatings. The n of metal deposited gold electrodes exposed to simple electrolytes is closer to unity for a smooth deposition of metal. We recall that the power factor of the CPE is an indicator of its fractal nature. For very smooth metal surfaces, the CPE approaches the regime of perfect capacitance with a power factor of 1. In the case of

partially coated smooth metal deposited gold electrodes, both n's have similar values (Table 2). The discriminant in this case is the n of the CPE.

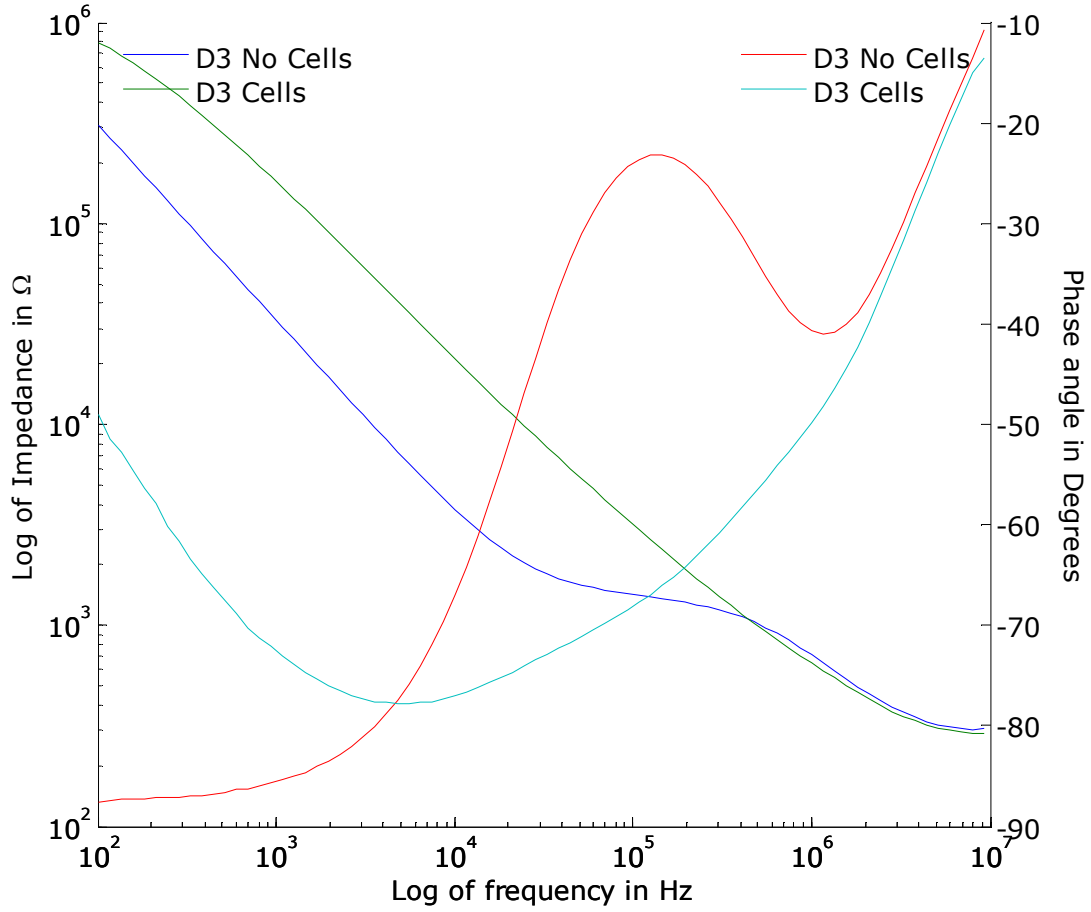

Figure 44: Bode diagram of device 3 with and without cells.

Figure 44 is the comparison of Bode diagrams of OvCa429 and HBSS systems. In the Bode magnitude plot, besides the similarity of the high frequency aspect, the lower frequency section, i.e. the double layer capacitance and solution resistance are considerably altered. The cell layer impedance appears as a single slope. This characteristic is due to the overlap of time constants of the RC elements in the equivalent circuit. In such situations, visual analysis of impedance spectra is rendered difficult. The convolution of time constants is also observed in the complex admittance plot in Figure 45.

The only plane where the semi-circles are discernible is the complex permittivity plane (Figure 41). The equivalent circuit fitting however leads to well determined parameters of the circuit of Figure 42.

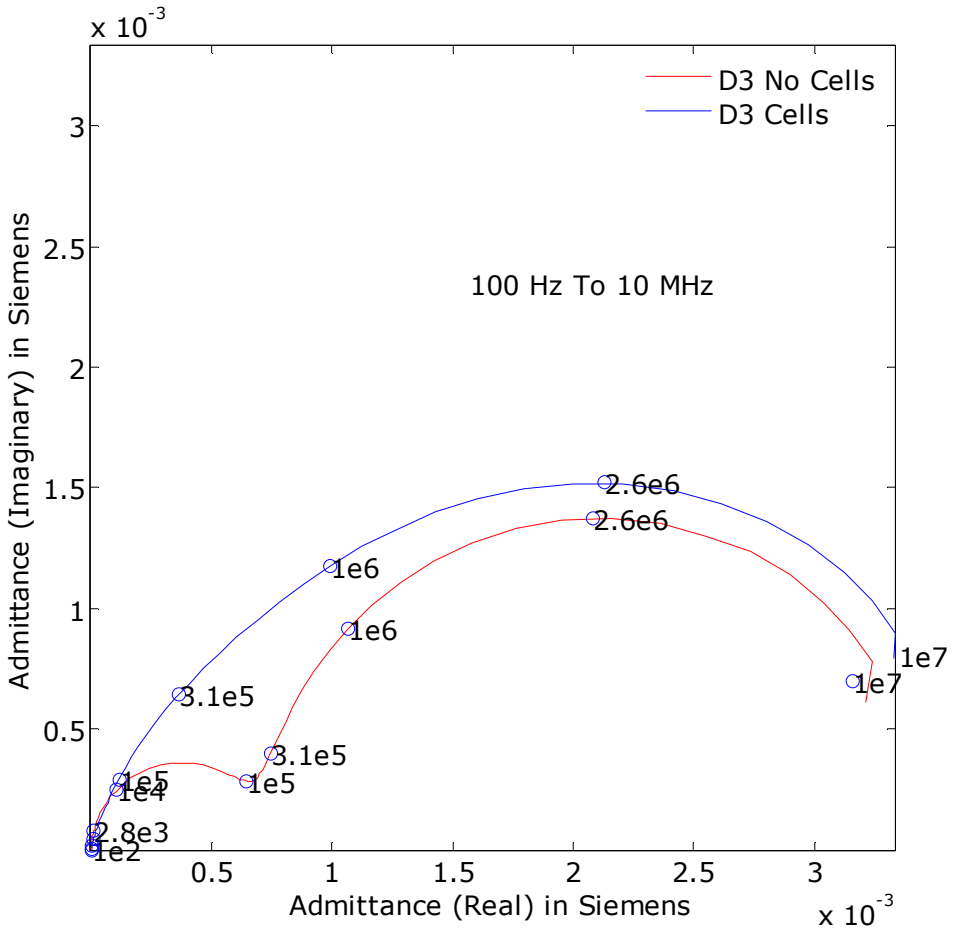

Figure 45: Complex admittance plot of HBSS and OVCA systems.

5.5 Summary

The OvCa429 ovarian cancer cell layers were characterized in terms of electrical equivalent circuit elements. The trans-layer resistance and capacitance are 153.61 Ω-cm^2 and 8.755 μF/cm^2, respectively. Equivalent circuit models developed for device containing HBSS and OvCa429 ovarian cancer cells indicate that the polymer coated regions contribute to the impedance spectrum above a frequency of approximately 100 KHz.

Measurements at high frequencies have facilitated the development of a detailed model which accounts for a variety of effects such as lead inductance and coating capacitance. This model will provide a more accurate basis for physiological parameter estimations using the ECIS cultureware™ than lesser detailed models.

Chapter 6: Effect of Electrode Area on Impedance Evaluation of Tissue and Cell Culture

6.1 Introduction

In this chapter, the effect of microelectrode geometry on the impedance response of four analytes of varying morphological complexity is studied. This experiment was performed to understand a) area dependent material and interfacial parameters, b) material dependent electrode geometry effects and c) the lower limits of microelectrode's geometry for the characterization of various types of biologically relevant materials. The systems chosen for this study are simple electrolyte of conductivity (14.28 mS/cm) comparable to biological fluids, a viscous electrode gel used to reduce the electrode contact resistance in ECG measurements, Human Umbilical Vein Endothelial Cell (HUVEC) culture and excised human skin tissue. With this choice of analytes, a wide range of systems of varying structural complexity are covered, from a simple electrolyte to complex, high impedance, heterogeneous skin tissue.

Electrodes are widely used in medicine to electrically measure, image, and treat cell/tissue conditions [81-83]. Microelectrode based devices offer many advantages over their conventional counterparts such as spatial resolution, small signal, batch fabrication, and portability among other advantages. In microbiological and cell culture studies, the spatial resolution of microelectrodes offers the ability to investigate a single cell or a group of cells. Planar microelectrodes are becoming increasingly common in electrical investigation of biological matter. Unlike the parallel plate configuration, the

field distribution in planar electrodes is not simple in the case of coplanar geometries. Consequently, the measured impedance response is influenced by the geometry of the electrodes. Optimization of electrode geometry and the study of field distribution effects for specific applications have been subjects of much research interest recently [84-86].

Despite the advantages, microelectrodes face the challenge of interfacial polarization in bipolar measurements. Interfacial polarization occurs due to the inability of charge carriers to move across the solid-liquid barrier. The result of this barrier is accumulation of charges in response to an applied potential to the electrode. This space-charge distribution gives rise to a capacitive effect. Since capacitance is directly proportional to area, interfacial polarization is an area dependent property. In the case of microelectrodes, this effect can lead to enormous impedances easily reaching the limit of contemporary measurement equipment, particularly at low frequencies. At small electrodes, high current density can lead to heating and other non-linear effects.

6.2 Materials Used

a) Potassium Chloride (KCl)

The binary electrolyte used in this study is a commercially available 0.85% potassium chloride (KCl) standard solution with a conductivity of 14.28 mS/cm. KCl, a very stable salt, is a standard for conductivity measurements.

b) HUVEC cell culture

Human umbilical endothelial cells, HUVECs, (Clonetics Corp., San Diego, CA) were cultured at 37°C and 5% CO_2 in endothelial cell growth medium (EGM; Clonetics Corp.) which was supplemented with the following: 10 ng/ml human recombinant epidermal growth factor, 1 µg/ml hydrocortisone, 50 µg/ml getamicin, 50 ng/ml amphotericin B, 12 µg/ml bovine brain extract, and 2% fetal bovine serum (amounts indicate final concentration). HUVECs were subcultured when they were 70% confluent, and the medium was

changed every 48 hours thereafter. HUVECs passaged less than six times were used in experiments. Twenty-four hours after inoculating cells in the cylinders attached to the electrodes, the normal medium was replaced by Hanks' Balanced Salt Solution (HBSS; Mediatech, Inc., Herndon, VA) without phenol red.

c) Spectra 360™ Electrode gel

Spectra™ is a commonly used conductive gel for surface application in electrical recordings through human skin such as Electrocardiogram (ECG), Electrical Impedance Tomography (EIT) etc. It reduces contact resistance and promotes even contact between skin and recording electrode. It is clear blue in color and free of salts (manufacturer description).

d) Skin tissue

The skin samples were obtained from the U.S. Cell and Tissue Bank in Ohio, and were kept in a freezer until measurements were performed. Shortly before the experiments, sufficient samples were transported in dry ice from the freezer to the experimental setting. Samples were sectioned to ensure full coverage of the electrodes. They were dabbed on dry paper to remove any excess water and then placed on the Electrode (stratum corneum (SC) side down) and lightly pressed to ensure good contact.

6.3 Experimental Methods

6.3.1 Microelectrode Fabrication

Multiple microelectrode devices each with an array of four micro-electrodes were fabricated using photolithography and micromachining techniques. The fabrication proceeds by depositing chromium (250 Å) and gold (1400 Å) onto a 2-inch glass wafer. Next, photolithography was performed to define the electrode length using S1813 positive photoresist. After development, the resist thickness was measured using a profilometer to be approximately 2 μM. The electrodes were then electroplated with gold to an average

thickness of approximately 1.7 µm. The wafers were solvent cleaned in acetone and methanol, after which another photolithography process was performed to define the 4 different electrode areas (electrode tips). The average gold thickness on the tips was approximately 4 µm. After removing the Cr/Au seed layer, 2 layers of S1813 resist were spun onto the wafers for another photolithography process. This lithography covers all other areas of the device except the contact pads and the electrode tips (Figure 46, i). The bonding pads were used to apply voltage/current to the tips. The fabricated devices are shown in Figure 46. The four devices of various electrode tip sizes are identified in Figure 46 (ii). The electrode diameters are 500 µm (a), 250 µm (b), 100 µm (c) and 50 µm (d). Upon completion of device fabrication, 5 mm internal diameter cloning cylinders are attached to the microelectrode devices (Figure 46, iii) for characterization of KCl and HUVECs

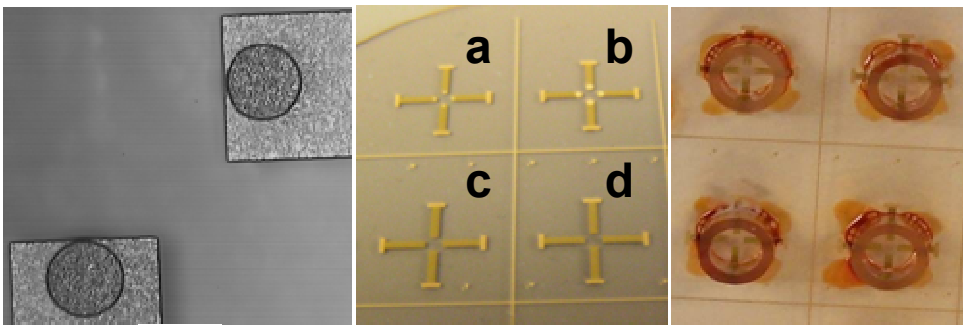

(i) (ii) (iii)

Figure 46: (a) Enlarged optical image of 2 microelectrode sensors showing lithographically defined electrode tips. (b) Photograph of 4 gold-plated microelectrodes devices on a glass wafer. (c) Photograph of electrode devices with cloning cylinders attached using photoresist as adhesive.

6.3.2 Impedance Measurements

An Agilent 4294A impedance analyzer and a pseudo 4 point probe which facilitates bipolar measurements, in tandem with a Cascade™ microprobe station was used for impedance measurements.. Cabling and open-short-load calibrations were performed to null the connection and fixture parasitics.

Measurements were performed from 40 Hz to 100 MHz, with a signal level of 25 mV. The measurement setup is shown in Figure 32.

First, measurements were performed with split thickness skin samples placed on the electrodes (Figure 46, ii). After completion of skin sample measurements, spectra™ was dispensed onto the electrodes to record its impedance. KCl and HUVEC measurements were performed on separate devices.

6.4 Results

6.4.1 Impedance Characterization of KCL

Figure 47 is the Bode plot of KCl for the four electrode sizes, a-d in Figure 46, (ii). The interfacial polarization regime is identified by the low frequency (<10 kHz) power law behavior of impedance magnitude. This slope shifts upwards with a decrease in electrode area due to the inverse relationship between electrode area and interfacial capacitance. At high frequencies (>10 kHz), a second frequency dispersion is observed, arising from the effect of polymer coating (Figure 46, i). The polymer coating is used to define the area of electrodes (electrode tips) by lithography and isolate the rest of metallic electrical contact from contributing to the electrochemical impedance. Although not contributing to the electrochemical impedance, the polymer coated area adds a separate impedance component known as coating impedance. The second dispersion is also visible in the Bode phase plot, where a second phase minima is seen for all electrode sizes except the 500 µm electrode. The absence of second dispersion from the largest area electrode is attributed to the lower interfacial impedance of the larger (500 µm) electrode. The Au-KCl system does not exhibit any apparent non-linearity as a function of electrode area. The low frequency noise component gains slight prominence for the lowest electrode area (50 µm) and could be due to the performance of measurement electronics, which is impedance range dependent [17]. For 50 µm electrode diameter the impedance is

approximately 8 MΩ, as opposed to lower values (approximately 100 KΩ) for larger electrodes (500 μm). This leads to relatively higher phase noise for the smaller device.

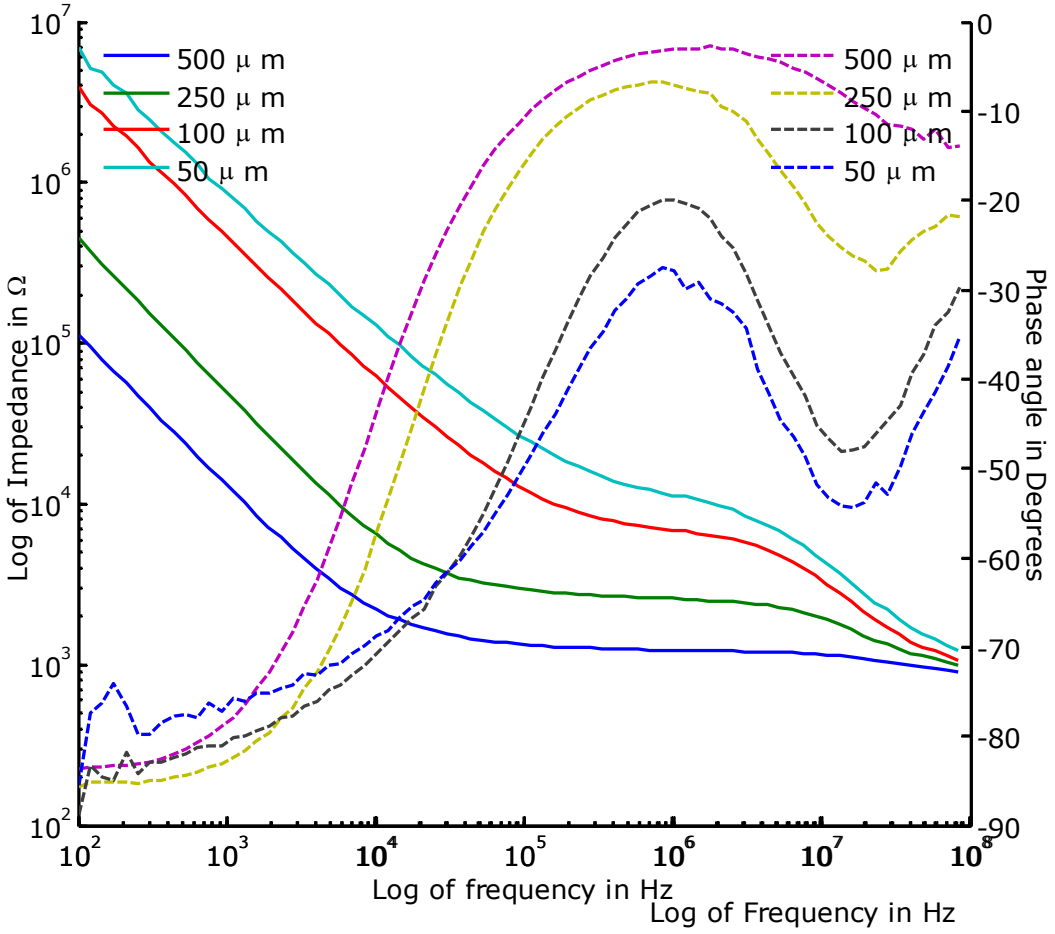

Figure 47: Bode diagram of KCl in four devices of varying electrode area.

The complex admittance representation of the KCl dataset is shown in Figure 48. In the admittance plane, frequency descends from right to left. The full formed semi-circles at lower frequencies are due to the double layer capacitance and solution resistance. The semi-formed semi-circles are due to the dispersion in the coating. It is worthy to note the inverse behavior of coating and double layer capacitance. For the devices where the double layer semi-circle is more completely formed the semi-circle due to the coating

capacitance is less completely formed. For a fixed total area of the electrode; either the double layer or the coating capacitance can increase only at the expense of the other, hence the contrasting behavior. The resistance determines the radius of the complex plane plot, where as the capacitance determines the extent of the semi-circle in the complex plane.

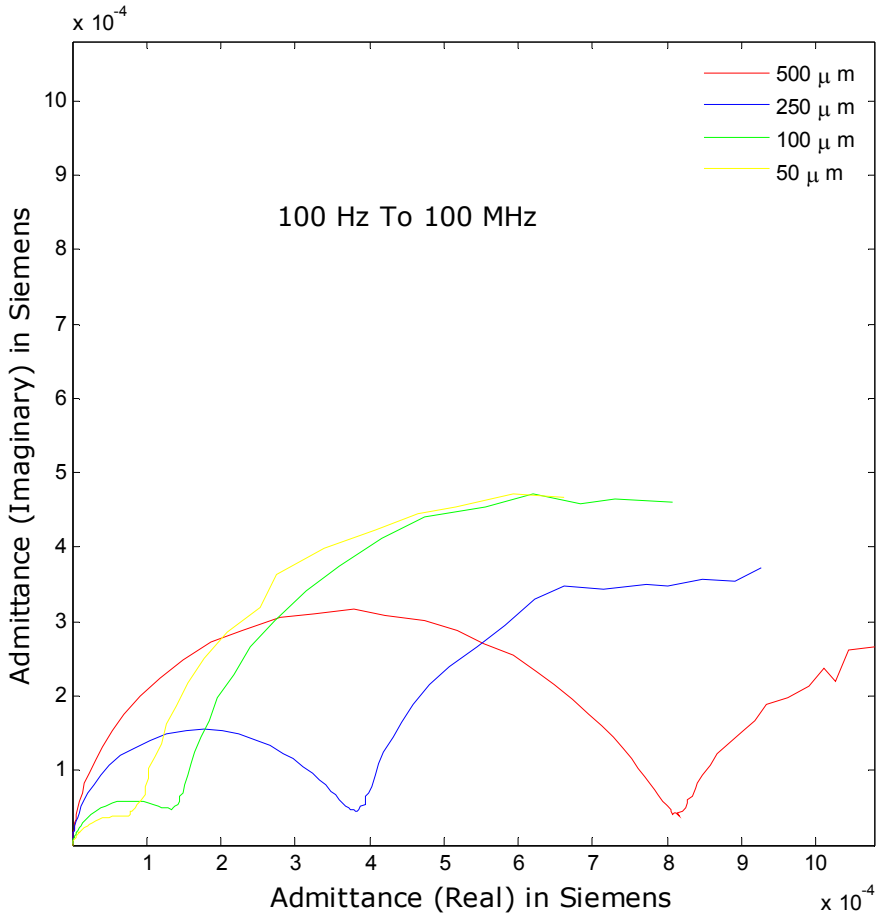

Figure 48: Complex admittance plot of KCL in four devices of varying electrode area.

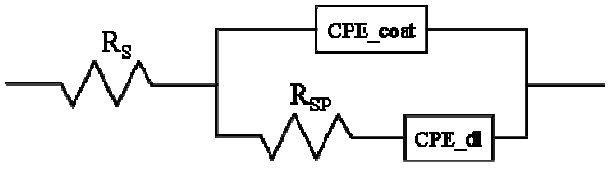

Figure 49: Equivalent circuit used to model the data of KCl. The R_s element is omitted in the modeling of Spectra™.

The electrical equivalent circuit shown in Figure 49 is used to parameterize the Au-KCl system. The extracted parameters are listed in Table 4. The quantity R_s was not required in the parameterization of 500 μm electrode. This is also consistent with the absence of high frequency coating dispersion for this electrode, as explained earlier. The spreading resistance (R_{sp}) and double layer capacitance (C_{dl}) are strongly correlated to the electrode area, consistent with their physical basis. It is worthy to note the trends of n-dl and n-coat from Table 4. These are power factors of double layer and coating CPE's respectively. The quantity n-dl decreases with decrease in electrode area. This can be attributed to non-uniform current distribution. Considering n-dl and n-coat together, one decreases (n-dl) and the other (n-coat) increases. As the electrode area decreases, more of the AC signal travels through the coated area, hence the coating CPE power factor (n-coat) increases. On the other hand, with decrease in electrode area, the current is more unevenly distributed and not confined to the gold electrode tips. This leads to a lower value of n-dl due to non-uniform current distribution.

The spreading resistance given by the eq. (5.1), is expected to increase with electrode area.

$$R_{sp} = \frac{2\rho}{4r} \quad \text{.....5.1}$$

where ρ is the resistivity of the KCl solution in ohm-cm, and r is the radius of the electrode sensors and R_{sp} is the spreading resistance.

In the measured frequency range, the contribution of coating capacitance can be reduced by either increasing the exposed area of the electrode or by increasing the thickness of the polymer coating. The use of hydrophobic coatings such as SU-8 can reduce the drift in the sensor due to water uptake in the polymer. Alternatively, several other approaches can be adopted to

increase the interfacial capacitance including electroplating and surface roughening.

Table 4: Electrical equivalent parameters of the impedance data for KCl electrolyte.

Parameter/electrode	500 μm	250 μm	100 μm	50 μm
Rsol (Ω)		7.19E2	7.78E2	7.62E2
Rsp (Ω)	1.33E3	2.16E3	7.30E3	1.36E4
Ydl (S.sn)	2.02E-8	4.61E-9	7.76E-10	5.36E-10
ndl	0.94	0.95	0.89	0.86
Ycoat(S.sn)	4.50E-9	4.43E-10	4.20E-11	4.71E-11
ncoat	0.57	0.77	0.87	0.85

The parameterization of spreading resistance into spreading and solution resistances was necessary to achieve a good fit, although not intuitive. It is necessitated due to the coating capacitance. In the normal gold-electrolyte system, the high frequency impedance is purely due to solution resistance. Beyond the interfacial regime, the impedance response would be a horizontal line (resistive) well into the GHz frequency. For planer electrodes the value of resistance commonly referred to as the spreading resistance is determined by the area of the metal in contact with the electrolyte. In the present scenario, at lower frequencies, the solution resistance is due to the exposed area of the electrode (lithographically defined). However, at higher frequencies the AC signal begins to permeate through the coated area of the electrode. This necessitates the inclusion of two separate resistances to achieve a good fit. Since the exact area of the coated metal that contributes to the impedance is ill defined, this parameter is not well characterized.

There is approximately 20 to 60 μF/cm^2 of (double layer) capacitance for every cm^2 of electrode area for metal in an electrolyte. This is supported by the measured data: 20.6 μF/cm^2 (500 μm electrode), 18.8 μF/cm^2 (250 μm electrode), 19.8 μF/cm^2 (100 μm electrode), and 54.6 μF/cm^2 (50 μm electrode). The much larger value of double layer capacitance for 50 μm electrode could be due to the increased current density.

6.4.2 Impedance Characterization of Spectra™ Gel

The impedances of the four electrode sizes measured by using spectra™ as the analyte are fairly similar to KCL impedances as seen in Figure 50. The measurements beyond 13 MHz are excluded from this dataset as they were deemed to be parasitic. The interfacial polarization is indicated by the low frequency power law slope. As the electrode size decreases the magnitude of the impedance increases, which is consistent with the impedance behavior of a capacitor. One departure from the expected behavior is the impedance magnitude of 50 μm electrode, which exhibits a sharper coating dispersion (steep slope) in comparison with the other electrodes. This can be attributed to the higher current density effects. The inverse relationship between impedance magnitude and electrode area seen in Figure 50 is anticipated due to the relationship in eq. (5.2). In particular, as the area increases, capacitance increases (as per the equation 5.2), and subsequently impedance decreases.

$$C = \frac{\varepsilon_o \varepsilon_r A}{d} \quad \text{.....5.2}$$

where ε_o = 8.86x10^{-14} F/cm (permittivity of free space), ε_r is the relative permittivity, A is the area, d is the screening length (electrolyte dependent) i.e., the distance from the electrode surface where the potential falls to 1/e of the potential at the surface of the metal.

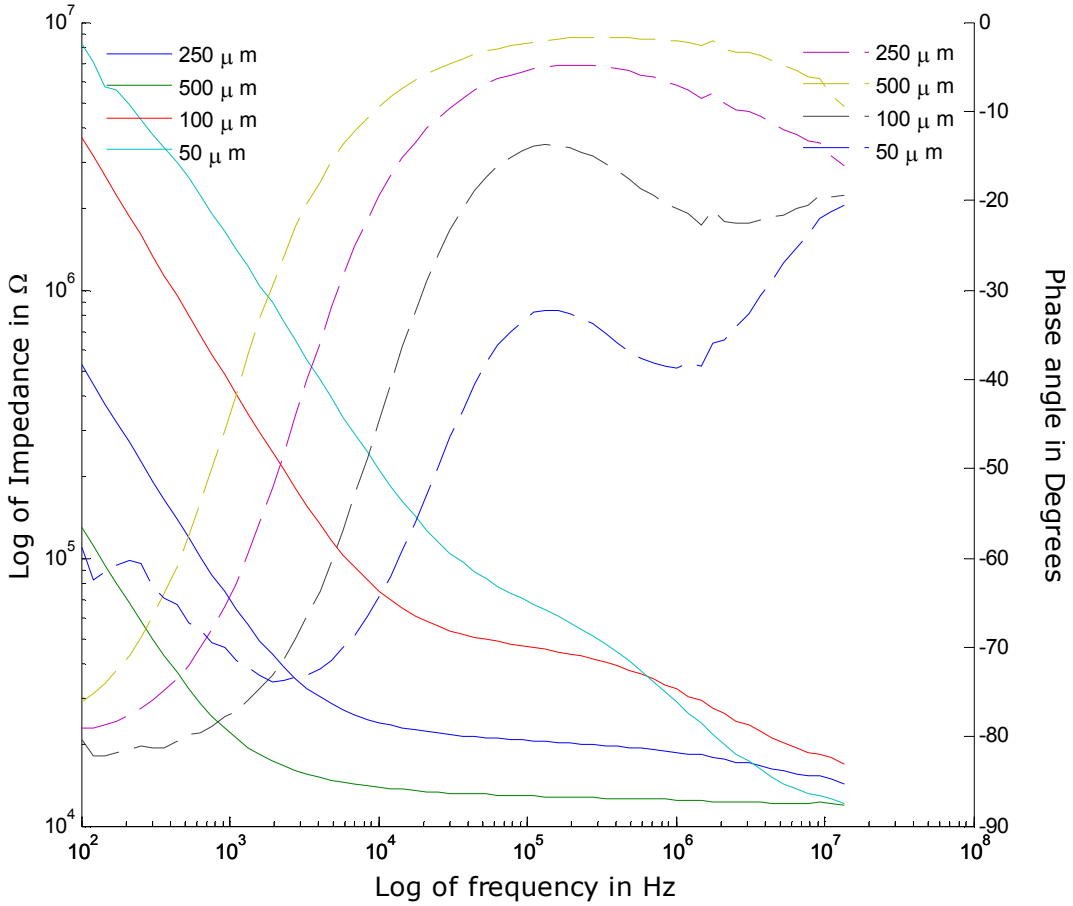

Figure 50: Bode diagram of spectra 360 electrode gel for four devices of different electrode geometries.

In comparing spectra™ with KCl, the resistance of spectra™ is lower than the KCl. This is noted from the extrapolation of plateau region on to the y-axis of the Bode plot, or by the x-intercept of the semi-circle in the admittance plot (Figure 48). Consequently, the coating dispersion occurs much earlier in the frequency scale for spectra™. This indicates excellent conductivity of this gel, comparable to the liquid electrolyte.

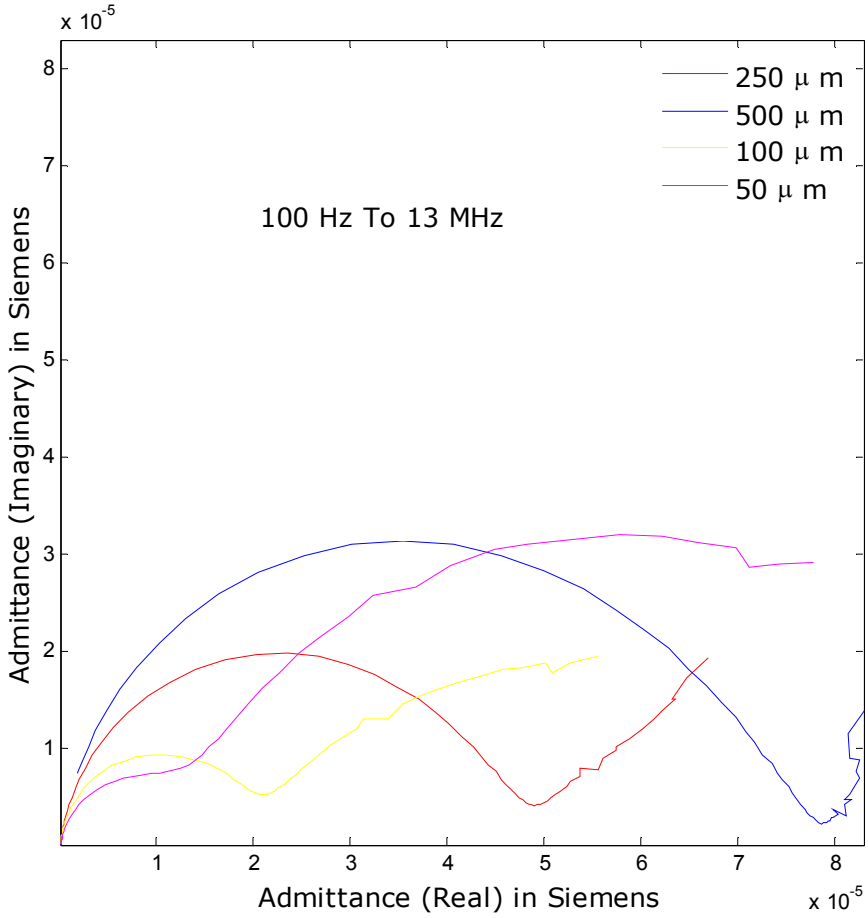

Figure 51: Complex admittance plot of spectra in four devices of varying electrode area.

The complex admittance plots in Figure 51 indicate a similar trend as the complex admittance plots of KCL (Figure 48). Table 5 summarizes the extracted parameters of the Au-spectra™ system. The impedance data of spectra™ was also fitted using the circuit of Figure 52. The solution resistance element was not necessary for data fitting in this case, due to the truncated frequency range. The fit for 250 μm electrode was unsatisfactory and hence omitted. The parameters listed in the Table 5 display good correlation with electrode geometry. It is noted that the spectra™ impedance values are close to those of KCl. This implies good conductive characterestics of spectra™.

Table 5: Electrical equivalent parameters of the impedance data for Spectra™ electrode gel.

Parameter/electrode	500 µm	250 µm	100 µm	50 µm
Rsp (Ω)	6.22E3	6.96E3	1.53E4	2.13E4
Ydl(S.sn)	1.05E-7	3.13E-7	5.68E-8	7.98E-8
ndl	7.43E-1	7.41E-1	6.89E-1	6.70E-1
Ycoat(S.sn)	4.78E-12	1.16E-6	2.95E-13	2.09E-13
ncoat	9.00E-1	1.94E-1	1.00	1.00

6.4.3 Impedance Characterization of HUVEC

The HUVEC culture system consists of a cultured cell above the planar electrodes. The cells form a confluent adherent layer on the electrode. The closest approach of the cell layer (cell-substrate separation) to the electrodes is few tens of nanometers. The screening length in electrolytes of physiological concentrations is comparable to that of KCl. The expected impedance behavior of this system would comprise of an interfacial component, a cell layer component and the coating component.

From the Bode diagram of HUVEC (Figure 52), a mid frequency (~ 10 kHz) dispersion attributed to the cell layer is observed in addition to the two dispersions observed in the KCL system. The impedance of an electrode-coating-electrolyte system is modified by the growth of a confluent cell layer. In the examination of impedance data with multiple dispersions, it is challenging to deconvolute the individual impedance contributors.

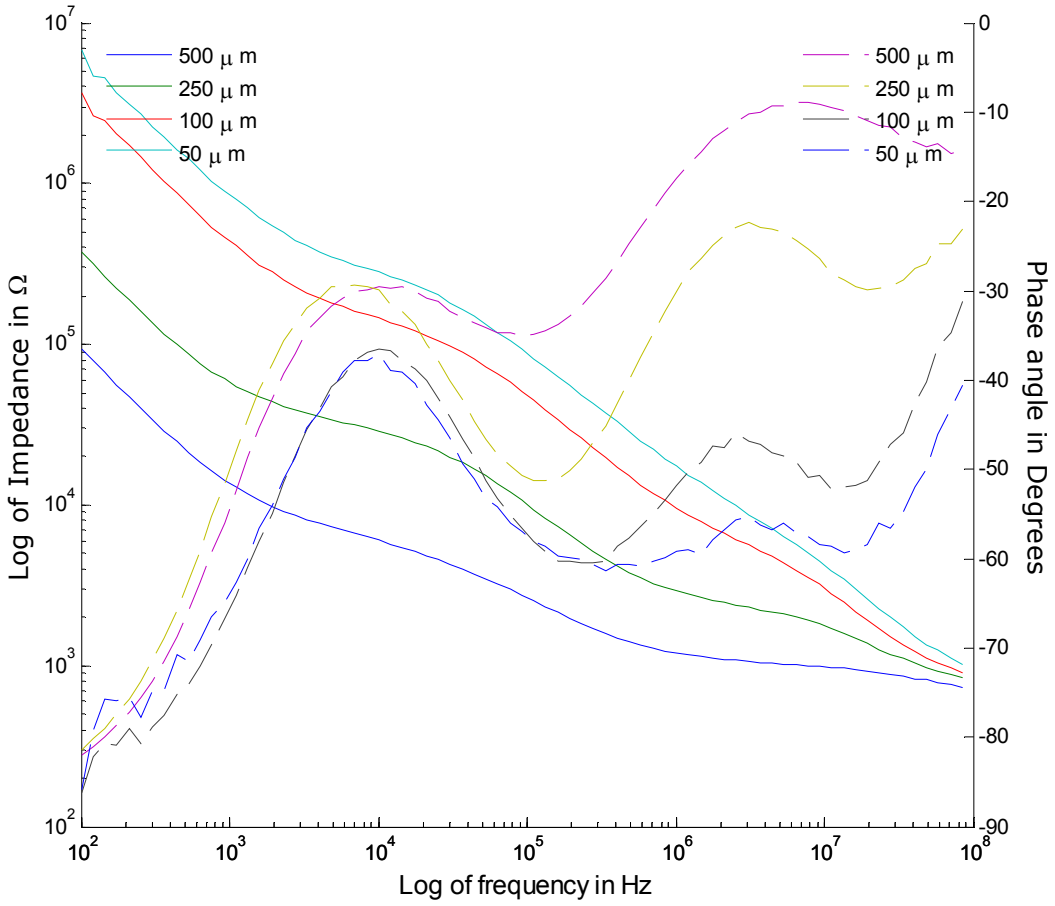

Figure 52: Bode diagrams of HUVEC in four devices of varying electrode area. Three phase minimas are observed due double layer, cells and coating in that order.

The sequence in which the dispersions due to the double layer, coating and cell CPE appear is dependent upon the penetration depth of the AC signal and hence the magnitudes of these CPE's. In the present case, the AC signal has to first get through the double layer capacitive barrier. At even higher frequencies (approximately 50 KHz), the AC signal can penetrate the cell layer which is adjacent to the electrode surface. At the higher frequencies (approximately 1 MHz), the coating impedance becomes comparable to the series combination of double layer and cell layer capacitances; hence AC passes indiscriminately from all areas of the electrode. At this point the cell

constant is ill defined, unless measurement is recorded at high enough frequencies (>10 MHz) where a resistance plateau can be attained. At these frequencies a new cell constant can be defined, which is representative of the overall area of the electrode (coated and exposed).

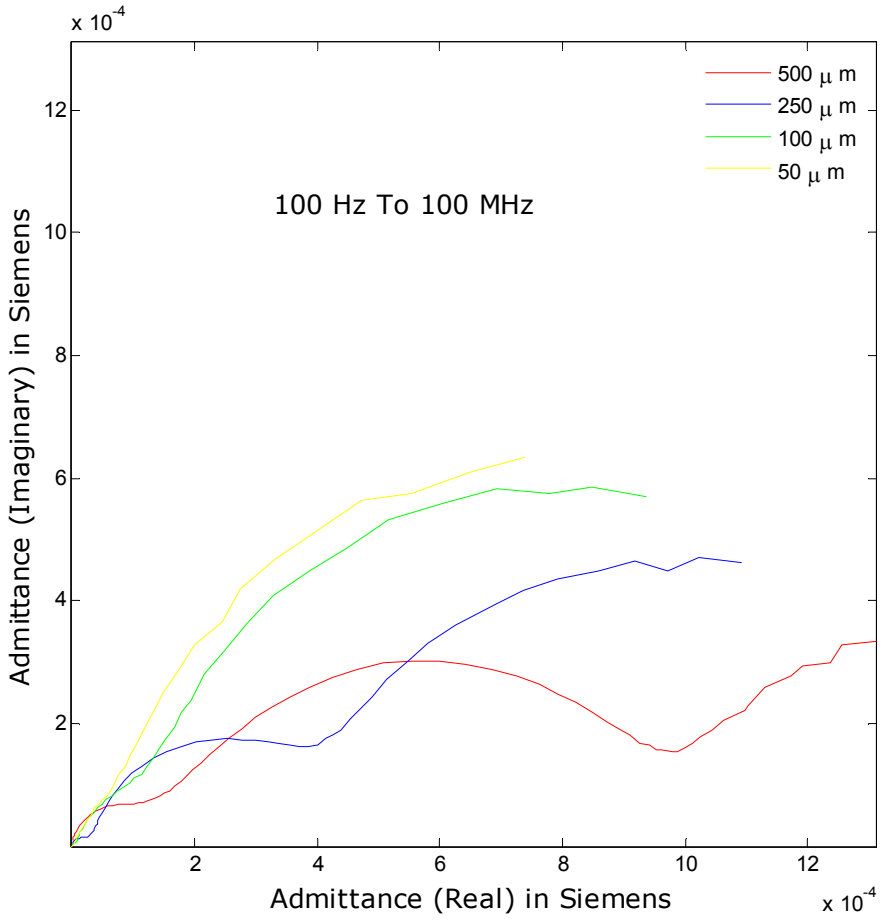

Figure 53: Complex admittance plot of HUVEC on devices of variable electrode area.

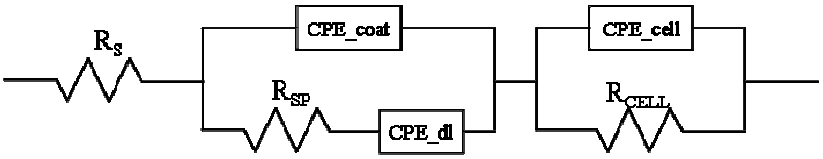

Figure 54: Equivalent circuit used to model the impedance response of HUVECs cultured on microelectrode devices. R_s is solution resistance, R_{sp} is the spreading resistance, CPE_dl is the double layer constant phase element (CPE), CPE_coat is the coating CPE, CPE_cell is the cell CPE, and R_{cell} is the cell layer resistance.

Figure 53 is the admittance spectra of HUVEC culture on four different electrodes of varying geometry. The three dispersions can be clearly seen in 250 and 500 μm electrodes while it is less defined in the other two electrode sizes. It is noteworthy that the separation of semi-circles in the admittance plane is in accordance with the magnitude of the phase minima. Larger electrode size leads to lower phase minima and well separated semi-circles in the complex admittance plane.

Table 6 lists the extracted parameters of HUVEC by equivalent circuit fitting, using the circuit in Figure 54. The cellular parameters can be clearly distinguished by the value of constant phase element. The cell layer resistance is well above the value of solution resistance, as expected, due to the high resistance of the cell layer. Besides contributing an additional R-CPE element, the cell layers considerably alter the interfacial polarization due to redistribution of ionic charge in the near vicinity of the electrode.

Table 6: Electrical equivalent parameters of the impedance data for HUVEC.

Parameter/electrode	500 µm	250 µm	100 µm	50 µm
Rsol(Ω)	5.91E2	6.78E2	6.89E2	5.80E2
Rsp (Ω)	3.53E2	1.42E3	3.61E3	4.07E3
Ydl(S.sn)	2.19E-8	5.49E-9	6.52E-10	4.04E-10
ndl	0.96	0.95	0.94	0.91
Ycoat(S.sn)	2.24E-11	5.18E-11	2.45E-11	3.82E-11
ncoat	0.95	0.90	0.93	0.91
Rcell(Ω)	6.72E3	3.22E4	1.39E5	2.83E5
Ycell(S.sn)	4.53E-8	1.94E-9	3.01E-10	3.03E-10
ncell	0.69	0.81	0.83	0.79

6.4.4 Impedance Characterization of Human Skin

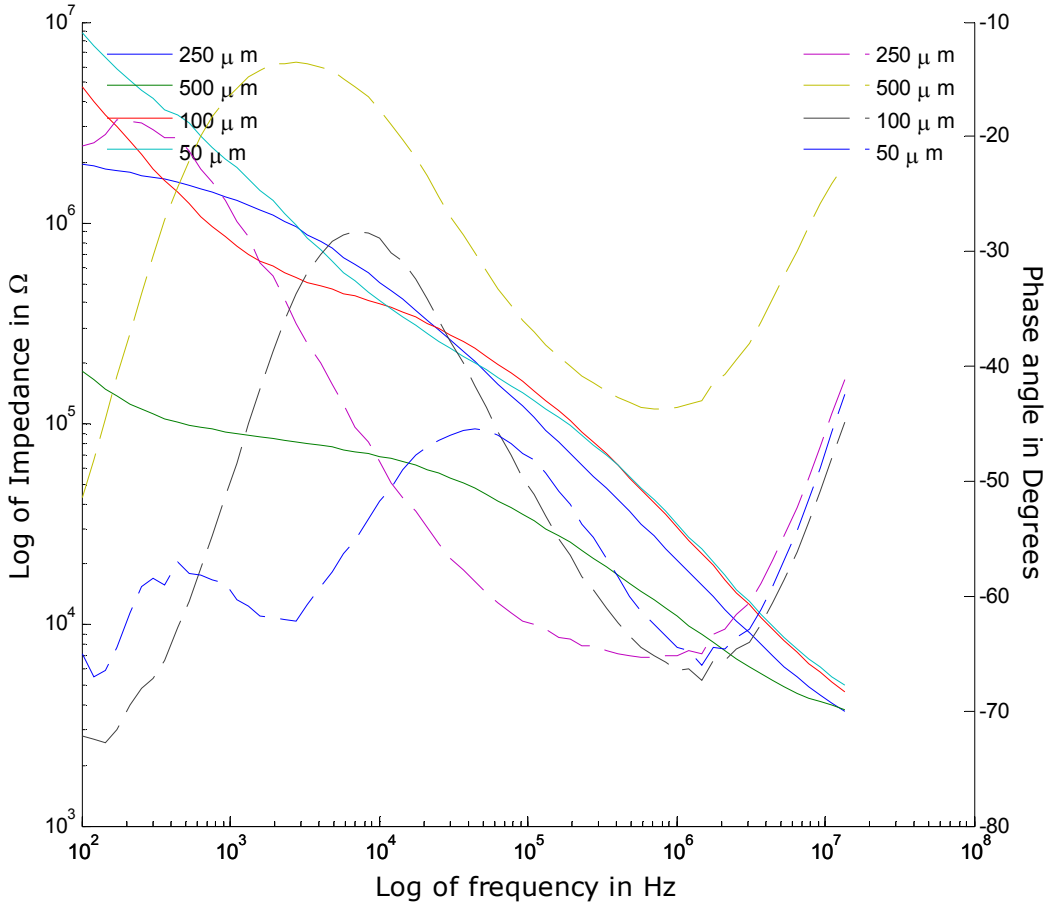

Figure 55: Bode diagram of human split skin tissue measured on devices of different electrode areas.

Figure 55 is the Bode magnitude plot of excised human skin tissue measured with four devices of varying electrode area. The impedance plots of skin are a marked departure from the previous three systems, namely, KCl, spectra™ and HUVEC. There is no clear relation between electrode area and interfacial or bulk properties. This highlights the challenge in the impedance evaluation of complex heterogeneous tissue such as skin using microelectrodes. Skin tissue is highly heterogeneous, comprising of Stratum Corneum (SC), fat, hair follicles among other heterogeneities. The impedance depends on the placement and orientation of the sample. In the case of microelectrodes, the

measured impedance is highly localized depending upon the constituent of skin tissue in the near vicinity of electrode. Unless the position of the electrode is precisely controlled, on a predetermined area of the skin sample to measure its impedance, the impedance data will be a function of electrode position.

6.5 Summary

To summarize, the impedance response of KCl and spectra™ show interfacial polarization and solution resistance effects. The parameter n-dl shows a decreasing trend with electrode size, falling sharply below 100 μm electrode diameter, indicating non-linear current distribution effects. The HUVEC electrode system exhibits distinct frequency dispersion at approximately 50 KHz due to the resistance and capacitance of the cell layer. The impedance response of excised skin could not be correlated with the electrode size due to the high degree of heterogeneity in skin tissue. All electrode sizes, displayed high frequency dispersion due to the polymer coating on the electrodes. The frequency of occurrence of this dispersion was material dependent, occurring at approximately 8 MHz for KCl and approximately 3 MHz for spectra™.

Chapter 7: CellMap System Implementation

7.1 Introduction

In this chapter, the CellMap system is implemented to study the adhesion, spreading, confluence and detachment of OvCa429 Ovarian cancer cells. A detailed account of the CellMap system is provided in Chapter 3. OvCa429 cell culture is monitored using the CellMap system beginning in a suspended state, through progression to confluence and ending in cell detachment. The impedance of cell culture medium (HBSS) is monitored for 160 hours to serve as a control. OvCa429 impedance is monitored for 116 hours. The objective of the work presented in this chapter is a) to detect the in-vitro behavior of OvCa429 cells, b) to identify the cell-substrate and cell-cell impedance parameters that reflect adhesion, spreading, motility, confluence and detachment of OvCa429 cells on the substrate and c) to show that the impedance of cell culture medium alone does not exhibit the impedance characteristics of those of OvCa429 cell cultures.

7.2 Experimental Method

Impedance of the cell culture medium (HBSS) was monitored by inoculating the culture cylinder with medium. IS scans were performed on all 8 electrodes at various times. A total of 6 recordings were performed over a period of 160 hours. The medium containing electrode array was placed inside a 37 °C incubator between measurements. This was done to replicate the procedure with which cell culture measurements are performed.

OvCa429 cell behavior was monitored by inoculating the culture cylinder with 10^6 cells/cm^2 concentration of OvCa429 cells. The culture inoculated electrode array was left inside the incubator for a period of 2 hours to allow the cells to stabilize. If the stabilization procedure was not followed, cells would not have grown on the substrate (experimentally verified). Culture containing electrode array was transported to the measurement lab for impedance measurements. The electrode array is placed inside a 5% CO_2 incubator at 37 °C between measurements. A total of 15 measurements were obtained over a period of 116 hours. The cell culture medium was replaced by 0.25% Trypsin-EDTA at 68 hours of cell culture.

7.3 Impedance of Cell Culture Medium

Figure 56 is the 3D Bode phase diagram of OvCa29 cell culture medium monitored for 160 hours. The first row of phase diagrams indicates time as zero because of rounding. These measurements were performed within the first hour of dispensing the cell culture medium. The Bode phase angle plots display very small deviation over time, with the shape of the phase curve essentially unchanged over a period of 160 hours. The observed shape of the phase curve is that of an equivalent circuit containing a capacitor in series with a resistor. At lower frequencies, the phase angle is capacitive (approximately 75 degrees) due to the blocking effect of the interfacial capacitance and at higher frequencies it is resistive (approximately 5 degrees) due to the solution resistance.

Consequent to the observed shape of the phase curve a series equivalent circuit comprising a Constant Phase Element (CPE) and a resistor, shown in Figure 28 (a), is used to model the impedance data of HBSS. We recall that the CPE represents the interfacial capacitance and the resistance models the spreading resistance of the medium. The plots of the estimated parameters namely, solution spreading resistance, CPE-magnitude and CPE-n, are shown in Figure 57 through Figure 59 respectively.

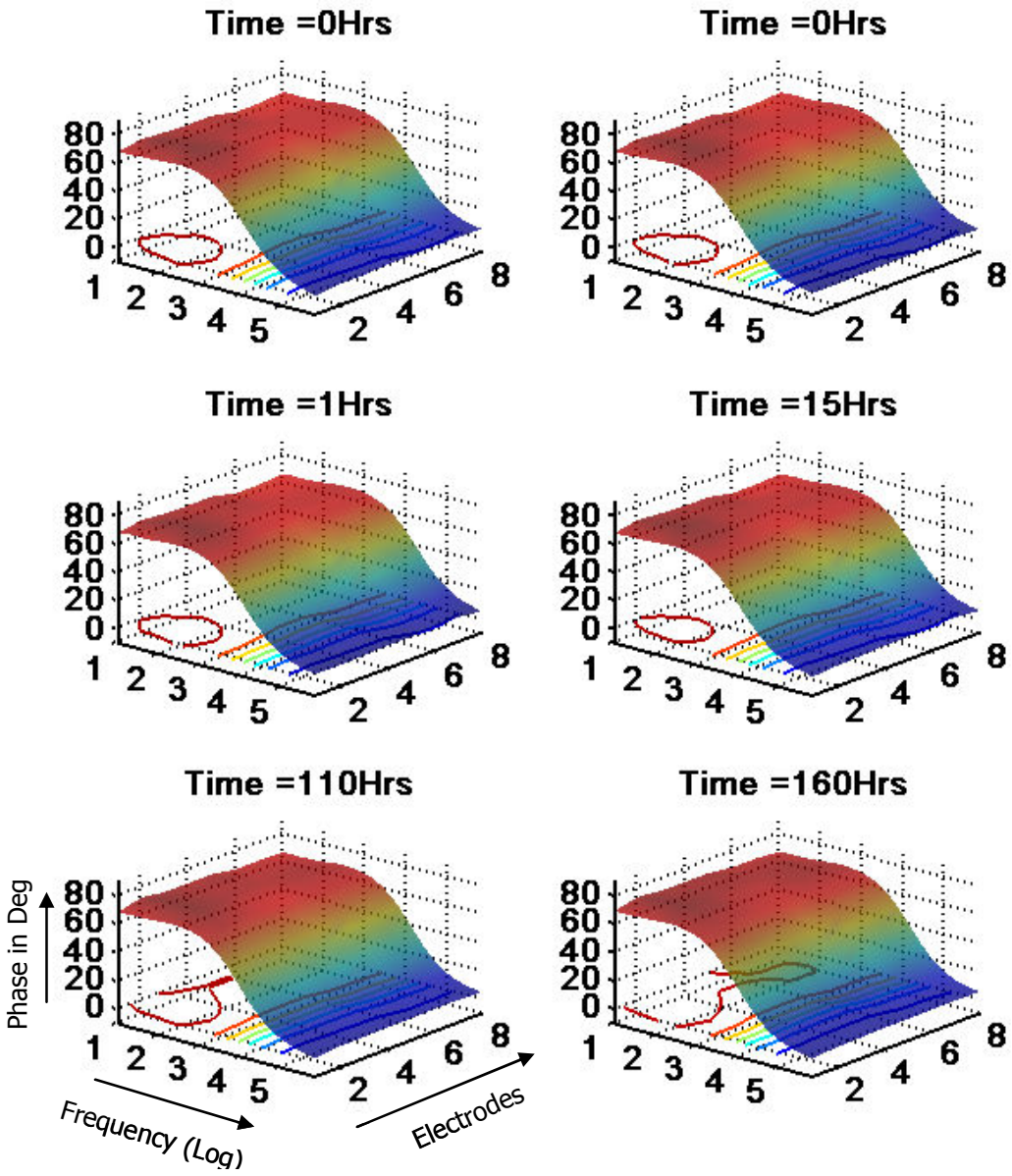

Figure 56: Bode phase diagram of HBSS medium monitored for 160 hours. The first two readings are taken within the first hour of dispensing; they are represented as time zero due to rounding.

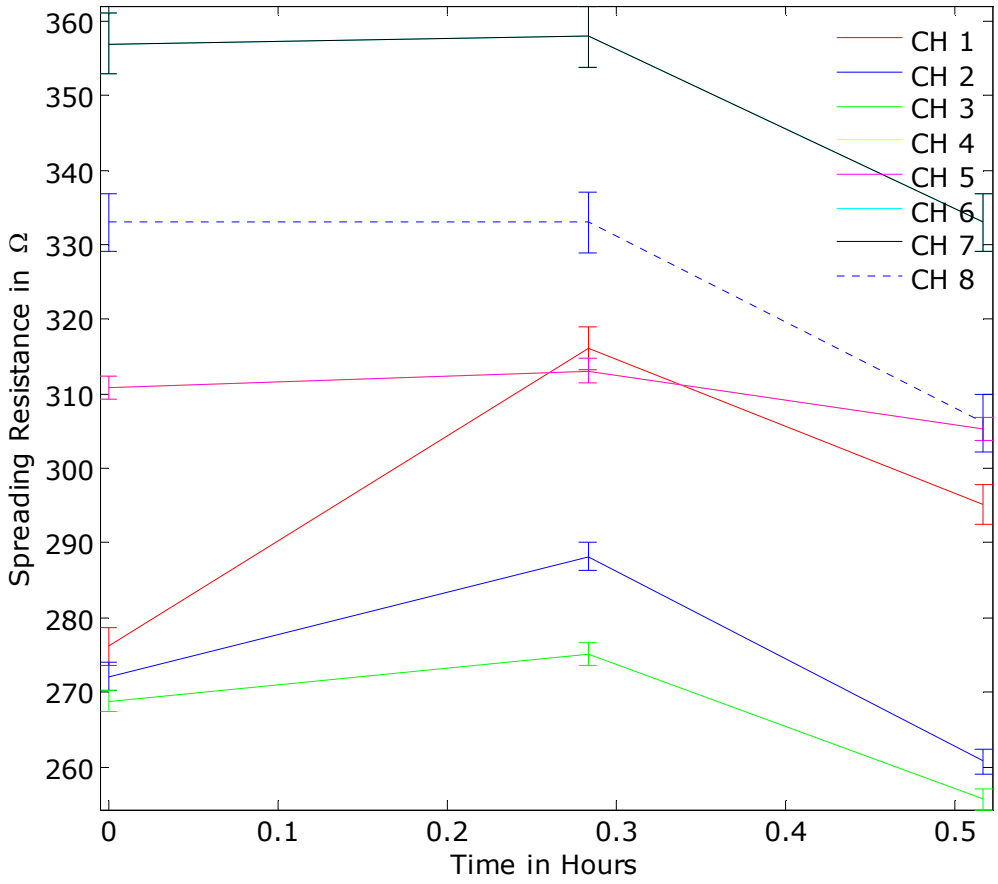

Figure 57: Spreading resistance of cell culture medium (HBSS) as a function of time for 8 electrodes. An approximately 20 Ω range is observed for individual electrodes over a period of 160 hours.

From Figure 57, which is the plot of spreading resistance of electrodes as a function of time, it is observed that the spreading resistance maintains a steady value within a range of approximately 20 Ω. This is approximately 6% deviation from the average value of spreading resistance for each electrode. The deviation in solution resistance could be due to environmental effects such as temperature.

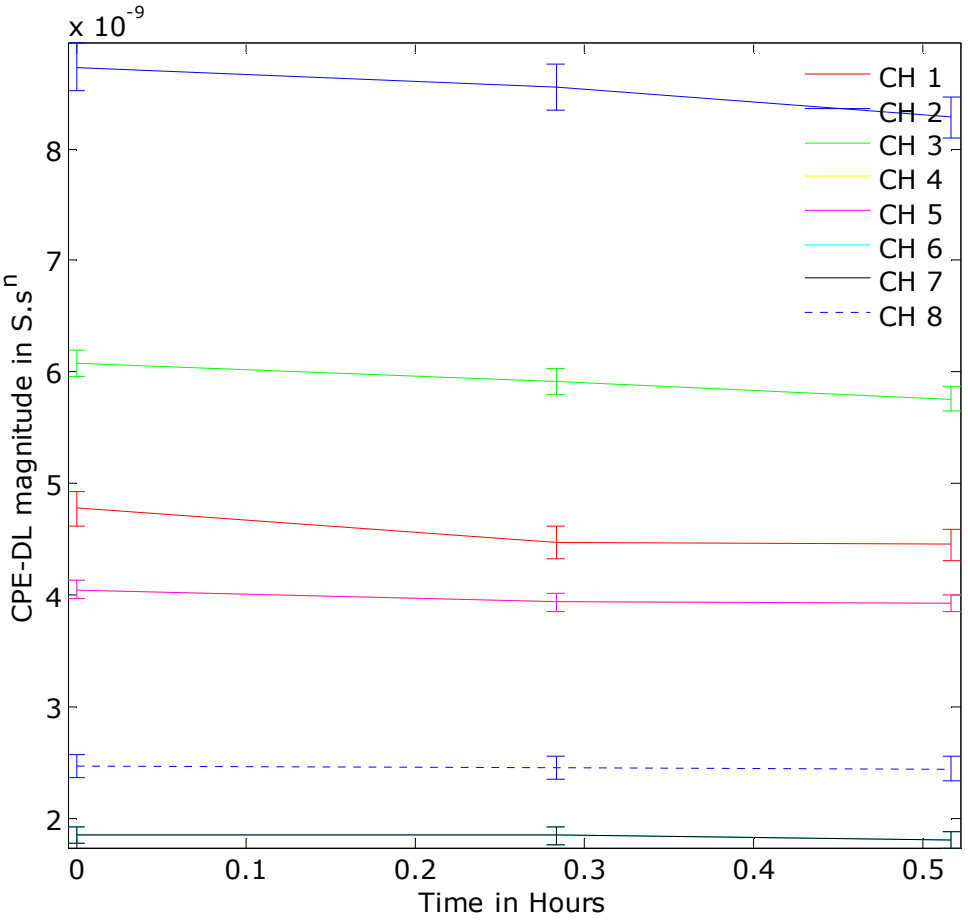

Figure 58: Magnitude of interfacial CPE of cell culture medium (HBSS) as a function of time for 8 electrodes. An approximately 2 nF range is observed for individual electrodes over a period of 160 hours. All electrodes exhibit a synchronous trend over time.

The magnitude of the interfacial CPE_{dl} plotted as a function of time (Figure 58) exhibits a steady rise over time within a range of 2 nF during 160 hours. This could be due to biofouling and degradation effects or simply due to the exhaustion of ionic species at the interface. The electrode was not maintained in a sterile environment. The drift is similar in all electrodes. The initial CPE_{dl}-magnitude is different for all electrodes due to the approximate method of placement of cell culture cylinder on the electrode array.

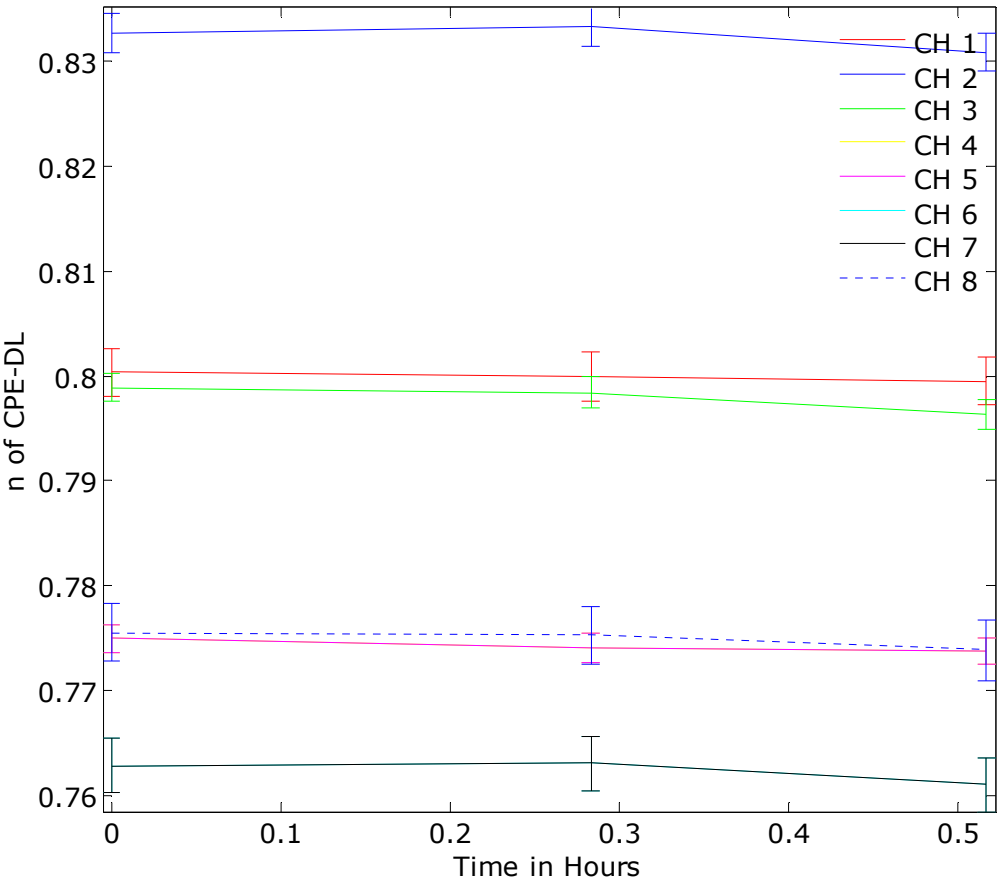

Figure 59: Power factor of interfacial CPE of cell culture medium (HBSS) as a function of time for 8 electrodes. An approximately 0.02 range is observed for individual electrodes over a period of 160 hours. All electrodes exhibit a synchronous trend over time.

The CPE power factor (CPE-n) is shown as a function of time in Figure 59. The CPE-n shows a similar trend to that of CPE-magnitude (Figure 58). The value of CPE-n is in the range of 0.8 for the electrodes used in this experiment. Typically for a thermal deposited metal, the CPE-n would be in the range of 0.9-0.95. The electrode array used in this experiment was fabricated by standard PCB process. The PCB traces were then electroplated to a thickness of approximately 2 μm. The surface of these electrodes is rougher in comparison to a thermal deposited gold electrode, hence the difference in CPE-n.

The important conclusion to be drawn from the cell culture medium measurements is that the shape of the phase curve does not change as function of time in the absence of cells, even though it might shift over a small range. Based on the data presented in this chapter and the preceding chapters, the gold (electrode) - medium (electrolyte) system can be confidently parameterized by a resistor - CPE series combination.

7.3.1 Adhesion, Spreading, Confluence and Detachment of OvCa429 Ovarian Cancer Cells

OvCa429 cell suspension was dispensed into the culture medium well attached to the 8-electrode device. Measurements were recorded over a period of more than 116 hours to monitor the activity of cells. The experimental method followed is discussed in section 7.2.

Figure 60 is the phase angle of impedance for electrode 1 as a function of frequency and time. The trace corresponding to the first time instance is recorded at 3 hours post inoculation of OvCa429 cells in the multielectrode sensor and the last time instance represents post trypsination. 0.25% Trypsin-EDTA (Trypsin) was added to the culture well after 68 hours of inoculation. The culture medium was removed prior to adding trypsin. The phase angle curves at these two time (0 and 71 hours) instances are similar to the phase angle curves observed in the case of electrode-cell culture medium alone (Figure 56). In the intervening time period between 0 and 71, the cells adhere, spread, move, become confluent and detach. These events are reflected in the shape of the phase curves. During evolution of the cell culture a secondary phase minimum develops in the Bode phase angle plot at approximately 40 KHz frequency. The phase minimum reaches a peak at approximately 48 hours, which is the known time of confluence of OvCa429 cells. The shape of the phase angle curve is also similar to the data reported in Chapters 4 and 5, where cells were cultured on gold electrodes and cell layer confluence verified by microphotographs.

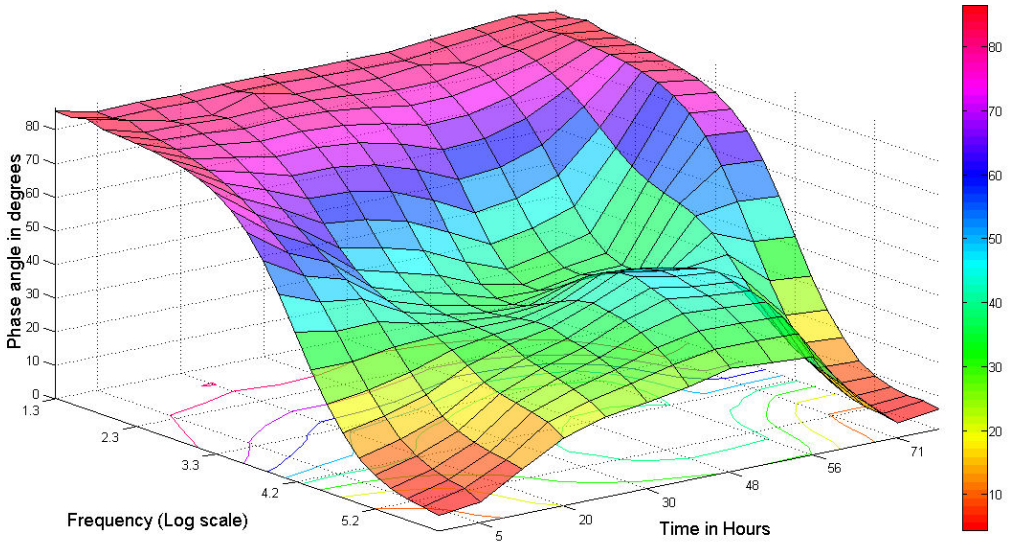

Figure 60: Surface plot of phase angle as a function of frequency and time.

The evidence presented above confirms that the change in the shape of phase angle curve is due to the presence of a cell layer. An examination of phase angle characteristics of all electrodes measured at various points in time will reveal the dynamics of cell culture evolution, presented below.

Figure 61 shows the time sequenced phase angle surface plot for all 8 electrodes. Each subfigure of Figure 61 constitutes a "frame," a set of measurements of 8 electrodes at a given point in time. With the progression of time, a second phase minimum develops around the 40 KHz frequency. The peak of this phase minimum coincides with the known time to confluence of OVCA429 cells. Beyond this point the peak amplitude declines, completely disappearing upon trypsination. Trypsin was added to the culture-well after approximately 68 hours of inoculation. The effect of trypsin is clearly visible in the next impedance reading at 71 hours, where substantial cell detachment has occurred. Following cell detachment, the device was washed thoroughly and filled with cell culture medium. The rest of the frames (beyond 71 hours) display phase angle characteristics of a gold-medium system as it should be.

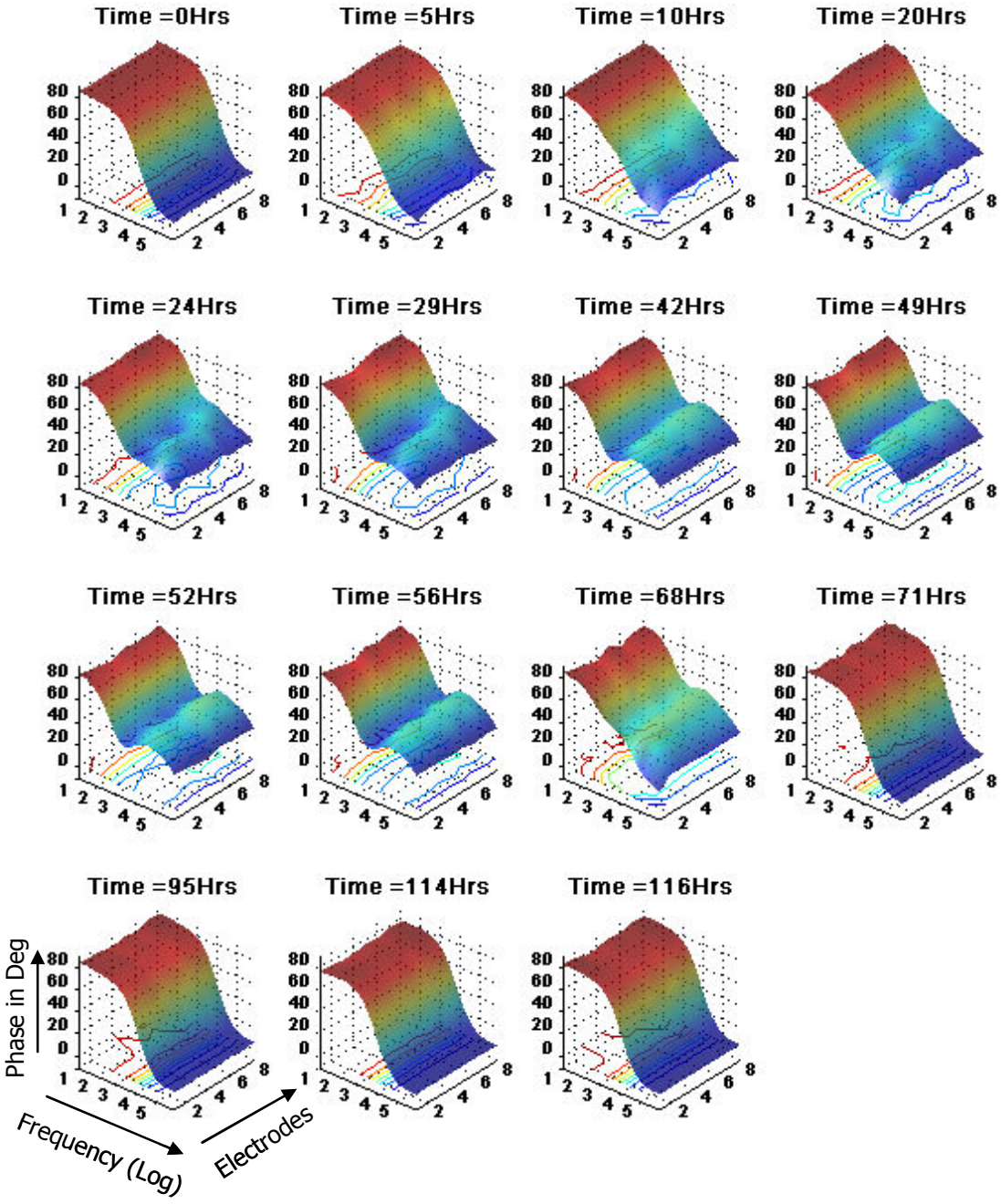

Figure 61: Phase angle of Impedance as a function of frequency, time and electrode position monitored for 116 hours.

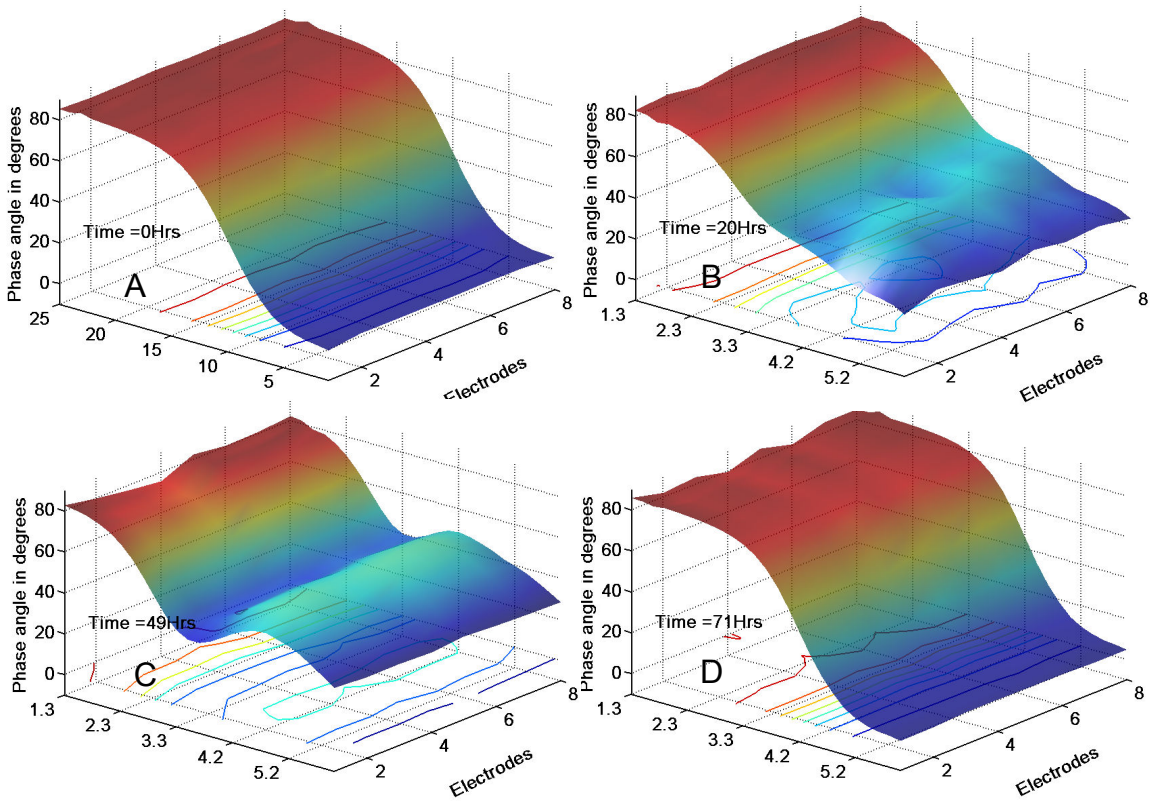

Figure 62: Abridged version of Figure 61, to indicate important events in cell culture progression. A-3 hours after inoculation, B-20 hours after inoculation; uneven cell distribution is noticed here, C- 49 hours past inoculation; even cell distribution is noticed, D- upon trypsination; cell layer detached.

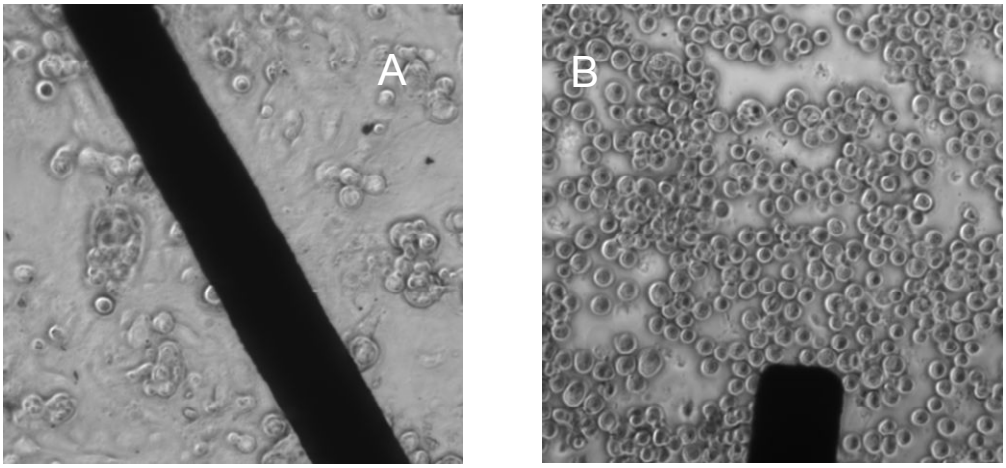

Figure 63: Microphotographs of cells on electrodes. A- confluent OvCa429 cell layer, B- after trypsination.

The spreading and growth of OvCa429 is clearly reflected in the phase angle characteristics. Figure 60 elucidates the effect of cell growth on the phase angle characteristics of electrode 1. This is the basis of visual detection of cell growth by impedance mapping, which can be easily quantified via computational tools using peak detection algorithms. The analysis of this dataset can be either shape-based (area under the curve, surface normalization) or parametric (equivalent circuit modeling). Equivalent circuit analysis is performed on the OvCa429 impedance dataset to determine the interfacial and cell-layer parameters. Parameter estimation by equivalent circuit modeling provides specific data pertaining to the interaction of cells with the substrate and with each other in a quantified manner.

An adaptive MATLAB algorithm is used to parameterize the impedance due to cell-substrate and cell-cell interactions. The lower frequencies reflect the cell-substrate interactions, whereas the higher frequencies reflect the cell-layer properties. Wegener et al [87] also used the low frequency capacitance as a measure of cell-substrate interaction. The thickness of the electrical double layer is a few nm. The closest approach of the cells to the substrate is a few tens of nm's. Consequently, cell coverage and motility are reflected in the impedance data in the lower frequency range (<1 KHz), whereas the cell layer capacitance and tight junctional resistance are reflected at higher frequencies. This is due to the penetration depth of the AC signal, which at higher frequencies can surpass the blocking effect of the double layer capacitance.

A well-formed confluent cell layer is represented by a parallel combination of cell layer capacitance and tight junctional resistance. In a two electrode system, the cell layer impedance is in series with the interfacial impedance. The circuit used to fit the electrode-cell system data consists of a series combination of resistance and CPE, in series with a parallel combination of resistance and CPE. The former represents the interfacial effects and the

latter represents cell layer effects. The circuit used for parameterization of cell covered electrodes is shown in Figure 28 (b).

7.4 Parameterization of Cell-Substrate and Cell-Cell Interactions

A variety of information is available from the CellMap system. Figure 64 through Figure 69 are the estimated parameters of the equivalent circuit of Figure 28 (b), used to parameterize the impedance of cell covered electrodes. The associated error bars in Figure 64 through Figure 69 indicate the confidence intervals of that particular parameter. The cell layer parameters were not required for the fit after tripsination (Time=71 hours) and at Time=0.

A MATLAB algorithm was used to extract the parameters of the impedance dataset shown in Figure 61. A two model fitting system was used to parameterize the impedance response of cell culture medium alone and cells in culture medium (Figure 28). In this method, the presence or absence of a cell layer is detected. The model in Figure 28 (a) is used to represent the lack of cell coverage and the model in Figure 28 (b) is used to represent cell adhesion and spreading. The extracted parameters and their interpretation is discussed in the following section.

7.4.1 Spreading Resistance

The spreading resistance of electrodes in the presence of cells as a function of time is plotted in Figure 64. The spreading resistance shows a decreasing trend with the progression of cell culture. This may be due to the availability of additional ions from the ionic activity of the cells. The spreading resistance shows a slight increase near confluence followed by a drop in resistance during detachment. From the observed trend, spreading resistance appears to be a function of proximity of cells to the substrate and gap junction. The spreading decreases in the time duration (20 - 60 hours) when the cells are in close proximity to the electrodes, but not tightly bound to each other. This inference is drawn from the observed increase in spreading resistance at

confluence but a decrease on either side of confluence time interval (40-50 hours). Outside this time window (20-60 hours), when cells are not in close proximity the spreading resistance increases. This trend is observed in all electrodes. The confidence interval of spreading resistance is the highest for all electrodes at Time=0 (cell suspension), Time=49 (confluent layer) and Time =71 (Trypsination).

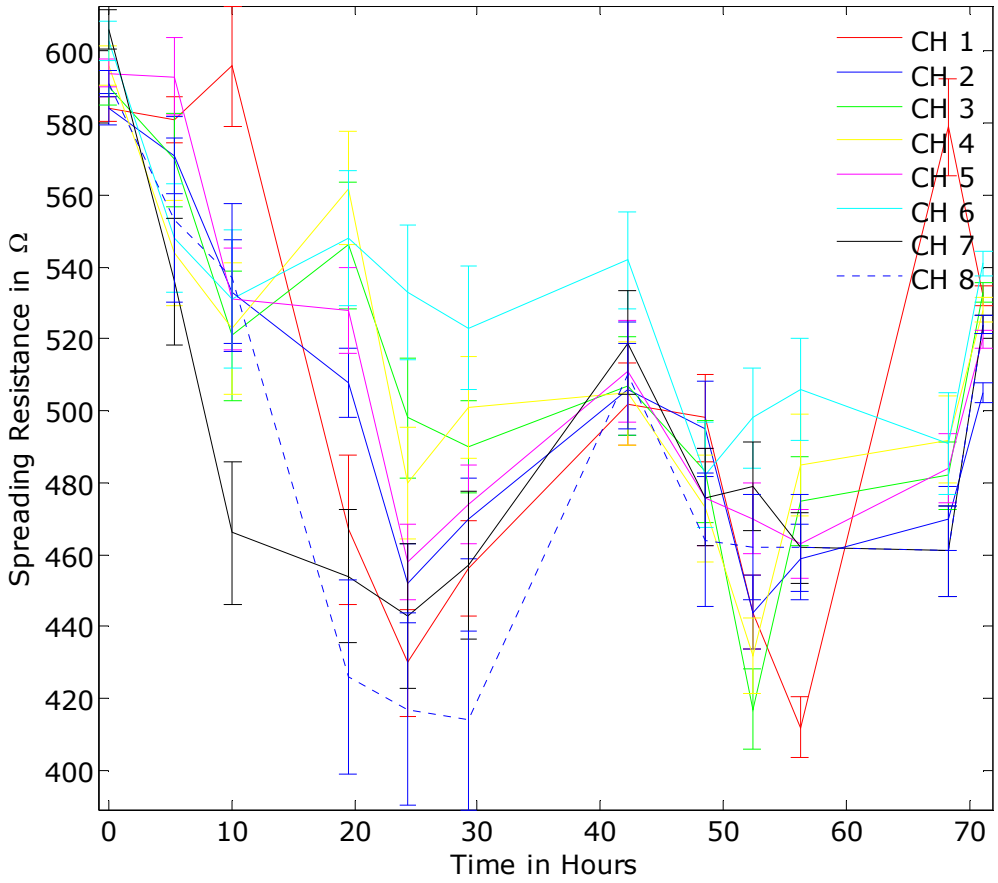

Figure 64: Spreading Resistance as a function of time for all 8 electrodes. Trypsin was added at Time=68 hours.

It is worth contrasting the trends of spreading resistances in Figure 57 (Au-Cell layer system) and Figure 64 (Au-HBSS system). The range of resistance is much broader (approximately 150 Ω) in the case of Au-cell culture system

as opposed to approximately 20 Ω for Au-HBSS system. The trend of spreading resistance is synchronous for the electrodes in Au-HBSS system indicating a steady drift affecting all electrodes, a trend that could be attributed to an environmental parameter affecting all electrodes equally.

7.4.2 The Interfacial Capacitance

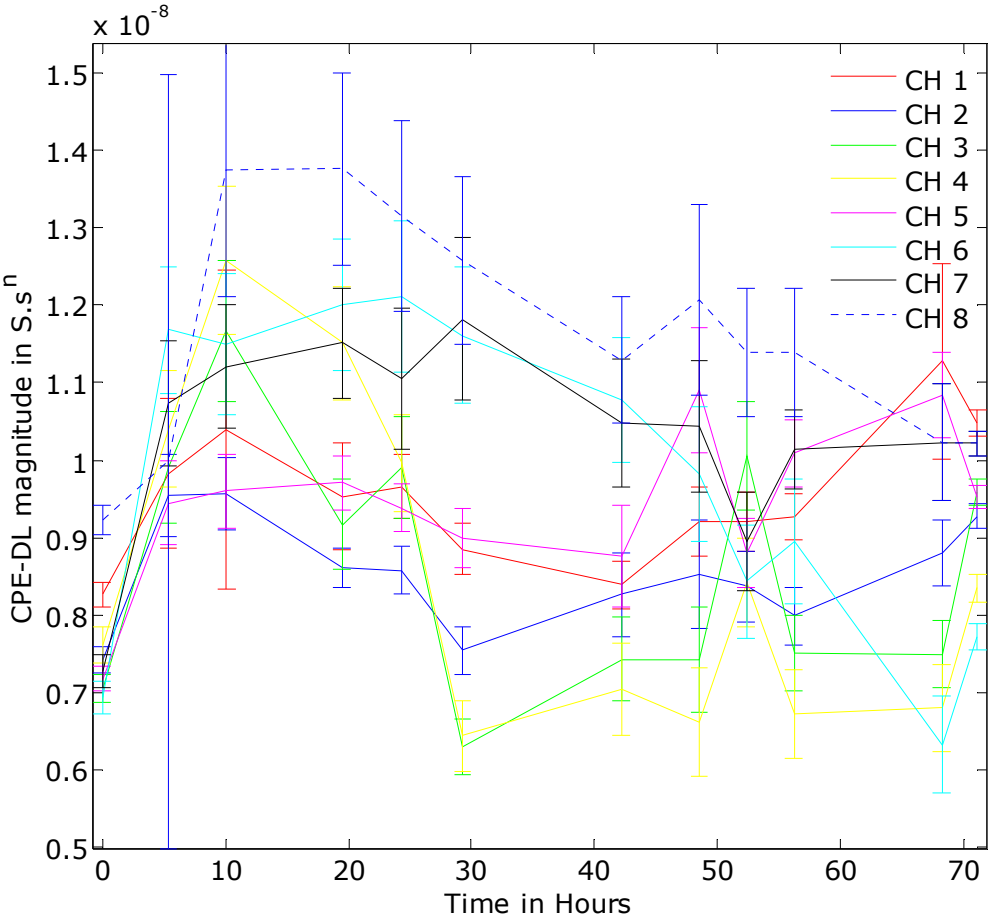

Figure 65: Magnitude of the double layer capacitance as a function of time for all 8 electrodes.

It is difficult to delineate the trends displayed in the CPE-magnitude of electrodes due to the adhesion and spreading of cells. A noticeable aspect is that the electrodes used in the AU-HBSS system are electroplated in contrast to thermal deposited electrodes used in the Au-Cell layer system. The

electroplated gold (on top of PCB track metal) is much rougher than thermal evaporated gold. This should result in higher electrode area for electroplated metal and consequently higher capacitance. On the contrary the Au (thermal deposited)-Cell layer system has an order of magnitude higher capacitance.

In contrast to Figure 58 which is the CPE-magnitude of the Au-HBSS system, the CPE-magnitudes of Au-Cell layer system display a higher degree of variability. Although this is attributed to the activity of the cells, it is difficult to point trends in this data.

A similar conclusion can be drawn from the plot of n of the double layer CPE as a function of time (Figure 66). More understanding is needed to analyze the exact nature of cell-substrate interactions. However, consistent with the stated objective of this research, the extracted parameters do reflect the activity of the cells in culture. From the vast information available through the CellMap system, some information is readily discernible whereas other information will require more insightful analysis to discern trends.

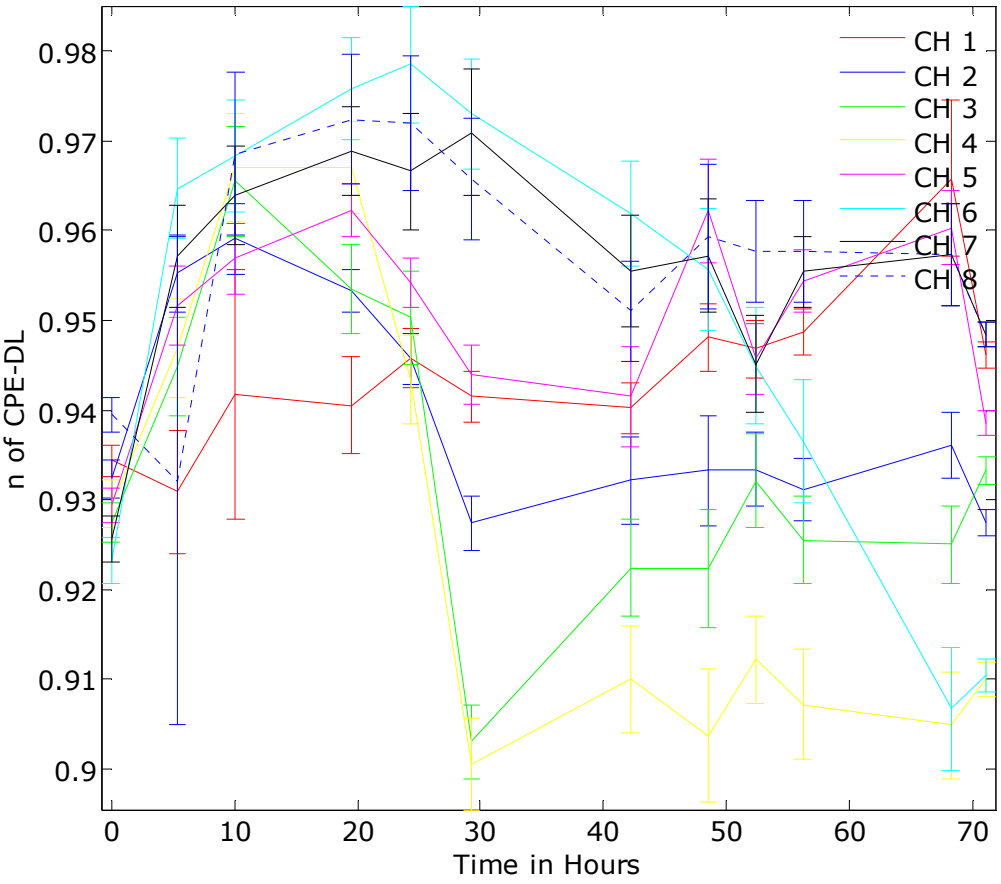

Figure 66: Power factor (n) of double layer CPE as a function of time.

7.4.3 Cell Layer (Tight-Junctional) Resistance

Figure 67 is the plot of cell layer resistance (tight junctional) as a function of culture time. The trend in this parameter is readily discernible. The tight-junctional resistance increases as a function of culture time until confluence, and decreases thereafter. Figure 67 indicates that detachment begins around 50 hours post inoculation. This is consistent with known times of detachment of OvCa429 cells when left in the same culture medium since inoculation. The nutrients in the medium are consumed and the medium turns acidic. Cells begin to detach and die. Upon trypsination, the junctional resistance vanishes.

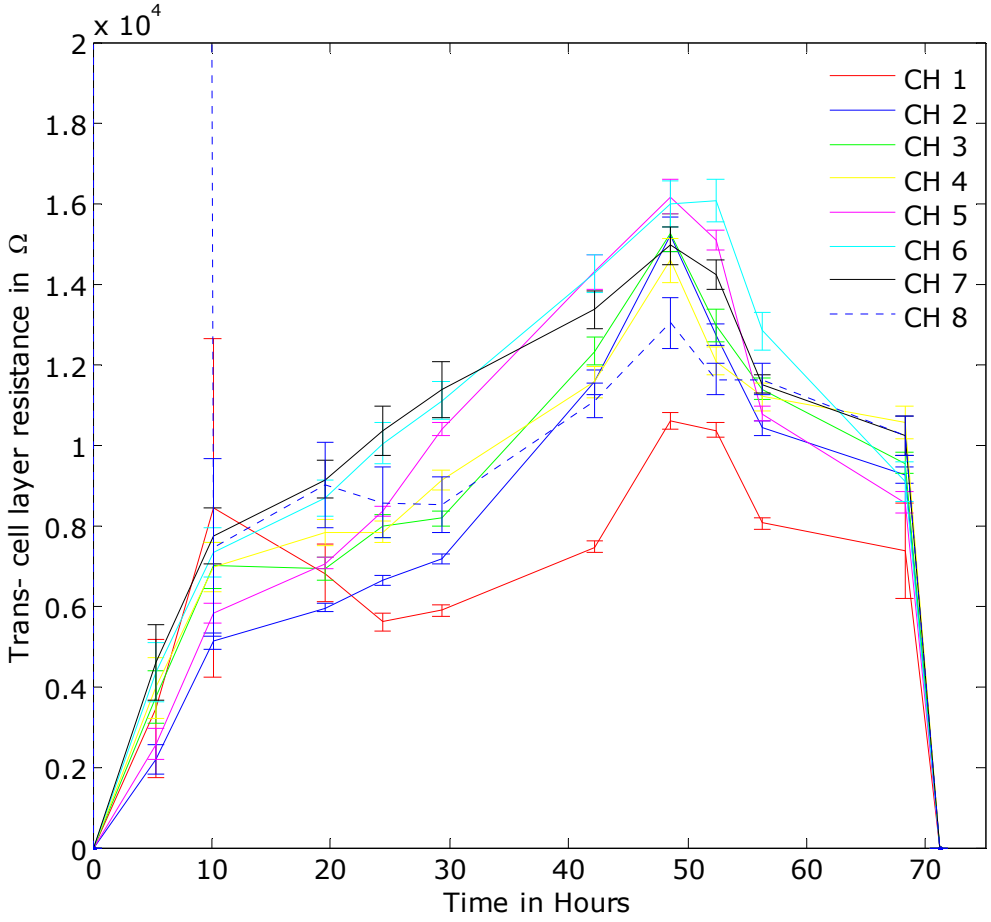

Figure 67: Tight-junctional resistance as a function of time for all 8 electrodes.

7.4.4 Cell Layer CPE-Magnitude

The cell layer capacitance displays an increasing trend when plotted as a function of time Figure 68. In the early stages of cell culture (approximately 5 hours) this parameter has lowest confidence interval, meaning it is not an important parameter in modeling impedance data corresponding to that time period. This is intuitive, given that the cell layer is only beginning to form at this stage. Beyond 5 hours, this parameter has a high confidence interval, meaning it is an important parameter in the overall model. The CPE-magnitude shows a general increasing trend until tripsination.

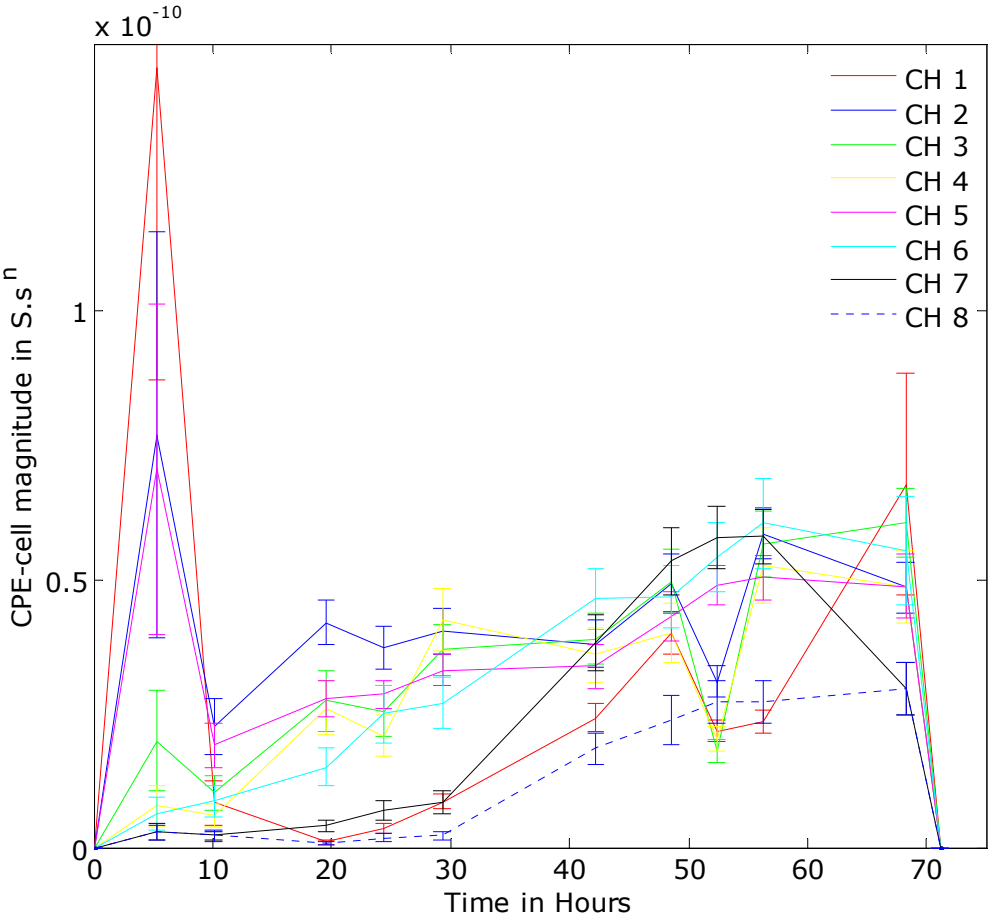

Figure 68: Cell layer CPE magnitude as a function of time for all 8 electrodes.

An interesting trend is observed in the CPE-cell magnitude values of electrodes 1,8 and 7, which are considerably lower than those of the other electrodes. This is probably due to the presence of a cluster of loosely bound cells (cell cluster). This interpretation is supported by the fact that electrodes 1, 8 and 7 are adjacent to each other forming a triangular sector. In due course of time, the cell layer reaches the same level of confluence as other parts of the culture space (Time=49 hours). This indicates that the CellMap system is capable of resolving non-uniform cell density distribution across the 2 dimensional culture space.

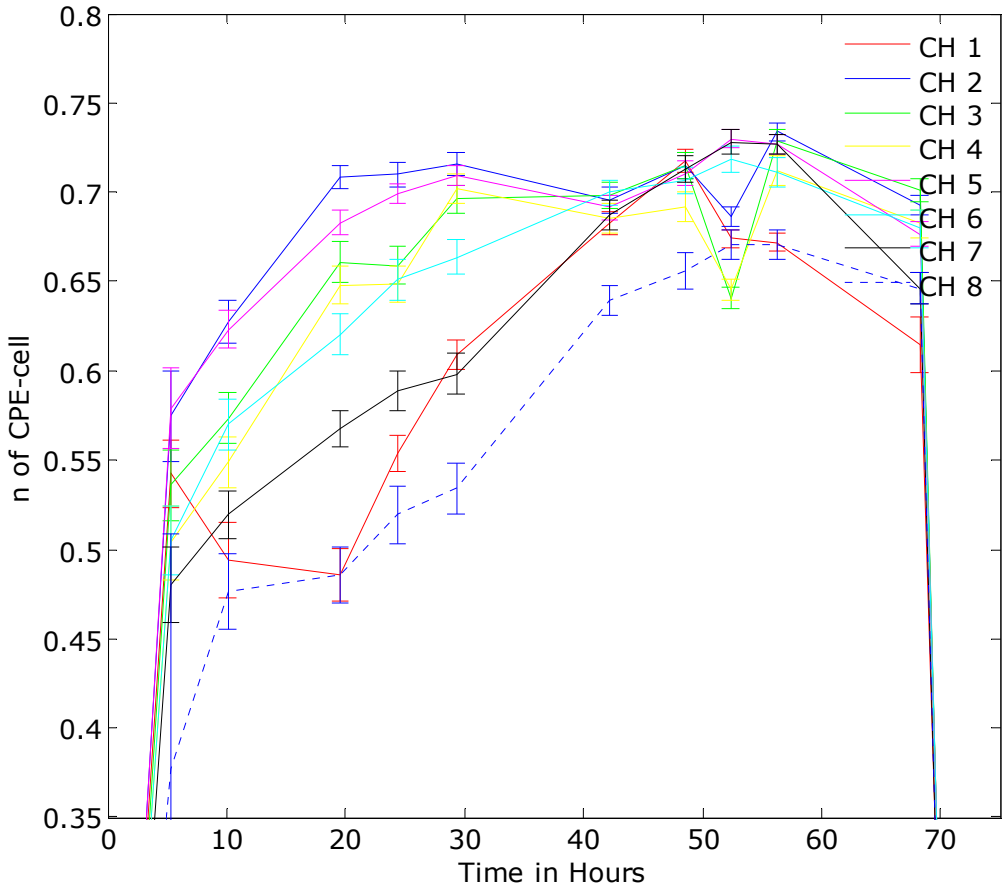

Figure 69: Cell layer CPE power factor (n) as a function of time for all 8 electrodes.

7.4.5 Power Factor of CPE-Cell Layer

The time evolution of power factor (CPE-n) for the cell layer is shown in Figure 69. A similar trend to the one observed for CPE-magnitude (Figure 68) is seen here. Consistent with the observation in Figure 68 for CPE-magnitude, the CPE-n for electrode 1, 7 and 8 are markedly lower. In similarity with CPE-magnitude the CPE-n also achieves consistency with the rest of the culture space around 49 hours, which is the known time to confluence of this cell type.

7.5 Summary

A fully automated system (CellMap) for impedance recording, data acquisition, analysis, visualization and parameter estimation has been implemented for monitoring in-vitro behavior of OvCa429 ovarian cancer cells. The parameter representing cell layer resistance shows clear trends during confluence and cell detachment. The CPE_{cell} magnitude and power factor parameters are more sensitive to cell layer non-uniformity. The scalability of the CellMap system to higher number of electrodes may result in improved sensitivity for cell behavior monitoring. In addition to quantitative parameterization of cell behavior, several 2D and 3D visualization options are available in the software package. The multielectrode scans can also provide statistical correlation.

Chapter 8: Conclusions and Future Work

The significant outcome of this research is that the CellMap system has been implemented to monitor adhesion, spreading, confluence and detachment of OvCa429 cells in culture. Quantitative electrical descriptors of cell-substrate and cell-cell interactions that were previously unavailable on an automated basis have been successfully identified and extracted from the impedance response. The CellMap system can be implemented for cell culture monitoring with any two port impedance measurement instrument.

The evolution of specific parameters of cell-substrate and cell-cell interactions such as interfacial capacitance, tight junctional resistance and cell layer capacitance have been analyzed as a function of culture time. The tight-junctional resistance increases as a function of culture time until the cell layer attains confluence, and decreases thereafter. Similar trend was observed for cell layer Constant Phase Element (CPE) and its power factor. The cell layer CPE and its associated n indicate a non-uniform cell distribution in the early stage of the cell culture (< 30 hours), which was visually confirmed from the shape of the phase angle curve. At around the known time of confluence (approximately 48 hours) of OvCa429 cells, the cell layer parameters attain similar values on all eight electrodes, indicating confluence.

During the development cycle of CellMap system, many experiments were performed with the aim of gaining a better understanding on aspects of impedance-based cell-substrate sensing. The results of these experiments provided insight into fundamental aspects of cell layer frequency response, device parasitic identification and impedance response parameterization

(Chapter 4). A crucial set of experiments to study the effect of electrode area on impedance response of analytes of various morphologies provided information on non-uniform current distribution effects. From the results of this experiment, the lower limit of electrode size was determined to be approximately 50 μm for aqueous based analytes (Chapter 5).

Future versions of the CellMap system can benefit from an increased number of Working Electrodes (WEs') without introducing much parasitics. This is possible due to the out of plane positioning of Counter Electrode (CE), which ensures that the gap between each working electrode and counter electrode is the same. However, the current configuration of CE is not batch fabricatable (suspended CE). For multi-well assays, it is beneficial to batch fabricate this device. The CE can be integrated in the device by isolating it with a thick photoresist such as SU-8. For successful implementation as a High-Throughput-Screening (HTS) system, CellMap has to be expanded into a multi-well assay. The currently used commercial impedance measurement instruments can be replaced by a small footprint card-based impedance analyzer. A portable impedance measurement unit with an integrated switching mechanism and wireless data transfer will make the CellMap system capable of remote monitoring. The current usage of MATLAB for data processing and visualization can be replaced with algorithms in open-sourced programming languages such as C++ and JAVA.

Other research groups should be encouraged to adopt the CellMap system to study various other cell types. This will stimulate research in cell motility pattern recognition and other unexplored areas of cell substrate research.

References

1. Woolf, N., Cell, Tissue and Disease: The Basis of Pathology. 2000, Edinburgh; New York: W.B.Saunders Ltd.

2. Kilani, M.M., et al., Respiratory Syncytial Virus Causes Increased Bronchial Epithelial Permeability. Chest, 2004. 126(1): p. 186-191.

3. Xiao, C., et al., Assessment of cytotoxicity using electric cell-substrate impedance sensing: concentration and time response function approach. Anal Chem, 2002. 74(22): p. 5748-53.

4. Lo, C.M., C.R. Keese, and I. Giaever, pH changes in pulsed CO2 incubators cause periodic changes in cell morphology. Exp Cell Res, 1994. 213(2): p. 391-7.

5. Abassi, Y.A., et al., Label-free, real-time monitoring of IgE-mediated mast cell activation on microelectronic cell sensor arrays. J Immunol Methods, 2004. 292(1-2): p. 195-205.

6. Yin, H., et al., Bioelectrical Impedance Assay to Monitor Changes in Aspirin-Treated Human Colon Cancer HT-29 Cell Shape during Apoptosis. Analytical Letters, 2007. 40(1): p. 85-94.

7. Harrison, D.J., et al., ``From micromotors to micro-fluidics the blossoming of micromachining technologies in chemistry, biochemistry, and biology,''. Proc Transducers. 99: p. 7-10.

8. Buehring, G.C. and R.R. Williams, Growth Rates of Normal and Abnormal Human Mammary Epithelia in Cell Culture. Cancer Res, 1976. 36(10): p. 3742-3747.

9. Yu, N., et al., Real-time monitoring of morphological changes in living cells by electronic cell sensor arrays: an approach to study G protein-coupled receptors. Anal Chem, 2006. 78(1): p. 35-43.

10. Peters, M.F., et al., Evaluation of Cellular Dielectric Spectroscopy, a Whole-Cell, Label-Free Technology for Drug Discovery on Gi-Coupled GPCRs. J Biomol Screen, 2007.

11. Buitenweg, J.R., et al., Measurement of sealing resistance of cell-electrode interfaces in neuronal cultures using impedance spectroscopy. Medical and Biological Engineering and Computing, 1998. 36(5): p. 630-637.

12. Asami, K., et al., Dielectric spectroscopy of biological cells. Bioelectrochemistry and Bioenergetics, 1996. 40(2): p. 141-145.

13. Underwood, J.C.E., Introduction to Biopsy Interpretation and Surgical Pathology. 1987: Springer-Verlag.

14. en.wikipedia.org. Histology - Wikipedia, the free encyclopedia. 2007 [cited 20 August 2007]; Available from: http://en.wikipedia.org/wiki/Histology

15. Fawcett, D.W. and W. Bloom, A textbook of histology. 1994: Chapman & Hall New York.

16. Ramos-Vara, J.A., Technical Aspects of Immunohistochemistry. Veterinary Pathology Online, 2005. 42(4): p. 405-426.

17. Cole, K.S. and H.J. Curtis, Electric Impedance of the Squid Giant Axon During Activity. The Journal of General Physiology, 1939. 22(5): p. 649-670.

18. Cole, K.S., Electric Impedance of Suspensions of Spheres. The Journal of General Physiology, 1928. 12(1): p. 29-36.

19. Schwan, H.P., Electric Characteristics of Tissues. Radiation and Environmental Biophysics, 1963. 1(3): p. 198-208.

20. Simpson, R.W., et al., Nonlinear AC and DC Polarization of Platinum Electrodes. Biomedical Engineering, IEEE Transactions on, 1980: p. 166-171.

21. McAdams, E.T. and J. Jossinet, Tissue impedance: a historical overview. Physiol Meas, 1995. 16(Suppl A): p. A1-A13.

22. Harrison, R.G., et al., Observations of the living developing nerve fiber. The Anatomical Record, 1907. 1(5): p. 116-128.

23. Witkowski, J.A., Experimental pathology and the origins of tissue culture: Leo Loeb's contribution. Med Hist, 1983. 27(3): p. 269-88.

24. Cheville, N.F., Cell Pathology. 1976: Iowa State University Press.

25. Wong, J.Y., R. Langer, and D.E. Ingber, Electrically Conducting Polymers can Noninvasively Control the Shape and Growth of Mammalian Cells. Proceedings of the National Academy of Sciences, 1994. 91(8): p. 3201-3204.

26. Bard, A.J. and L.R. Faulkner, Electrochemical Methods: Fundamentals and Applications. 2001, Wiley & Sons, New York.

27. Eugenii Katz, I.W., Probing Biomolecular Interactions at Conductive and Semiconductive Surfaces by Impedance Spectroscopy: Routes to Impedimetric Immunosensors, DNA-Sensors, and Enzyme Biosensors. Electroanalysis, 2003. 15(11): p. 913-947.

28. Guan, J., Y.U.Q. Miao, and Q. Zhang, Impedimetric Biosensors. Journal of Bioscience and Bioengineering, 2004. 97(4): p. 219-226.

29. Thielecke, H., et al., Evaluation of impedance spectroscopy for the characterization of small biological samples in tissue-based test systems. Engineering in Medicine and Biology Society, 2004. EMBC 2004. Conference Proceedings. 26th Annual International Conference of the, 2004. 1.

30. Frew, J.E. and H.A. Hill, Electrochemical biosensors. Anal Chem, 1987. 59(15): p. 933A-944A.

31. Johnson, M.D., et al., Chemical sensing capability of MEMS implantable multichannel neural microelectrode arrays. Engineering in Medicine and Biology Society, 2003. Proceedings of the 25th Annual International Conference of the IEEE, 2003. 4.

32. Tresset, G. and S. Takeuchi, A microfluidic device for electrofusion of biological membranes. Micro Electro Mechanical Systems, 2004. 17th IEEE International Conference on.(MEMS), 2004: p. 25-28.

33. Lin, Y.C., et al., A microchip for electroporation of primary endothelial cells. Sensors and Actuators A: Physical, 2003. 108(1): p. 12-19.

34. Muller, T., et al., A 3-D microelectrode system for handling and caging single cells and particles. Biosensors & Bioelectronics, 1999. 14(3): p. 247-256.

35. Cho, Y.H., et al., MEMS-based biochip for the characterization of single red blood cell. 2005 3rd IEEE/EMBS Special Topic Conference on Microtechnology in Medicine and Biology (IEEE Cat. No. 05EX937), 2005: p. 60-63.

36. Gomes, H.L., et al., A microelectrode impedance method to measure interaction of cells. Proceedings of the IEEE Sensors 2004 (IEEE Cat. No.04CH37603), 2004: p. 1011-1013 Volume 2.

37. Huang, X., et al. Impedance based biosensor array for monitoring mammalian cell behavior. 2003.

38. Bashir, R., BioMEMS: state-of-the-art in detection, opportunities and prospects. Adv Drug Deliv Rev, 2004. 56(11): p. 1565-1586.

39. Giaever, I. and C.R. Keese, Micromotion of Mammalian Cells Measured Electrically. Proceedings of the National Academy of Sciences, 1991. 88(17): p. 7896-7900.

40. Keese, C.R., et al., A biosensor that monitors cell morphology with electrical fields. Engineering in Medicine and Biology Magazine, IEEE, 1994. 13(3): p. 402-408.

41. Schwartz, D.R., et al., Gene Expression in Ovarian Cancer Reflects Both Morphology and Biological Behavior, Distinguishing Clear Cell from Other Poor-Prognosis Ovarian Carcinomas. Cancer Res, 2002. 62(16): p. 4722-4729.

42. Szent-Gyorgyi, A., The Living State and Cancer. PNAS, 1977. 74(7): p. 2844-2847.

43. Kasza, K.E., et al., The cell as a material. Curr Opin Cell Biol, 2006.

44. Li, N., A. Tourovskaia, and A. Folch, Biology on a chip: microfabrication for studying the behavior of cultured cells. Crit Rev Biomed Eng, 2003. 31(5-6): p. 423-88.

45. web.indstate.edu. Extracellular Matrix (ECM). 2007 [cited 12 June 2007]; Available from: http://web.indstate.edu/thcme/mwking/extracellularmatrix.html

46. Wang, N. and D.E. Ingber, Control of cytoskeletal mechanics by extracellular matrix, cell shape, and mechanical tension. Biophysical Journal, 1994. 66(6): p. 2181-2189.

47. users.rcn.com. The Extracellular Matrix. 2004 [cited 12 June 2007]; Available from: http://users.rcn.com/jkimball.ma.ultranet/BiologyPages/E/ECM.html

48. Burridge, K., et al., Focal Adhesions: Transmembrane Junctions Between the Extracellular Matrix and the Cytoskeleton. Annual Review of Cell Biology, 1988. 4(1): p. 487-525.

49. users.rcn.com. Junctions Between Cells. 2007 [cited 12 June 2007]; Available from: http://users.rcn.com/jkimball.ma.ultranet/BiologyPages/J/Junctions.html

50. Atienza, J.M., et al., Dynamic monitoring of cell adhesion and spreading on microelectronic sensor arrays. J Biomol Screen, 2005. 10: p. 795-805.

51. Borkholder, D.A., Cell-based biosensors using microelectrodes. 1999, Stanford University: United States -- California.

52. Keese, C.R. and I. Giaever. A whole cell biosensor based on cell-substrate interactions. 1990. Philadelphia, PA, USA: Publ by IEEE, Piscataway, NJ, USA.

53. Xiao, C. and J.H.T. Luong, On-Line Monitoring of Cell Growth and Cytotoxicity Using Electric Cell-Substrate Impedance Sensing(ECIS). Biotechnology Progress, 2003. 19(3): p. 1000-1005.

54. Martinsen, O.G., S. Grimnes, and H.P. Schwan, Interface phenomena and dielectric properties of biological tissue. Encyclopedia of Surface and Colloid Science, 2002: p. 2643–52.

55. Liu, H.-B., et al., Sensing minute changes in biological cell monolayers with THz differential time-domain spectroscopy. Biosensors and Bioelectronics. In Press, Corrected Proof.

56. Molckovsky, A. and B.C. Wilson, Monitoring of cell and tissue responses to photodynamic therapy by electrical impedance spectroscopy. Phys. Med. Biol, 2001. 46: p. 983–1002.

57. Huang, X., et al., Impedance based biosensor array for monitoring mammalian cell behavior. Sensors, 2003. Proceedings of IEEE, 2003. 1.

58. Asami, K., Dielectric dispersion in biological cells of complex geometry simulated by the three-dimensional finite difference method. J. Phys. D: Appl. Phys, 2006. 39: p. 492–9.

59. Lo, C.M., et al., Cell-substrate separation: effect of applied force and temperature. European Biophysics Journal, 1998. 27(1): p. 9-17.

60. Schmidt, M.H.H., et al., SETA/CIN85/Ruk and its binding partner AIP1 associate with diverse cytoskeletal elements, including FAKs, and modulate cell adhesion. Journal of Cell Science, 2003. 116(14): p. 2845-2855.

61. Hug, T.S., Biophysical Methods for Monitoring Cell-Substrate Interactions in Drug Discovery. Assay and Drug Development Technologies, 2003. 1(3): p. 479-488.

62. Goda, N., et al., Evaluation of micromotion of vascular endothelial cells in Electrical Cell-substrate Impedance Sensing (ECIS) method using a mathematical model. Journal of Mechanics in Medicine and Biology, 2005. 5(2): p. 357-368.

63. Xiao, C., et al., An in-depth analysis of electric cell-substrate impedance sensing to study the attachment and spreading of mammalian cells. Analytical Chemistry, 2002. 74(6): p. 1333-1339.

64. Lo, C.M., C.R. Keese, and I. Giaever, Impedance analysis of MDCK cells measured by electric cell-substrate impedance sensing. Biophysical Journal, 1995. 69(6): p. 2800-2807.

65. Wegener, J., M. Sieber, and H.J. Galla, Impedance analysis of epithelial and endothelial cell monolayers cultured on gold surfaces. Journal of Biochemical and Biophysical Methods, 1996. 32(3): p. 151-170.

66. Lo, C.M., C.R. Keese, and I. Giaever, Cell-substrate contact: another factor may influence transepithelial electrical resistance of cell layers cultured on permeable filters. Experimental Cell Research, 1999. 250(2): p. 576-580.

67. Barsoukov, E. and J.R. Macdonald, Impedance spectroscopy : theory, experiment, and applications. 2nd ed. 2005, Hoboken, N.J.: John Wiley. xvii, 595.

68. Huang, X., et al., Impedance based biosensor array for monitoring mammalian cell behavior. Proceedings of IEEE Sensors 2003 (IEEE Cat. No.03CH37498), 2003: p. 304-309 Vol.1.

69. Nguyen, D.D., Impedance based sensing of mammalian cell colonization, spreading, proliferation, and drug response. 2004, Carnegie Mellon University: United States -- Pennsylvania.

70. Matthew, A., Current biosensor technologies in drug discovery. Drug Discovery, 2006: p. 69.

71. Zhu, J., et al., Dynamic and label-free monitoring of natural killer cell cytotoxic activity using electronic cell sensor arrays. J Immunol Methods, 2006.

72. Ciambrone, G.J., et al., Cellular Dielectric Spectroscopy: A Powerful New Approach to Label-Free Cellular Analysis. Journal of Biomolecular Screening, 2004. 9(6): p. 467.

73. Jonscher, A.K., Dielectric relaxation in solids. 1983, London: Chelsea Dielectrics Press. xiii, 380.

74. Macdonald, J.R., Linear Relaxation - Distributions, Thermal-Activation, Structure, and Ambiguity. Journal of Applied Physics, 1987. 62(11): p. R51-R62.

75. Schwan, H.P., Electrical properties of tissue and cell suspensions. Adv Biol Med Phys, 1957. 5: p. 147-209.

76. Shapiro, H.M., Cell membrane potential analysis. Methods Cell Biol, 1990. 33: p. 25-35.

77. Jossinet, J., Variability of impedivity in normal and pathological breast tissue. Medical & Biological Engineering & Computing, 1996. 34(5): p. 346-350.

78. Blad, B., et al., Electrical impedance index to distinguish between normal and cancerous tissues. Journal of Medical Engineering and Technology, 1999. 23(2): p. 57-62.

79. Kun, S. and R.A. Peura. Tissue ischemia detection using impedance spectroscopy. 1994. Baltimore, MD, USA: IEEE, Piscataway, NJ, USA.

80. Gimsa, J., et al., Dielectric spectroscopy of single human erythrocytes at physiological ionic strength: dispersion of the cytoplasm. Biophysical Journal, 1996. 71(1): p. 495-506.

81. Morimoto, T., et al., Measurement of the electrical bio-impedance of breast tumors. Eur Surg Res, 1990. 22(2): p. 86-92.

82. Rossi, S., et al., Percutaneous treatment of small hepatic tumors by an expandable RF needle electrode. American Journal of Roentgenology, 1998. 170(4): p. 1015-1022.

83. Silver, I.A., Microelectrodes in medicine. Philos. Trans. R. Soc. Lond. Series B. Biol. Sci, 1987. 316: p. 161-167.

84. Cho, S. and H. Thielecke, Design of electrode array for impedance measurement of lesions in arteries. Physiological Measurement, 2005. 26(2): p. S19-S26.

85. Franks, W., et al., Impedance characterization and modeling of electrodes for biomedical applications. Biomedical Engineering, IEEE Transactions on, 2005. 52(7): p. 1295-1302.

86. Linderholm, P., A. Bertsch, and P. Renaud, Resistivity probing of multi-layered tissue phantoms using microelectrodes. Physiological Measurement, 2004. 25(3): p. 645-658.

87. Wegener, J., C.R. Keese, and I. Giaever, Electric cell-substrate impedance sensing (ECIS) as a noninvasive means to monitor the kinetics of cell spreading to artificial surfaces. Exp Cell Res, 2000. 259: p. 158-166.

About the Author

Abdur Rub Abdur Rahman received the bachelor of engineering degree in electrical and electronics engineering from the University of Madras, India in 1997 and master of engineering in electrical engineering from University of Cincinnati in 2001. Upon completion of his masters degree, he served as a process engineer and senior process engineer at Form Factor Inc and Standard MEMS Inc respectively (2000–2002). He has recently (June 28, 2007) completed his doctoral degree in MEMS and Nanotechnology at the University of South Florida. His interests include MEMS based Impedance spectroscopy, fuel cells, and system on a chip.